Improvisations in Phototrophy

Protein engineering and functional investigation of rhodopsin proton-pumps

Srividya Ganapathy

Improvisations in Phototrophy

Protein engineering and functional investigation of rhodopsin proton-pumps

ISBN: 978-94-6233-826-5

Cover design: Srividya Ganapathy

Printing: Gildeprint, The Netherlands

Funded by: Buchem BV, The Netherlands

This research was financially supported by the BioSolar Cells consortium and Leiden university. The project was carried out in the research programme of BioSolar Cells (BSC core project grant C2.9 to W.J. de Grip and K. J. Hellingwerf), co-financed by the Dutch Ministry of Economic Affairs.

Improvisations in Phototrophy

Protein engineering and functional investigation of rhodopsin proton-pumps

PROEFSCHRIFT

ter verkrijging van

de graad van Doctor aan de Universiteit Leiden,

op gezag van de Rector Magnificus Prof. Mr. C. J. J. M. Stolker,

volgens besluit van het College voor Promoties te

verdedigen op Dinsdag 12 December 2017

klokke 16.15 uur

door

Srividya Ganapathy

geboren te Rochester, U.S.A in 1987

Promotiecommissie

Promoters:	Prof. dr. W. J. de Grip
	Prof. dr. H. J. M. de Groot
Overige Leden:	Prof. dr. H. S. Overkleeft
	Prof. dr. J. M. F. G Aerts
	Prof. dr. J. T. M. Kennis
	Prof. dr. J. Lugtenburg
	Prof. dr. A. Matysik-Alia
	Prof. dr. K. J. Hellingwerf
	Dr. R. van der Steen
	Dr. A. Pandit

For all my inner and outer guides…

“Willingness to be puzzled by what seem to be obvious truths is the first step towards gaining understanding of how the world works” - Noam Chomsky

Table of Contents

Abbreviations

A1	all-*trans*-retinal
A2	all-*trans*-3,4-dehydroretinal
ACRs	anion channelrhodopsins
ALL-E	all-*trans*-all-E-locked-retinal
AR3	Archaerhodopsin3
ATP	adenosine triphosphate
bR	Bacteriorhodopsin
CCCP	carbonyl cyanide m-chlorophenyl hydrazine
CCRs	cation channel rhodopsins
cfu	colony forming units
ChR2	Channelrhodopsin2
DDM	aqueous solution of 1-n-dodecyl-β-D-maltopyranoside
DPC	dodecyl phosophocholine
DMAR	all-*trans*-3-dimethylamino-16-nor-1,2,3,4-didehydroretinal
DMF	dimethylformamide
DTT	1,4-dithiothreitol
GR	*Gloeobacter violaceus* rhodopsin
GR_{CTRL}	*E. coli* MG1655Δ*isc*S MUT pJBS1257- IPTG
GR_{MUT}	*E. coli* MG1655Δ*isc*S-MUT pJBS1257-IPTG, retinal, arabinose
GR_{WT}	*E. coli* MG1655Δ*isc*S-MUT pJBS1257-IPTG, retinal
GR:A1	pigment of GR with A1 as the chromophore
GR-FS	GR single mutant F260S
IPTG	Isopropyl β-D-1-thiogalactopyranoside
HR	Halorhodopsin
MMAR	all-*trans*-3-methylamino-16-nor-1,2,3,4-didehydroretinal

MOA2	all-*trans*-3-methoxy-3,4-dehydroretinal
MSP	membrane scaffold protein
MUT	mutagenesis plasmid
OG	octyl-β-D-glucopyranoside
OGNG	octyl glucose neopentyl glycol
PAR	photosynthetically active radiation
PHE	all-*trans*-1,2,3,4-didehydro-1,5-desmethyl-retinal
pmf	proton motive force
PR	Proteorhodopsin from Monterey Bay SAR86 ϒproteobacterium
PR_{CTRL}	*E. coli* MG1655Δ*isc*S MUT pJBS1255 IPTG
PR_{MUT}	*E. coli* MG1655Δ*isc*S-MUT pJBS1255 IPTG, retinal, arabinose
PR_{WT}	*E. coli* MG1655Δ*isc*S-MUT pJBS1255 IPTG, retinal
PR:A1	pigment of PR with A1 as the chromophore
PR-DNFS	PR double mutant D212N, F234S
PR-TA	PR single mutant T101A
NIR	near-infrared
Rh	bovine visual rhodopsin
RT	room temperature
SB	starvation buffer
SBAz	starvation buffer supplemented with 30 mM sodium azide
SMA	styrene maleic acid copolymer
ssNMR	solid-state nuclear magnetic resonance spectroscopy
SRI	Sensory rhodopsin I
SRII	Sensory rhodopsin II
TD-DFT	time dependent density functional theory
WT	wild type

Chapter 1

Introduction to this thesis

Our planet faces a challenging situation driven by the depletion of fossil fuels and the imminent threat of global warming. In the near future, we anticipate a time when the available fuel supplies will no longer meet the rising demands of the population and industry. Thus, we urgently require alternative means to generate and harness energy, to reduce our over-reliance on fossil fuels. The solution clearly lies in renewable sources of energy, of which solar energy is the most prevalent form available to us. Photosynthesis and phototrophy are among the most important biological processes on the planet, and these already make efficient use of the incident solar flux to generate chemical energy for the growth and survival of organisms [1]. Photosynthetic microorganisms represent promising systems for the sustainable production of biofuels or important biochemicals. However, photosynthesis is expensive with respect to the resources required. Organisms have only evolved the photosynthetic capabilities to meet their energy requirements for growth and survival, within the environmental constraints imposed on them. Furthermore, non-photochemical quenching limits the amount of light that can be converted to product. From a bioengineering perspective, the complexity of photosynthetic light harvesting processes imposes another challenge.

Retinal-based microbial phototrophy may present an attractive alternative to harness solar energy. Microbial rhodopsins are relatively simple tunable photosystems, which are highly amenable for a host of bioengineering strategies targeted towards solar-fuel conversion [2, 3].

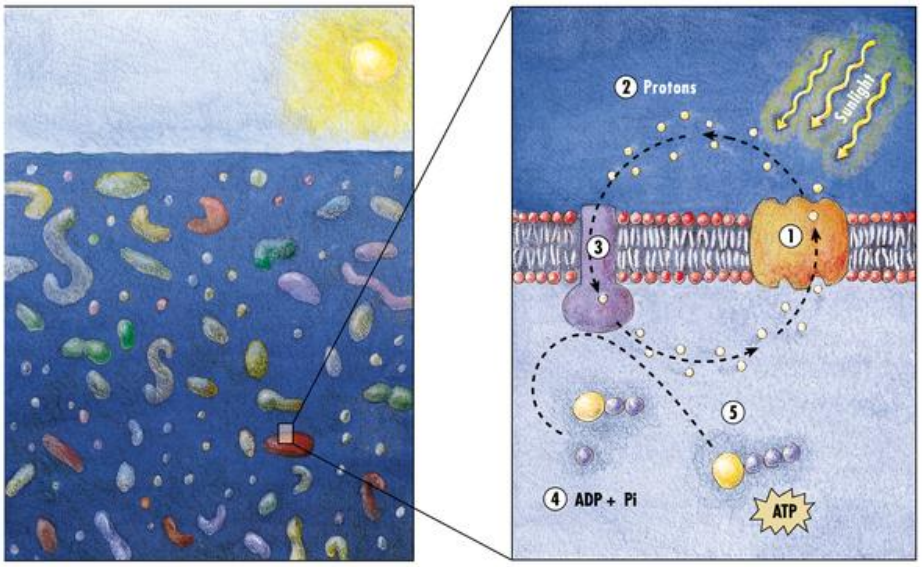

Figure 1.1 An artist's illustration of the distribution and function of microbial proton-pumping rhodopsins in aquatic microbes [4]. Illumination induces proton transport across the cell membrane, which is coupled to ATP synthesis.

1.1 Microbial rhodopsins

Microbial or type-I rhodopsins are light-driven seven-helical transmembrane proteins found in a broad phylogenetic range of microbial life (Figure 1.1) [5]. These proteins bind a molecule of retinal as a chromophore (Figure 1.2) and use visible light, in the range of 400-700 nm, to facilitate various functions in their hosts. These functions include the active transport of ions via proton, sodium, potassium or chloride pumps as well as sensory signaling pathways. The ion transporting rhodopsins provide energy to their hosts by hyperpolarizing the cell membrane. This energy is used during conditions of stress or nutrient limitation, when the respiratory electron transport activity is low. Sensory rhodopsins allow cells to sense and respond to their immediate environment using phototactic signaling mechanisms. Consequently, these proteins are physiologically important for the survival and adaptation of their hosts.

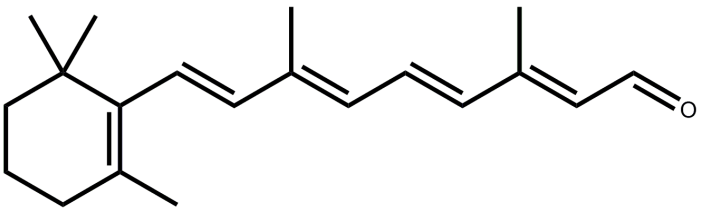

Figure 1.2 The all-*trans* retinal chromophore, common to all microbial rhodopsins

The light-driven outward proton pump bacteriorhodopsin (bR) was the first microbial rhodopsin to be discovered. It was detected in 1971 in the purple membrane of the halophilic marine archaeon *Halobium salinarum* [6]. This archaeon was later shown to also contain an inward chloride pump halorhodopsin (HR) [7] and the positive and negative phototaxis sensors sensory rhodopsin-I (SRI) and II (SRII) respectively [8]. These four archaeal rhodopsins have served as functionally distinct prototypes of the microbial rhodopsin family, and have been investigated by various crystallographic and spectroscopic techniques over the past four decades [9].

At the turn of the 21st century, scientists discovered that microbial rhodopsin genes are far more widespread and functionally diverse than previously imagined. No longer confined to Archaea, variants of these proteins were now also found in Eubacteria, such as proteobacteria [10], cyanobacteria [11] and Eukarya, such as fungi [12], algae [13], as illustrated by the various classes presented in figure 1.3. Metagenomic analyses have shown that lateral gene transfer may have facilitated this distribution across divergent microbial populations [14]. Thus, microbial rhodopsin-based phototrophy is ubiquitous in all three domains of life, making it the most abundant light-driven process on the planet.

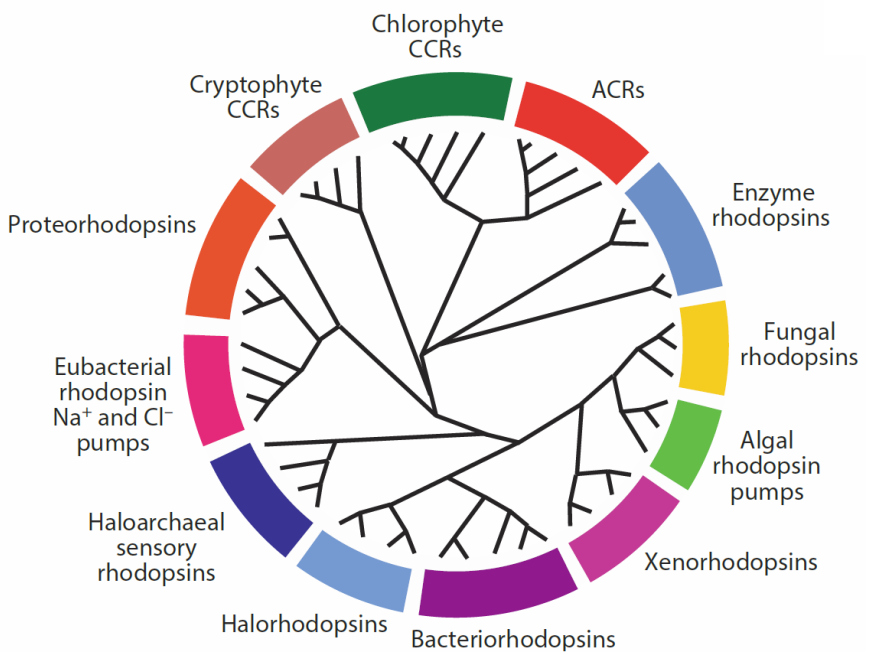

Figure 1.3 Cladogram showing the relatedness (black lines) between the major classes of the microbial rhodopsin superfamily [3]. The proteorhodopsin family of proton-pumps discussed below is represented by the orange arc.

In this thesis, we focus on two eubacterial rhodopsin proton-pumps, which have stimulated considerable interest recently, namely proteorhodopsin and *Gloeobacter* rhodopsin.

1.2 Proteorhodopsin

Proteorhodopsins are the first rhodopsins to be isolated from eubacteria. They are an archetype of the class of rhodopsin proton-pumps, showing ~22% homology to the well-studied bR. The first proteorhodopsin (PR; λ_{max} 520 nm, Figure 1.4a) was discovered in 2000 during a metagenomic screen of marine uncultured gamma-proteobacteria from Monterey Bay in California [10]. Since then, PR-like variants have been found widely distributed in various organisms across the photic zone, making them a hot topic of current research [15].

Since its discovery in bacteria, homologs of PR have been found in archaeal and eukaryotic hosts [16-20], and even in some giant viruses [21]. These hosts inhabit diverse ecosystems, ranging from marine [22, 23] and freshwater habitats [24, 25], to Antarctic sea ice [26], permafrost [27], hot-springs [28], and even samples from terrestrial leaf surfaces [29]. Furthermore, they are found stratified in deep or shallow environs, and are spectrally tuned to the light availability at that depth [30]. Though their exact physiological role is unclear, various studies have shown that PRs generate a light-driven proton-motive force *in vivo*, which can be coupled to ATP synthesis [31]. This contributes towards the growth and survival of host organisms under energy limiting conditions. For instance, upon illumination, PR was shown to stimulate the growth of a marine flavobacterium *Dokdonia* sp. MED134 under carbon limitation [32], and of *Vibrio* sp. during starvation [33]. Due to these light driven functions and their prolific distribution, PRs are thought to be key players in maintaining the phototrophic energy balance in various biospheres.

PR can also be recombinantly expressed in heterologous hosts such as *Escherichia coli* in good quantities [10], unlike bR which shows poor bacterial expression [34]. Its phototrophic potential can be exploited to drive physiological activities in *E. coli*, like flagellar motility [35] or ATP synthesis [36]. One study showed that upon illumination, PR could contribute towards the growth of *E. coli* under anaerobic conditions [37]. Furthermore, heterologous co-expression of PR with a hydrogenase could drive the production of bio-hydrogen [38]. These studies, taken in concert, demonstrate that PR has broad potential for a variety of light-driven biotechnology applications.

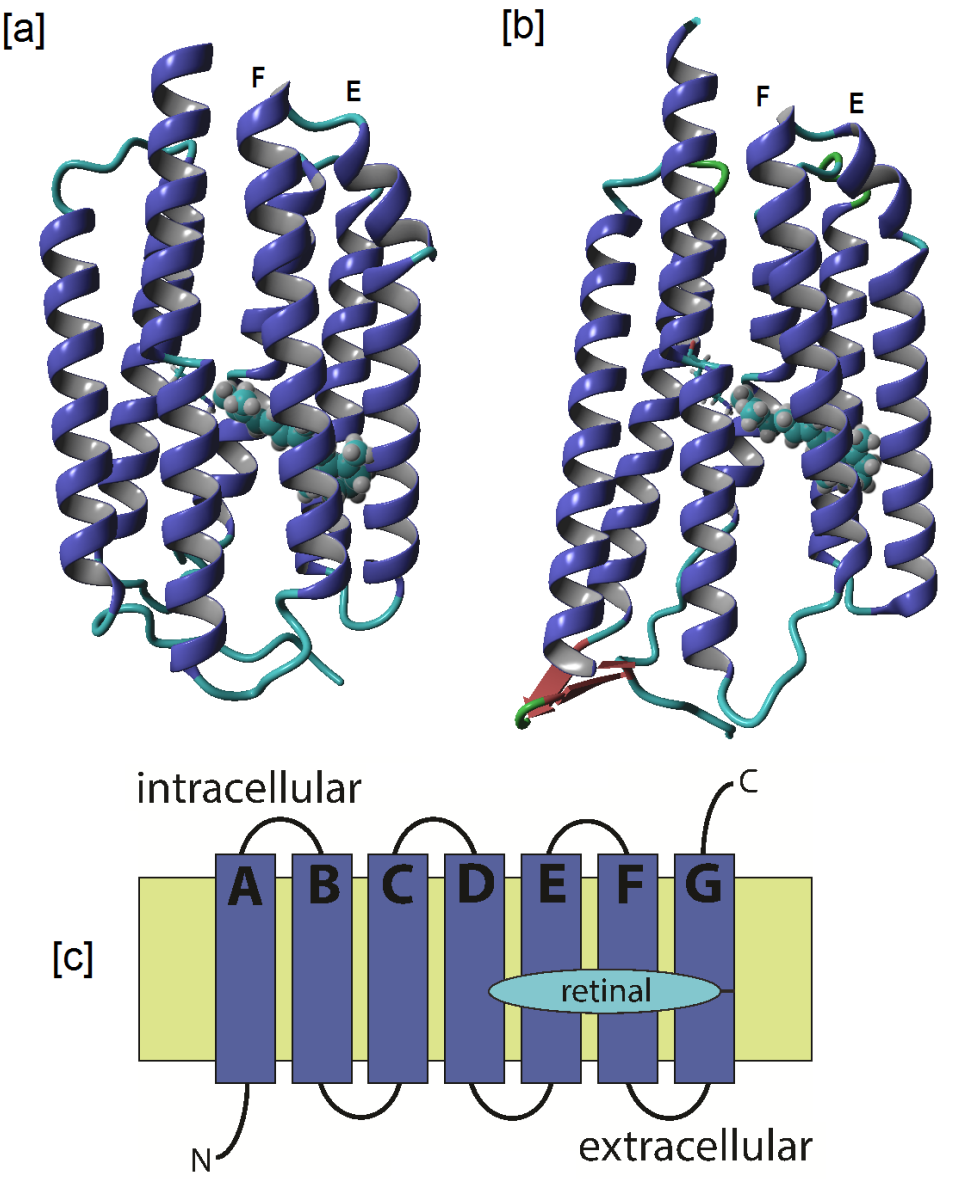

Figure 1.4 Homology model of [a] proteorhodopsin (PR) and [b] *Gloeobacter* rhodopsin (GR), generated using YASARA (www.yasara.org). See chapter 2 for further information. The labeling of helices E and F is indicated. The homology model of GR indicates the presence of a small β-sheet shown in red. The retinylidene chromophore is displayed in cyan as a space filled residue. [c] 2-D snake plot displaying the labeling of the seven helices of PR and GR.

1.3 *Gloeobacter* rhodopsin

Gloeobacter rhodopsin (GR; $\lambda_{max} = 540$ nm, Figure 1.4b), a distant relative of PR, has been studied less extensively. It was discovered in the thylakoid-less cyanobacterium *Gloeobacter violaceus* PCC 7421, isolated from a calcareous rock in Switzerland [39]. GR also functions as a light driven proton-pump in its native host [40] and shares ~30% sequence identity with PR, while conserving several key residues involved in its proton pumping function [40, 41]. GR shows excellent heterologous expression in *E. coli* as well [42] and can contribute towards light-driven ATP production *in vivo* [43].

Phylogenetically, GR is closely related to the eubacterial proton pump xanthorhodopsin (XR), which binds the carotenoid salinixanthin, in addition to the retinylidene chromophore [44, 45]. *In vitro* reconstitution experiments have shown that GR binds the carotenoids salinixanthin [42], and echinenone [46]. The carotenoid is speculated to behave as an antenna, by facilitating energy transfer to the retinal [47], in the order of 30% [48]. The enhanced spectral sensitivity of this phototrophic system, in addition to its rapid photocycle [49] and ease of bacterial expression make GR another highly amenable candidate for bioengineering applications.

1.4 Mechanism and photocycle of PR and GR

PR and GR contain the typical seven trans-membrane α-helical protein motif common to all microbial rhodopsins, called the "opsin". Residues from all helices, which are labeled from A to G (Figure 1.4), contribute towards the formation of the retinal-binding pocket. The holo-protein is formed upon binding a molecule of all-*trans* retinal, via a covalent linkage with the ε-amino group of a lysine residue in helix G (Figures 1.4 and 1.5; K231 in PR, K257 in GR). This generates the retinylidene Schiff-base (SB), which is protonated (PSB) in the resting state. In the dark-adapted form of

PR, the retinylidene moiety predominantly remains in an all-*trans*-15-*anti* conformation [50, 51]. This is in contrast to bR, which contains a mixture of the all-*trans*-15-*anti*, and 13-*cis*-15-*syn* retinal isomers in its dark state [52]. Light excitation drives the isomerization of retinylidene, followed by thermal relaxation of the chromophore and the opsin. A series of conformational changes ultimately result in the transfer of one proton across the cell membrane per photon absorbed. Using ultra-fast spectroscopy, this entire photocycle can be spectrally and kinetically resolved into distinct intermediates[53].

The photocycle is initiated by electronic excitation of the PSB from the ground state (S_0) to its first excited state (S_1), upon the absorption of a single photon of light. The transfer of an electron from the lower energy π-bonding orbital to the higher energy π* anti-bonding orbital induces rotation about the C13-C14 bond, leading to the isomerization of the PSB from an all-*trans* to a 13-*cis* configuration (Figure 1.5). This isomerization takes place in less than 200 femtoseconds, forming the red-shifted J and K-intermediates [54, 55]. The J intermediate is a vibrationally hot form of the subsequent K state, which contains a highly strained 13-*cis* chromophore.

Relaxation of the 13-*cis* chromophore leads to structural rearrangement within the protein, causing a proton to be transferred from the PSB to a nearby Asp residue (D97 in PR, D121 in GR). The deprotonated SB accumulates over a time scale of ms, forming the blue-shifted M-intermediate, which often exists in equilibrium with an earlier L-state [56, 57]. The deprotonated SB is re-protonated by a Glu residue (E108 in PR, E132 in GR) situated midway between the retinylidene and the cytoplasmic side, forming the red-shifted N-intermediate [41]. This Glu picks up a proton from the cytoplasm, while the retinal thermally re-isomerizes into a twisted all-*trans* form, characteristic of the O-intermediate [58]. In the last step of the photocycle, D97/D121 undergoes deprotonation leading to

extracellular proton release, accompanied by relaxation of retinal back to the ground state. The entire photocycle is completed within a time scale of milliseconds.

The photocycle can thus be simplified into the following main stages: isomerization of the PSB, deprotonation to form the SB, reprotonation of the SB, proton-uptake from the cytoplasm and extracellular proton-release. The photocycle of PR resembles that of bR. However, there are some differences, the most notable being the lack of ionizable proton release groups. In bR, Asp residues are involved in proton release to the extracellular surface [59, 60], which are absent in PR and GR. The strongly hydrogen bonded network in the retinal binding pocket could play an important role in proton transport via a bucket brigade of water molecules [61], and proton uptake from the cytoplasm is shown to be influenced by the mobile loop between helices E and F (Figure 1.4) [62]. However, the precise mechanism of extracellular proton release and proton uptake for PR and GR is still unclear.

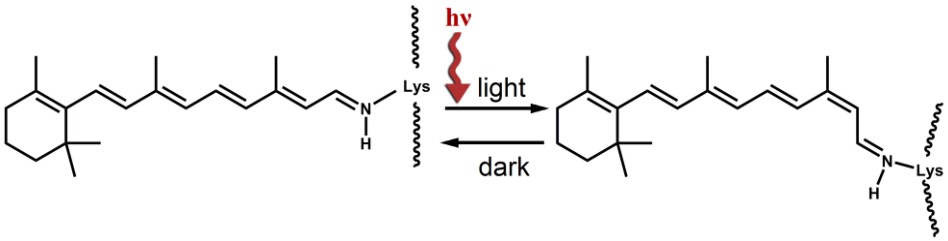

Figure 1.5 Light induced isomerization of the all-*trans* to the 13-*cis* retinylidene group bound to the opsin, eliciting reorganization of the protein environment.

Despite the ambiguity in atomic details of its mechanism, the overall proton-pumping function of PR has been well investigated under a range of conditions. Its function is strongly pH dependent. It shows outward directed proton-pumping in alkaline pH [58], and it has been claimed that the direction of proton transport can be reversed under acidic conditions

[56, 63], though this is the subject of some debate [64]. Nevertheless, there is a clear consensus that the primary proton acceptor D97 has to be deprotonated [65] for a normal photocycle to proceed. The pKa of D97 is reported to be ~7.1 [58], which is much higher than the pKa of the analogous D85 in bR, which is ~2.9 [66]. A nearby His residue, namely H75 in helix B, is thought to have an influence on this high pKa of D97. Solid-state nuclear magnetic resonance (NMR) analyses in combination with mutagenesis have revealed the importance of a specific hydrogen bonding interaction between H75 and D97 [67], which also has an effect on the photocycle of PR. The acidity of D97 is further influenced by the formation of a complex counterion with the residues D227 and R94, as shown in figure 1.5. At alkaline pH, a water molecule forms a complex with the two Asp residues, and the proton from the PSB [56, 68]. R94 further contributes a weak coupling interaction with D97, and possibly also to H75 [69].

Figure 1.6 highlights the important residues discussed above, which influence proton transfer and stability of the counterion complex. It also highlights residues which affect the spectral tuning of proteorhodopsins in general. In the next section, we discuss some of these tuning processes.

1.5 Colour tuning mechanisms

The colour of microbial rhodopsins originates from the electronic transitions occurring within the all-*trans* retinylidene chromophore. Retinal consists of a β-ionone ring attached to an elongated polyene chain, which has the characteristic chemical structure of alternating single and double bonds, as shown in figure 1.2. A delocalization of π electrons over the polyene chain results in a main absorbance band peaking at 360-380 nm for free retinal, which is visually seen as a yellow compound. Studies on SB model compounds have shown that the unprotonated retinylidene SB is relatively insensitive to the solvent environment, with a slightly blue-shifted absorbance band (relative to free retinal) in the UV region [70].

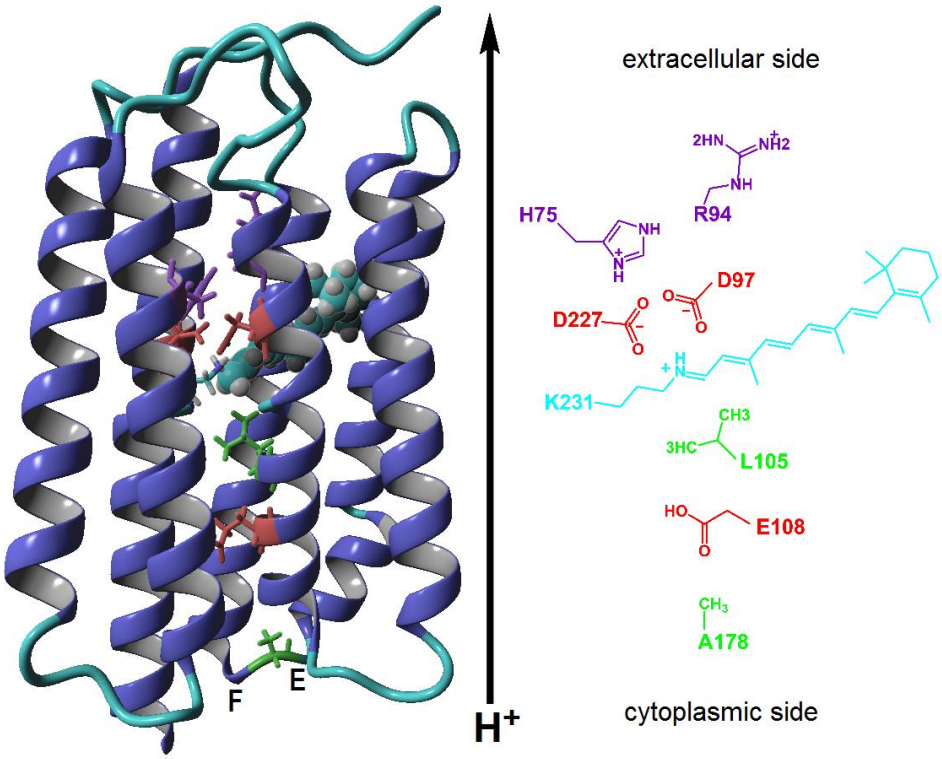

Figure 1.6 Homology model of PR highlighting important residues for the proton pumping function (red), for stability of the counter-ion complex (purple) or residues affecting colour tuning (green). The retinal bound via a protonated SB to a lysine residue is displayed in cyan. The labeling of helices E and F is indicated.

The PSB, however is significantly red-shifted to ~440 nm in methanol, and is much more sensitive to its microenvironment [70, 71]. Upon binding to the opsin, the interaction with the protein environment further shifts this absorbance band towards the much longer wavelengths of $\lambda_{max} = 520$ and $\lambda_{max} = 540$ nm for PR and GR respectively, which is called the "opsin-shift". The distance of the PSB from the counterion and specific interactions with residues lining the binding pocket influence the energy gap between the ground and excited state of the retinylidene chromophore, and therefore the resulting colour of the pigments. A smaller energy gap represents a bathochromic shift and a larger gap corresponds with a hypsochromic shift

in the absorbance band of the pigment (Figure 1.7d). These effectors are examined in further detail below.

The interaction with the negatively charged counterion is an important factor affecting the colour of the retinylidene SB in the binding pocket (Figure 1.7). In the ground state, the PSB is positively charged. The excited state has a tendency to displace this positive charge in the direction of the β-ionone ring, thereby neutralizing the PSB. The counterion however stabilizes the positive charge on the ground state, increasing the pKa of the Schiff base, and leading to a blue shift (Figure 1.7a). The overall effect of the opsin environment, therefore, is to modulate this blue shift induced by the counterion. To further understand this phenomenon, mutational studies have been used to identify specific amino acid residues, which impact the absorbance band of the pigment. Several mutations of PR have thus been described by site-specific mutagenesis [72] or random mutagenesis screens [73], which exert an effect on the PSB via direct or long-range interactions.

A detailed solid-state NMR study in combination with site-directed mutagenesis probed the effect of the EF loop on the photocycle and spectral properties of PR [62]. A specific Ala residue on this loop (Figure 1.6) was shown to exert a long-range effect on the retinal binding pocket, with the A178R mutation leading to a 20 nm red-shift in the absorbance band. This was accompanied by a longer photocycle, due to an elongated life-time of the N/O intermediate, the decay of which is correlated with the re-protonation pathway. One can thus conclude that a complex interaction pathway exists between the EF loop and the retinal-binding pocket, which influences both the colour and photocycle of PR.

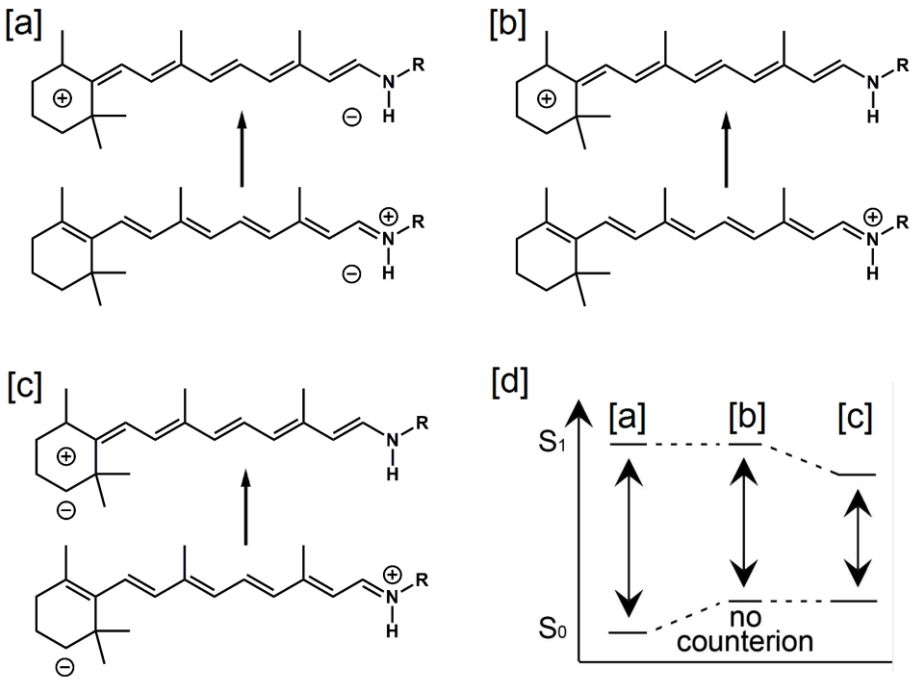

Figure 1.7 Photoexcitation causes switching of the bond alteration and a displacement of positive charge towards the β-ionone ring. Scenarios when the counterion is located: [a] close to the protonated SB, [b] absent, [c] near the β-ionone ring. [d] Electrostatic interactions with the counterion or other residues will increase or decrease the energy gap between the ground and excited states of the retinylidene chromophore.

Two main spectral variations of PR have been described, namely a blue absorbing PR (BPR, λ_{max} 490 nm) [74, 75] and the green absorbing PR (PR, λ_{max} 520 nm), included in this study. From structural modeling and mutagenesis, it was seen that a single amino acid substitution at position L105 in the retinal binding pocket of PR, (which is a Q in BPR) functions as a colour tuning switch (Figure 1.6). The mutation PR L→Q shifts the absorbance maxima into the blue, while the reverse mutation shifts it back to the green form [30, 75]. This mutation is thought to represent an ecological adaptation strategy, to spectrally tune PR to the light-availability at the depth where its respective host is located.

The conformational properties of the ligand also have an influence on the spectral properties and function of these proteins. The electronic distribution in the chromophore will affect the pKa of the SB [76-78], and its structure and fit into the binding pocket will determine the distance to the counterion and proton acceptor, and may also have long-range effects on the protein structure and thereby the interaction with the protein. From a bioengineering perspective, the influence of the PSB and its binding pocket on the colour and function of these proteins is very convenient. Spectrally tuned variants of these proton pumps can be generated by modifying the electronic properties of retinal, or with specific opsin mutations. These proteins can thus be engineered to exploit desired wavelengths of light for specific applications, especially the near-infrared part of the solar spectrum, which is discussed further below.

1.6 Potential of near-infrared active proteorhodopsins

PR and GR are attractive model systems for various synthetic biology applications. However, a great challenge in many of these applications is to extend the action spectrum into the far-red and near-infrared (NIR) range of the electromagnetic spectrum ($\geq$ 700 nm), a range which is relatively unexplored. It has been suggested that PRs can complement oxo-phototrophy when their spectral band is shifted bathochromically to utilize photons outside the range of photosynthetically active radiation (PAR; 400-700 nm) [79], which is hardly exploited by oxygenic photosynthesis [80, 81]. A step has been made in this direction, by expressing PR in the cyanobacterium *Synechocystis* sp. PCC 6803, where it was shown to stimulate growth upon illumination, when compared to a non-functional PR mutant [82].

Red-light activation is also extremely desired in the field of optogenetics, where microbial rhodopsins like Channelrhodopsins are used to modulate the activity of neurons or other mammalian cells by light [83]. Light $\geq$ 700

nm penetrates much further into biological tissue, which for instance would be very useful for the optogenetic stimulation of deeper brain regions. Recently, a red-shifted variant of the widely used Channelrhodopsin2 (ChR2) termed ReaChR was engineered by opsin modification [84]. ReaChR can be activated by 630 nm illumination, and is thus far the most shifted red-light activable optogenetic tool available for the stimulation of neurons.

Chromophore modification strategies have been the most successful in the spectral modulation of microbial rhodopsins. The largest spectral red-shift (~225 nm) reported thus far was obtained with the azulenic pigment of bR, displaying a λ_{max} at 795 nm [85]. However subsequent studies showed that the resulting pigments could not undergo a complete photocycle [86], thereby lacking pump activity which represents a major drawback. Altering the retinylidene environment can significantly affect the isomerization and proton transfer reactions within the retinal-binding pocket, thereby influencing the function of these proteins. Thus, generating a NIR active microbial rhodopsin is still a significant challenge, and the spectral window >700 nm remains largely elusive.

1.7 Structural characterization of proteorhodopsins

Protein and chromophore engineering require an understanding of the structure-function relationship of the system at hand. This is greatly facilitated by detailed and precise structural information available via crystallographic or NMR analyses [87, 88]. These techniques typically require a highly purified intact protein sample, which in the case of membrane proteins is also stabilized in a micellar or lipid bilayer microenvironment. Recombinant protein expression in heterologous hosts is the most convenient and preferred method towards this end. The gram-negative bacterium *E. coli* is widely used as a model organism for the

inducible expression, purification and characterization of many membrane proteins, due to its high turnover, transformation efficiency and well-characterized genetic toolbox. Both PR and GR can be recombinantly expressed in *E. coli* with high yields in the order of 10^5-10^6 molecules/cell [10, 41]. Due to their insoluble nature, PR and GR require prior solubilization and purification with a detergent such as n-dodecyl-β-D-maltopyranoside (DDM), and if required, can subsequently be embedded into an artificial membrane environment in the form of liposomes or nanodiscs [89]. The above-described photophysical and spectral properties of PR have been investigated both in detergent micelles, as well as in a more native-like liposome environment.

The quarternary structure of membrane proteins has an important impact on their function. Cryo-electron and atomic force microscopy have shown that PR exists predominantly in a pentameric or hexameric assembly, both in lipid bilayers and in DDM micelles, which is likely to represent its native oligomeric state [90, 91]. This is in contrast to bR, which is embedded in the purple membrane as a hexagonal lattice composed of trimeric units. Trimers of GR have also been reported, due to an involvement of the His-Asp cluster [92]. Till date, no crystal structure of PR has been reported. However, solid and liquid-state NMR have been used to investigate the structure of PR in liposomes and detergent micelles respectively [93, 94], though these NMR structures deviate from the crystal structure of BPR [95]. Therefore, one can conclude that reliable structural information for these proteins in a native-like membrane environment is still lacking, and a more detailed characterization under such conditions is imperative.

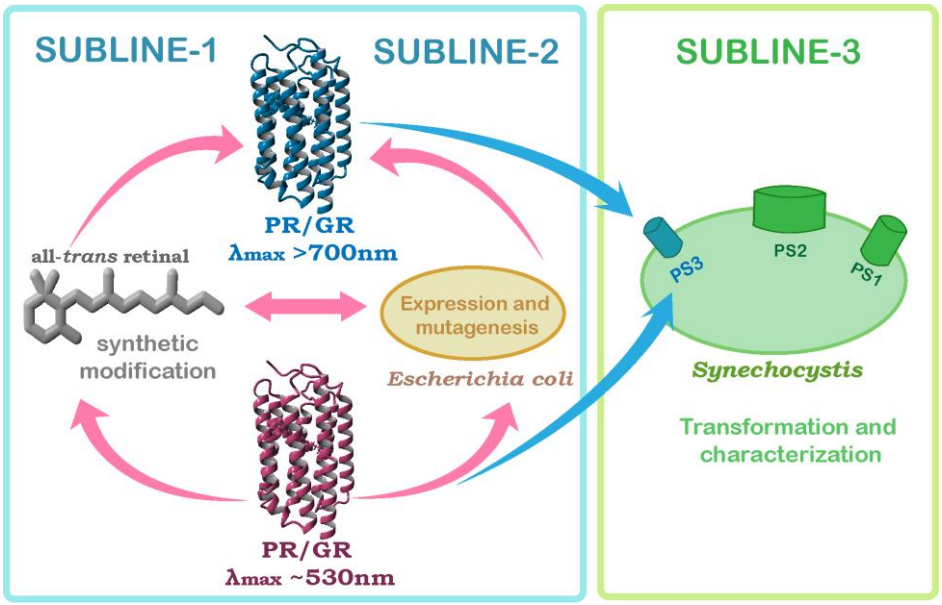

Figure 1.8 An overview of the research goals of this project. Sublines-1 and 2 refer to the spectral modulation of WT PR and GR, by modification of the retinal chromophore and the opsin, to generate a NIR active proton pump with a λ_{max} >700nm. Both the WT and NIR active proto-pumps (PS3) are incorporated into the cyanobacterium *Synechocystis*, to assess their contribution towards phototrophic growth of the organism.

1.8 Research goals

The major goal of this research is to generate and characterize a NIR active rhodopsin proton pump, towards the ultimate intention of complementing natural photosynthesis. Figure 1.8 shows a broad overview of this project, which can be defined by the following sublines. Sublines-1 and 2 refer to the engineering of NIR active PR and GR, and the characterization of their spectral properties and proton-pump activity using *E. coli* as a model organism. **Subline-1** involves the use of synthetically engineered analogs of all-*trans* retinal to regenerate the wild type (WT) proteo-opsins. In **subline-2**, site-directed mutagenesis and/or directed evolution are used to generate red-shifted opsin mutants. The mutants are first tested with the native

ligand to characterize their properties, and then further combined with suitable retinal analogs obtained from subline-1.

From this combinatorial strategy, we aim to generate an active variant of PR/GR displaying an absorbance maximum >700 nm. This NIR active proton-pump, nicknamed photosystem-3 (PS3) will be incorporated in the cyanobacterium *Synechocystis* sp. PCC6803 in **subline-3**. This subline is undertaken by our collaborators in the University of Amsterdam, towards the aim of utilizing PS3 as a complement to photosystems-1 and 2 (PS1, PS2). For this subline, a suitable expression system for the proteorhodopsins in *Synechocystis* had to be generated, which was optimized using WT PR and GR. The ultimate goal is to express PS3 in *Synechocystis,* and assess its contribution towards phototrophic growth of the organism, using complementary or sole illumination >700nm.

1.9 Scope of this thesis

The central aim of this thesis project is to investigate the spectral modulation and characterization of PR and GR in various micro-environments. In **Chapter 2**, we tested retinal analogs containing specific ring modifications, and were able to generate active red and blue shifted variants of PR and GR. The red-shifted A2 analog studied in this chapter was further modified in **Chapter 3,** by elongating the conjugation on the retinal β-ionone ring. One promising retinal analog, in combination with a specific PR mutant, generated a novel near-infrared absorbing proton-pump. In **chapter 4**, we describe the construction of a novel concept for a directed evolution assay, which enables us to perform random mutagenesis as well as select for active red-shifted variants of PR and GR simultaneously *in vivo*. In **Chapter 5**, we investigate the influence of the membrane or detergent microenvironment on the stability and spectral properties of PR/GR and some of their red-shifted variants. The biotechnological

potential and future scope of the novel proteorhodopsin variants generated in this project is discussed in **Chapter 6**.

References

[1] Bryant, D. A. and Frigaard, N. U. "Prokaryotic photosynthesis and phototrophy illuminated", *Trends Microbiol*, 2006. **14**(11): p. 488-96.

[2] Walter, J. M., Greenfield, D. and Liphardt, J. "Potential of light-harvesting proton pumps for bioenergy applications", *Curr Opin Biotechnol*, 2010. **21**(3): p. 265-70.

[3] Govorunova, E. G., Sineshchekov, O. A., Li, H. and Spudich, J. L. "Microbial rhodopsins: diversity, mechanisms, and optogenetic applications", *Annu Rev Biochem*, 2017.

[4] DeLong, E. F. and Beja, O. "The light-driven proton pump proteorhodopsin enhances bacterial survival during tough times", *PLoS Biol*, 2010. **8**(4): p. e1000359.

[5] Spudich, J. L. and Jung, K.-H. "Microbial Rhodopsins: Phylogenetic and Functional Diversity", *Handbook of Photosensory Receptors*, 2005: p. 1--23.

[6] Oesterhelt, D. and Stoeckenius, W. "Rhodopsin-like protein from the purple membrane of *Halobacterium halobium*", *Nat New Biol*, 1971. **233**(39): p. 149-52.

[7] Schobert, B. and Lanyi, J. K. "Halorhodopsin is a light-driven chloride pump", *J Biol Chem*, 1982. **257**(17): p. 10306-10313.

[8] Spudich, J. L. and Bogomolni, R. A. "Mechanism of colour discrimination by a bacterial sensory rhodopsin", *Nature*, 1984. **312**(5994): p. 509-513.

[9] Ernst, O. P., Lodowski, D. T., Elstner, M., Hegemann, P., Brown, L. S. and Kandori, H. "Microbial and animal rhodopsins: structures, functions, and molecular mechanisms", *Chem Rev*, 2014. **114**(1): p. 126-63.

[10] Béjà, O., Aravind, L., Koonin, E. V., Suzuki, M. T., Hadd, A., Nguyen, L. P., Jovanovich, S. B., Gates, C. M., Feldman, R. A., Spudich, J. L., Spudich, E. N. and DeLong, E. F. "Bacterial rhodopsin: Evidence for a new type of phototrophy in the sea", *Science*, 2000. **289**(5486): p. 1902-1906.

[11] Jung, K.-H., Trivedi, V. D. and Spudich, J. L. "Demonstration of a sensory rhodopsin in eubacteria", *Mol Microbiol*, 2003. **47**(6): p. 1513-1522.

[12] Bieszke, J. A., Braun, E. L., Bean, L. E., Kang, S., Natvig, D. O. and Borkovich, K. A. "The nop-1 gene of Neurospora crassa encodes a seven transmembrane helix retinal-binding protein homologous to archaeal rhodopsins", *Proc Natl Acad Sci U S A*, 1999. **96**(14): p. 8034-8039.

[13] Nagel, G., Ollig, D., Fuhrmann, M., Kateriya, S., Musti, A. M., Bamberg, E. and Hegemann, P. "Channelrhodopsin-1: A light-gated proton channel in green algae", *Science*, 2002. **296**(5577): p. 2395.

[14] Frigaard, N.-U., Martinez, A., Mincer, T. J. and DeLong, E. F. "Proteorhodopsin lateral gene transfer between marine planktonic Bacteria and Archaea", *Nature*, 2006. **439**(7078): p. 847-850.

[15] Bamann, C., Bamberg, E., Wachtveitl, J. and Glaubitz, C. "Proteorhodopsin", *Biochim Biophys Acta*, 2014. **1837**(5): p. 614-25.

[16] Man-Aharonovich, D., Sabehi, G., Sineshchekov, O. A., Spudich, E. N., Spudich, J. L. and Béjà, O. "Characterization of RS29, a blue-green proteorhodopsin variant from the Red Sea ", *Photochem Photobiol Sci*, 2004. **3**(5): p. 459-62.

[17] Nguyen, D., Maranger, R., Balague, V., Coll-Lladó, M., Lovejoy, C. and Pedrós-Alió, C. "Winter diversity and expression of proteorhodopsin genes in a polar ocean ", *ISME J*, 2015. **9**(8): p. 1835-45.

[18] McCarren, J. and DeLong, E. F. "Proteorhodopsin photosystem gene clusters exhibit co-evolutionary trends and shared ancestry among diverse marine microbial phyla ", *Environ Microbiol*, 2007. **9**(4): p. 846-58.

[19] Slamovits, C. H., Okamoto, N., Burri, L., James, E. R. and Keeling, P. J. "A bacterial proteorhodopsin proton pump in marine eukaryotes ", *Nat Commun*, 2011. **2**: p. 183.

[20] Finkel, O. M., Beja, O. and Belkin, S. "Global abundance of microbial rhodopsins ", *ISME J*, 2013. **7**(2): p. 448-451.

[21] Yutin, N. and Koonin, E. V. "Proteorhodopsin genes in giant viruses ", *Biol Direct*, 2012. **7**: p. 34.

[22] Sabehi, G., Massana, R., Bielawski, J. P., Rosenberg, M., Delong, E. F. and Beja, O. "Novel proteorhodopsin variants from the Mediterranean and Red Seas ", *Environ Microbiol*, 2003. **5**(10): p. 842-9.

[23] de la Torre, J. R., Christianson, L. M., Beja, O., Suzuki, M. T., Karl, D. M., Heidelberg, J. and DeLong, E. F. "Proteorhodopsin genes are distributed among divergent marine bacterial taxa ", *Proc Natl Acad Sci U S A*, 2003. **100**(22): p. 12830-5.

[24] Sharma, A. K., Zhaxybayeva, O., Papke, R. T. and Doolittle, W. F. "Actinorhodopsins: proteorhodopsin-like gene sequences found predominantly in non-marine environments ", *Environ Microbiol*, 2008. **10**(4): p. 1039--1056.

[25] Atamna-Ismaeel, N., Sabehi, G., Sharon, I., Witzel, K.-P., Labrenz, M., Jurgens, K., Barkay, T., Stomp, M., Huisman, J. and Beja, O. "Widespread distribution of proteorhodopsins in freshwater and brackish ecosystems ", *ISME J*, 2008. **2**(6): p. 656-662.

[26] Koh, E. Y., Atamna-Ismaeel, N., Martin, A., Cowie, R. O., Beja, O., Davy, S. K., Maas, E. W. and Ryan, K. G. "Proteorhodopsin-bearing bacteria in Antarctic sea ice ", *Appl Environ Microbiol*, 2010. **76**(17): p. 5918-25.

[27] Petrovskaya, L. E., Lukashev, E. P., Chupin, V. V., Sychev, S. V., Lyukmanova, E. N., Kryukova, E. A., Ziganshin, R. H., Spirina, E. V., Rivkina, E. M., Khatypov, R. A., Erokhina, L. G., Gilichinsky, D. A., Shuvalov, V. A. and Kirpichnikov, M. P. "Predicted bacteriorhodopsin from *Exiguobacterium sibiricum* is a functional proton pump ", *FEBS Letters*, 2010. **584**(19): p. 4193-4196.

[28] Bohorquez, L. C., Ruiz-Perez, C. A. and Zambrano, M. M. "Proteorhodopsin-like genes present in thermoacidophilic high-mountain microbial communities ", *Appl Environ Microbiol*, 2012. **78**(21): p. 7813-7.

[29] Atamna-Ismaeel, N., Finkel, O. M., Glaser, F., Sharon, I., Schneider, R., Post, A. F., Spudich, J. L., von Mering, C., Vorholt, J. A., Iluz, D., Béjà, O. and Belkin, S. "Microbial rhodopsins on leaf surfaces of terrestrial plants ", *Environ microbiol*, 2012. **14**(1): p. 140-146.

[30] Man, D., Wang, W., Sabehi, G., Aravind, L., Post, A. F., Massana, R., Spudich, E. N., Spudich, J. L. and Beja, O. "Diversification and spectral tuning in marine proteorhodopsins ", *EMBO J*, 2003. **22**(8): p. 1725-31.

[31] Yoshizawa, S., Kawanabe, A., Ito, H., Kandori, H. and Kogure, K. "Diversity and functional analysis of proteorhodopsin in marine Flavobacteria ", *Environ Microbiol*, 2012. **14**(5): p. 1240-8.

[32] Gómez-Consarnau, L., González, J. M., Coll-Lladó, M., Gourdon, P., Pascher, T., Neutze, R., Pedrós-Alió, C. and Pinhassi, J. "Light stimulates growth of proteorhodopsin-containing marine Flavobacteria ", *Nature*, 2007. **445**(7124): p. 210-213.

[33] Gómez-Consarnau, L., Akram, N., Lindell, K., Pedersen, A., Neutze, R., Milton, D. L., González, J. M. and Pinhassi, J. "Proteorhodopsin phototrophy promotes survival of marine bacteria during starvation ", *PLoS Biol*, 2010. **8**(4): p. e1000358.

[34] Karnik, S., Doi, T., Molday, R. and Khorana, H. G. "Expression of the archaebacterial bacterio-opsin gene with and without signal sequences in *Escherichia coli*: the expressed proteins are located in the membrane but bind retinal poorly ", *Proc Natl Acad Sci U S A*, 1990. **87**(22): p. 8955-9.

[35] Walter, J. M., Greenfield, D., Bustamante, C. and Liphardt, J. "Light-powering *Escherichia coli* with proteorhodopsin ", *Proc Natl Acad Sci U S A*, 2007. **104**(7): p. 2408-12.

[36] Martinez, A., Bradley, A. S., Waldbauer, J. R., Summons, R. E. and DeLong, E. F. "Proteorhodopsin photosystem gene expression enables photophosphorylation in a heterologous host ", *Proc Natl Acad Sci U S A*, 2007. **104**(13): p. 5590-5.

[37] Wang, Y., Li, Y., Xu, T., Shi, Z. and Wu, Q. "Experimental evidence for growth advantage and metabolic shift stimulated by photophosphorylation of proteorhodopsin expressed in *Escherichia coli* at anaerobic condition ", *Biotechnol Bioeng*, 2015. **112**(5): p. 947-56.

[38] Kim, J. Y., Jo, B. H., Jo, Y. and Cha, H. J. "Improved production of biohydrogen in light-powered *Escherichia coli* by co-expression of proteorhodopsin and heterologous hydrogenase ", *Microb Cell Fact*, 2012. **11**: p. 2.

[39] Nakamura, Y., et al. "Complete genome structure of Gloeobacter violaceus PCC7421, a cyanobacterium that lacks thylakoids ", *DNA Res*, 2003. **10**: p. 137-145.

[40] Choi, A. R., Shi, L., Brown, L. S. and Jung, K. H. "Cyanobacterial light-driven proton pump, gloeobacter rhodopsin: complementarity between rhodopsin-based energy production and photosynthesis ", *PLoS One*, 2014. **9**(10): p. e110643.

[41] Miranda, M. R., Choi, A. R., Shi, L., Bezerra, A. G., Jr., Jung, K. H. and Brown, L. S. "The photocycle and proton translocation pathway in a cyanobacterial ion-pumping rhodopsin ", *Biophys J*, 2009. **96**(4): p. 1471-81.

[42] Imasheva, E. S., Balashov, S. P., Choi, A. R., Jung, K. H. and Lanyi, J. K. "Reconstitution of Gloeobacter violaceus rhodopsin with a light-harvesting carotenoid antenna ", *Biochemistry*, 2009. **48**(46): p. 10948-55.

[43] Lee, K. A. and Jung, K.-H. "ATP Regeneration System Using *E. coli* ATP Synthase and *Gloeobacter* Rhodopsin and Its Stability ", *J Nanosci Nanotechnol*, 2011. **11**(5): p. 4261-4264.

[44] Balashov, S. P. and Lanyi, J. K. "Xanthorhodopsin: Proton pump with a carotenoid antenna ", *Cell Mol Life Sci*, 2007. **64**(18): p. 2323-8.

[45] Luecke, H., Schobert, B., Stagno, J., Imasheva, E. S., Wang, J. M., Balashov, S. P. and Lanyi, J. K. "Crystallographic structure of xanthorhodopsin, the light-driven proton pump with a dual chromophore ", *Proc Natl Acad Sci U S A*, 2008. **105**(43): p. 16561-5.

[46] Balashov, S. P., Imasheva, E. S., Choi, A. R., Jung, K. H., Liaaen-Jensen, S. and Lanyi, J. K. "Reconstitution of gloeobacter rhodopsin with echinenone: role of the 4-keto group ", *Biochemistry*, 2010. **49**(45): p. 9792-9.

[47] Iyer, E. S., Gdor, I., Eliash, T., Sheves, M. and Ruhman, S. "Efficient femtosecond energy transfer from carotenoid to retinal in gloeobacter rhodopsin-salinixanthin complex ", *J Phys Chem B*, 2015. **119**(6): p. 2345-9.

[48] Chiang, H.-K. and Chu, L.-K. "Wavelength-dependent photocycle activity of xanthorhodopsin in the visible region ", *Biochem Biophys Rep*, 2016. **7**: p. 347-352.

[49] Vogt, A., Wietek, J. and Hegemann, P. "Gloeobacter rhodopsin, limitation of proton pumping at high electrochemical load ", *Biophys J*, 2013. **105**(9): p. 2055-63.

[50] Imasheva, E. S., Shimono, K., Balashov, S. P., Wang, J. M., Zadok, U., Sheves, M., Kamo, N. and Lanyi, J. K. "Formation of a long-lived photoproduct with a deprotonated Schiff base in proteorhodopsin, and its enhancement by mutation of Asp227 ", *Biochemistry*, 2005. **44**(32): p. 10828-38.

[51] Pfleger, N., Lorch, M., Woerner, A. C., Shastri, S. and Glaubitz, C. "Characterisation of Schiff base and chromophore in green proteorhodopsin by solid-state NMR ", *J Biomol NMR*, 2008. **40**(1): p. 15-21.

[52] Harbison, G. S., Smith, S. O., Pardoen, J. A., Winkel, C., Lugtenburg, J., Herzfeld, J., Mathies, R. and Griffin, R. G. "Dark-adapted bacteriorhodopsin contains 13-cis, 15-syn and all-*trans*, 15-*anti* retinal Schiff bases ", *Proc Natl Acad Sci U S A*, 1984. **81**(6): p. 1706-9.

[53] Kandori, H. "Ion-pumping microbial rhodopsins ", *Front Mol Biosci*, 2015. **2**: p. 52.

[54] Rupenyan, A., van Stokkum, I. H., Arents, J. C., van Grondelle, R., Hellingwerf, K. J. and Groot, M. L. "Reaction pathways of photoexcited retinal in proteorhodopsin studied by pump-dump-probe spectroscopy ", *J Phys Chem B*, 2009. **113**(50): p. 16251-6.

[55] Rupenyan, A., van Stokkum, I. H., Arents, J. C., van Grondelle, R., Hellingwerf, K. and Groot, M. L. "Characterization of the primary photochemistry of proteorhodopsin with femtosecond spectroscopy ", *Biophys J*, 2008. **94**(10): p. 4020-30.

[56] Friedrich, T., Geibel, S., Kalmbach, R., Chizhov, I., Ataka, K., Heberle, J., Engelhard, M. and Bamberg, E. "Proteorhodopsin is a light-driven proton pump with variable vectoriality ", *J Mol Biol*, 2002. **321**(5): p. 821-38.

[57] Varo, G., Brown, L. S., Lakatos, M. and Lanyi, J. K. "Characterization of the photochemical reaction cycle of proteorhodopsin ", *Biophys J*, 2003. **84**(2 Pt 1): p. 1202-7.

[58] Dioumaev, A. K., Brown, L. S., Shih, J., Spudich, E. N., Spudich, J. L. and Lanyi, J. K. "Proton transfers in the photochemical reaction cycle of proteorhodopsin ", *Biochemistry*, 2002. **41**: p. 5348-5358.

[59] Garczarek, F. and Gerwert, K. "Functional waters in intraprotein proton transfer monitored by FTIR difference spectroscopy ", *Nature*, 2006. **439**(7072): p. 109-112.

[60] Balashov, S. P., Imasheva, E. S., Ebrey, T. G., Chen, N., Menick, D. R. and Crouch, R. K. "Glutamate-194 to cysteine mutation inhibits fast light-induced proton release in bacteriorhodopsin ", *Biochemistry*, 1997. **36**(29): p. 8671-6.

[61] Gerwert, K., Freier, E. and Wolf, S. "The role of protein-bound water molecules in microbial rhodopsins ", *Biochim Biophys Acta*, 2014. **1837**(5): p. 606-13.

[62] Mehler, M., Scholz, F., Ullrich, S. J., Mao, J., Braun, M., Brown, L. J., Brown, R. C., Fiedler, S. A., Becker-Baldus, J., Wachtveitl, J. and Glaubitz, C. "The EF loop in green proteorhodopsin affects conformation and photocycle dynamics ", *Biophys J*, 2013. **105**(2): p. 385-97.

[63] Lorinczi, E., Verhoefen, M. K., Wachtveitl, J., Woerner, A. C., Glaubitz, C., Engelhard, M., Bamberg, E. and Friedrich, T. "Voltage- and pH-dependent changes in vectoriality of photocurrents mediated by wild-type and mutant proteorhodopsins upon expression in Xenopus oocytes", *J Mol Biol*, 2009. **393**(2): p. 320-41.

[64] Lakatos, M., Lanyi, J. K., Szakács, J. and Váró, G. "The photochemical reaction cycle of Proteorhodopsin at low pH", *Biophys J*, 2003. **84**(5): p. 3252-3256.

[65] Dioumaev, A. K., Wang, J. M., Balint, Z., Varo, G. and Lanyi, J. K. "Proton transport by proteorhodopsin requires that the retinal Schiff base counterion Asp-97 be anionic", *Biochemistry*, 2003. **42**(21): p. 6582-7.

[66] Mowery, P. C., Lozier, R. H., Chae, Q., Tseng, Y.-W., Taylor, M. and Stoeckenius, W. "Effect of acid pH on the absorption spectra and photoreactions of bacteriorhodopsin", *Biochemistry*, 1979. **18**(19): p. 4100-4107.

[67] Hempelmann, F., Hölper, S., Verhoefen, M.-K., Woerner, A. C., Köhler, T., Fiedler, S.-A., Pfleger, N., Wachtveitl, J. and Glaubitz, C. "His75−Asp97 cluster in green Proteorhodopsin", *J Am Chem Soc*, 2011. **133**(12): p. 4645-4654.

[68] Ikeda, D., Furutani, Y. and Kandori, H. "FTIR study of the retinal Schiff base and internal water molecules of proteorhodopsin", *Biochemistry*, 2007. **46**(18): p. 5365-73.

[69] Partha, R., Krebs, R., Caterino, T. L. and Braiman, M. S. "Weakened coupling of conserved arginine to the proteorhodopsin chromophore and its counterion implies structural differences from bacteriorhodopsin", *Biochim Biophys Acta Bioenerg*, 2005. **1708**(1): p. 6-12.

[70] Irving, C. S. and Leermakers, P. A. "Spectroscopic behavior of all-trans retinal and its Schiff bases in various media. The role of conformational perturbation", *Photochem Photobiol*, 1968. **7**(6): p. 665--670.

[71] Blatz, P. E., Mohler, J. H. and Navangul, H. V. "Anion-induced wavelength regulation of absorption maxima of Schiff bases of retinal", *Biochemistry*, 1972. **11**(5): p. 848-855.

[72] Engqvist, M. K., McIsaac, R. S., Dollinger, P., Flytzanis, N. C., Abrams, M., Schor, S. and Arnold, F. H. "Directed evolution of *Gloeobacter violaceus* rhodopsin spectral properties", *J Mol Biol*, 2015. **427**(1): p. 205-20.

[73] Kim, S. Y., Waschuk, S. A., Brown, L. S. and Jung, K. H. "Screening and characterization of proteorhodopsin color-tuning mutations in *Escherichia coli* with endogenous retinal synthesis", *Biochim Biophys Acta*, 2008. **1777**(6): p. 504-13.

[74] Beja, O., Spudich, E. N., Spudich, J. L., Leclerc, M. and DeLong, E. F. "Proteorhodopsin phototrophy in the ocean", *Nature*, 2001. **411**: p. 786-789.

[75] Wang, W. W., Sineshchekov, O. A., Spudich, E. N. and Spudich, J. L. "Spectroscopic and photochemical characterization of a deep ocean proteorhodopsin", *J Biol Chem*, 2003. **278**(36): p. 33985-91.

[76] Sheves, M., Albeck, A., Friedman, N. and Ottolenghi, M. "Controlling the pKa of the bacteriorhodopsin Schiff base by use of artificial retinal analogues", *Proc Natl Acad Sci U S A*, 1986. **83**(10): p. 3262-6.

[77] Baasov, T. and Sheves, M. "Alteration of pKa of the Bacteriorhodopsin protonated Schiff base. A study with model compounds", *Biochemistry*, 1986. **25**: p. 5249-5258.

[78] Gat, Y. and Sheves, M. "A mechanism for controlling the pKa of the retinal protonated Schiff base in retinal proteins. A study with model compounds", *J Am Chem Soc*, 1993. **115**(9): p. 3772-3773.

[79] Claassens, N. J., Sousa, D. Z., dos Santos, V. A. P. M., de Vos, W. M. and van der Oost, J. "Harnessing the power of microbial autotrophy ", *Nat Rev Micro*, 2016. **14**(11): p. 692-706.

[80] Blankenship, R. E., et al. "Comparing photosynthetic and photovoltaic efficiencies and recognizing the potential for improvement ", *Science*, 2011. **332**(6031): p. 805-9.

[81] Knöpfel, T., Lin, M. Z., Levskaya, A., Tian, L., Lin, J. Y. and Boyden, E. S. "Toward the second generation of optogenetic tools ", *J Neurosci*, 2010. **30**(45): p. 14998-5004.

[82] Chen, Q., van der Steen, J. B., Dekker, H. L., Ganapathy, S., de Grip, W. J. and Hellingwerf, K. J. "Expression of holo-proteorhodopsin in Synechocystis sp. PCC 6803 ", *Metab Eng*, 2016. **35**: p. 83-94.

[83] Kushibiki, T., Okawa, S., Hirasawa, T. and Ishihara, M. "Optogenetics: Novel tools for controlling mammalian cell functions with light ", *Int J Photoenergy*, 2014. **2014**: p. 1-10.

[84] Lin, J. Y., Knutsen, P. M., Muller, A., Kleinfeld, D. and Tsien, R. Y. "ReaChR: a red-shifted variant of channelrhodopsin enables deep transcranial optogenetic excitation ", *Nat Neurosci*, 2013. **16**(10): p. 1499-508.

[85] Asato, A. E., Li, X. Y., Mead, D., Patterson, G. M. L. and Liu, R. S. H. "Azulenic retinoids and the corresponding Bacteriorhodopsin analogs - unusually red-shifted pigments ", *J Am Chem Soc*, 1990. **112**(20): p. 7398-7399.

[86] Bell, J. R., Muthyala, R. S., Larsen, R. W., Alam, M. and Liu, R. S. H. "Photoactivities of the red-shifted azulenic Bacteriorhodopsin analogues ", *J Phys Chem A*, 1998. **102**(28): p. 5481-5483.

[87] Maslennikov, I. and Choe, S. "Advances in NMR structures of integral membrane proteins ", *Curr Opin Struct Biol*, 2013. **23**(4): p. 555-62.

[88] Moraes, I., Evans, G., Sanchez-Weatherby, J., Newstead, S. and Stewart, P. D. S. "Membrane protein structure determination — The next generation ", *Biochim Biophys Acta*, 2014. **1838**(1): p. 78-87.

[89] Denisov, I. G. and Sligar, S. G. "Nanodiscs for structural and functional studies of membrane proteins ", *Nat Struct Mol Biol*, 2016. **23**(6): p. 481-6.

[90] Klyszejko, A. L., Shastri, S., Mari, S. A., Grubmuller, H., Muller, D. J. and Glaubitz, C. "Folding and assembly of proteorhodopsin ", *J Mol Biol*, 2008. **376**(1): p. 35-41.

[91] Liang, H., Whited, G., Nguyen, C. and Stucky, G. D. "The directed cooperative assembly of proteorhodopsin into 2D and 3D polarized arrays ", *Proc Natl Acad Sci U S A*, 2007. **104**(20): p. 8212-7.

[92] Tsukamoto, T., Kikukawa, T., Kurata, T., Jung, K. H., Kamo, N. and Demura, M. "Salt bridge in the conserved His-Asp cluster in Gloeobacter rhodopsin contributes to trimer formation ", *FEBS Lett*, 2013. **587**(4): p. 322-7.

[93] Pfleger, N., Worner, A. C., Yang, J., Shastri, S., Hellmich, U. A., Aslimovska, L., Maier, M. S. and Glaubitz, C. "Solid-state NMR and functional studies on proteorhodopsin ", *Biochim Biophys Acta*, 2009. **1787**(6): p. 697-705.

[94] Reckel, S., Gottstein, D., Stehle, J., Lohr, F., Verhoefen, M. K., Takeda, M., Silvers, R., Kainosho, M., Glaubitz, C., Wachtveitl, J., Bernhard, F., Schwalbe, H., Guntert, P. and Dotsch, V. "Solution NMR structure of proteorhodopsin ", *Angew Chem Int Ed Engl*, 2011. **50**(50): p. 11942-6.

[95] Ran, T., Ozorowski, G., Gao, Y., Sineshchekov, O. A., Wang, W., Spudich, J. L. and Luecke, H. "Cross-protomer interaction with the photoactive site in oligomeric proteorhodopsin complexes ", *Acta Crystallogr D Biol Crystallogr*, 2013. **69**(10): p. 1965-80.

Chapter 2

Retinal analogs can modulate the spectral properties and proton pumping of PR and GR

Proteorhodopsins bind all-*trans* retinal A1 as a native ligand to absorb visible light (520-540 nm). Here, we describe the modulation of the absorbance band of Monterey Bay proteorhodopsin (PR), its red-shifted double mutant PR-D212N-F234S and *Gloeobacter* rhodopsin (GR). This was approached using three analogs of all-*trans* retinal A1, which differ in their electronic and conformational properties. We further probed the effect of these retinal analogs on the proton pump activity of the pigments. Our results indicate that, while the constraints of the retinal binding pocket differ for the proteorhodopsins, at least two of the retinal analogs are capable of shifting the absorbance bands of the pigments either bathochromically or hypsochromically, while maintaining their proton pump activity. Furthermore, the shifts implemented by the analogs add up to the shift induced by the double mutation in PR-DNFS. This type of chromophore substitution may present attractive biotechnological applications.

This chapter is published as: S. Ganapathy, O. Bécheau, H. Venselaar, S. Frölich, J. B. van der Steen, Q. Chen, S. Radwan, J. Lugtenburg, K. J. Hellingwerf, H. J. M. de Groot, W. J. de Grip **(2015)** *Biochemical Journal* 467: 333-343

2.1 Introduction

In this chapter, we investigate the effects of three retinal analogs, which differ in their electronic and conformational properties, on the action spectrum of wild type (WT) PR and GR and the red-shifted double mutant PR-D212N-F234S (PR-DNFS) [1]. The three all-*trans* analogs of the native retinal A1 are: retinal A2, Phe-retinal A1 and 6-s-*trans* locked retinal A1 (Figure 2.1). Retinal A2 has the same structural make-up as retinal A1, but contains an elongated π-conjugated polyene chain. This analog has been shown to red-shift the absorbance band of archaeal rhodopsins [2-5] and xanthorhodopsin (XR) [6]. We anticipated that this analog would have a similar effect on the proteorhodopsins. Phe-retinal A1 contains an even more complex conjugated system, but lacks the methyl groups in the ring element. This analog blue-shifts the absorbance band of bR [7, 8] and XR [6, 9]. In 6-s-*trans* locked retinal A1, the C6-C7 bond is locked in an s-*trans* configuration. The use of this analog corroborated evidence that the chromophore in bR and XR contains a 6-s-*trans* configuration [10]. Our results show that retinal analogs can significantly modulate the spectral properties of proteorhodopsins with at least partial preservation of proton pump activity, and that the binding pocket constraints differ for PR and GR. Further, we show that in PR-DNFS, the analog-induced spectral shifts are additive to the mutation-induced shift.

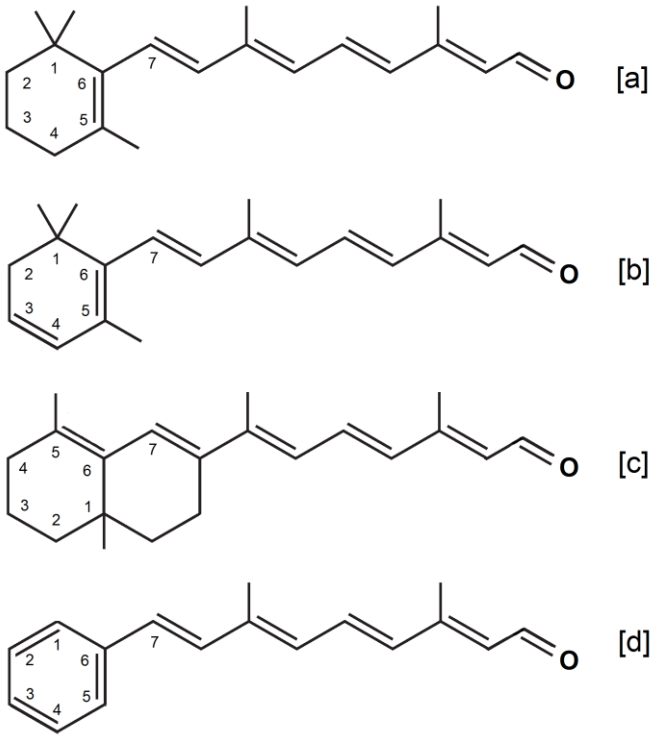

Figure 2.1 Chemical structures of retinal analogs used in this chapter [a] A1 [b] A2 [c] ALL-E [d] PHE. For spectral properties, see the Appendix figure A.2.

2.2 Experimental section

2.2.1 Materials:

E. coli strain UT5600 and the pKJ900 plasmids encoding PR or GR with a C-terminal 6-His tag were a generous gift from Dr. K. Jung, University of Seoul, South Korea [1]. UT5600 was used to express the recombinant proteins. All-*trans* retinal A1 (hereafter called A1) was obtained from Sigma-Aldrich. All-*trans* retinal A2 (A2) and all-E-6-s-*trans* locked retinal A1 (ALL-E) were prepared as described before [10, 11]. All-*trans*-phe-retinal A1 (PHE) was synthetized in analogy to A1 and A2, but starting from benzaldehyde, and the structure was confirmed by ^{1}H NMR [36]. The source of all other chemicals is outlined in the appendix (A.1)

2.2.2 Site-directed mutagenesis:

Site directed mutagenesis was performed on the PR gene using mis-match PCR. In brief, the pKJ900 plasmid containing PR was linearized by restriction with Esp3I and subjected to mis-match PCR using overlapping primers containing the corresponding mutation sites for the D212N and the F234S mutations. 25 cycles of PCR were run at 95°C for 30 s, 55°C for 30 s and 68°C for 60 s. The mutant gene was further amplified using outside vector primers with the same PCR program. The sequences of the primers are listed in the appendix (A.4). The amplified mutant gene and vector were restricted at HindIII and XbaI sites and run on an agarose gel. The bands corresponding to the restricted mutant gene and the empty vector were cut out, extracted using a Qiagen gel extraction kit and ligated overnight at 4°C. The ligated plasmid was then transformed into *E. coli* UT5600 made chemically competent using calcium chloride.

2.2.3 Bacterial cell culturing:

The cells were grown in LB medium with 50 μg/mL ampicillin at 30°C in an orbital shaker at 180 rpm. Overnight cultures were grown from frozen glycerol stocks of transformed cells, which were diluted 1:100 to get the working culture. At a cell density corresponding to an OD_{600} of 0.3-0.4, expression of the opsin was induced by the addition of isopropyl β-D-1-thiogalactopyranoside (IPTG) to a final concentration of 1 mM. The cells were allowed to grow further for 24 h at 30°C and then harvested.

2.2.4 Regeneration of proteo-opsin with retinal:

Retinals were stored at -80°C in hexane stock solutions, with the exception of PHE which was stored in methanol. The absorbance spectra and λ_{max} of the retinal analogs are presented in the appendix (A.2). The molar absorbance of A1 and A2 were taken as 49000 and 44000 $M^{-1}cm^{-1}$ respectively [12, 13]. The molar absorbance of ALL-E and PHE were

assumed to be similar to that of A1. At the time of use, the required aliquot of stock solution was evaporated and the residue re-dissolved in dimethylformamide (DMF) to obtain a concentration of 1 mM. This solution was then added to a crude cellular lysate or to isolated membrane vesicles containing the opsin to achieve a final retinal concentration of 5-10 µM, and incubated under dim light for up to 60 min at room temperature (RT) or, if necessary, overnight at 4°C.

2.2.5 Preparation and analysis of membrane vesicles:

The cells were harvested by centrifugation (3200xg, 20 min, RT), and the pellet was resuspended in an ice-cold solution of 50 mM Tris-HCl, 150 mM NaCl, pH 7 (10 mL per 50 mL of culture). The suspended cells were lysed by sonication at 4°C using a Sonics vibra-cell sonicator (10 min, 4 s pulses, 5 s pauses, 25% amplitude) and centrifuged to remove insoluble material and cellular debris (4000xg, 15 min, 4°C). The resulting supernatant with membrane vesicles was incubated with the selected retinal for one hour at RT and the vesicles were then pelleted by high-speed centrifugation (147,000xg, 1 h, 4°C). The pellet was resuspended in 150 mM NaCl (2 mL per 50 ml culture). For solubilisation of membrane proteins, DDM was added to a final concentration of 2% (w/v), and the suspension was incubated with shaking for an hour at 4°C, followed by overnight incubation at 4°C. The insoluble material was removed by centrifugation (16,000xg, 20 min, 4°C). The supernatant was used for spectral analysis.

2.2.6 Proteorhodopsin purification:

The cell pellet was resuspended in ice cold lysis buffer (5 ml/100 ml culture volume) containing 20 mM Tris, 50 mM NaCl, 20 mM imidazole, 0.1% DDM, pH 7, supplemented with an EDTA-free protease inhibitor tablet, benzonase (4 units/100 mL culture) and lysozyme (4 mg/100 mL culture). The suspension was sonicated at 4°C and centrifuged to remove cellular debris as described in the previous section. At this stage, the crude

mixture was incubated with the selected retinal for one hour at RT. DDM was then added to a final concentration of 1.5% (w/v) and the sample was kept rotating overnight at 4°C. The insoluble material was removed by centrifugation (4,000xg, 25 min, 4°C) and the resulting supernatant was utilized as a crude extract. For purification of the His-tagged proteorhodopsins, immobilized-metal affinity chromatography (IMAC) was exploited using 0.4 mL Ni^{2+}-NTA resin per 100 mL original culture volume. The resin was contained in a spin column and first equilibrated with buffer A (20 mM bis-tris propane, 0.5 M NaCl, 0.1% DDM, pH 8) containing 20 mM imidazole. The crude extract was then allowed to equilibrate with the column for 15 min at RT. The column was washed 5 times with 5 column volumes of buffer A containing 50 mM imidazole at RT. Finally, strongly bound protein was eluted using buffer A containing 250 mM imidazole and 0.01% DDM at RT. Fractions of 0.3 mL were collected. Fractions containing the purified proteorhodopsin were combined and analyzed by spectroscopy and SDS-PAGE. Thus purified proteorhodopsin could be stored at 4°C for several weeks, but was kept at -80 °C for long-term storage.

2.2.7 Spectroscopy:

The spectral properties of all samples were measured using a Shimadzu UV-Vis spectrophotometer (UV-1601). The pH-dependence of the main absorbance band of the proteorhodopsins was assessed in solubilised membrane vesicles at different pH values by diluting the samples 1:1 with buffers containing either 100 mM bis-tris-propane at pH 6.5 or 9.5, or 20 mM MES at pH 5. To isolate the major absorbance band of the proteorhodopsin out of the composite spectrum of membrane vesicles, hydroxylamine was added from a 1 M stock solution, pH 7, to a final concentration of 50 mM, followed by incubation at RT under ambient light. Hydroxylamine attacks the Schiff base and releases the retinal from the opsin binding pocket as retinaloxime. A difference spectrum then reveals

the major absorbance band of the proteorhodopsin present. Absorbance maxima were determined using the internal peak-pick function of the software UVProbe.

2.2.8 SDS-PAGE:

The crude and purified protein fractions were analysed by SDS-PAGE. In brief, aliquots of the samples were diluted with SDS sample buffer, incubated for 30 min at 37°C, and run on a 12.5% polyacrylamide gel at 20 mA for 2 h. The gel was stained using Coomassie brilliant-blue G for 2 hours according to the manufacturer's instructions and destained overnight using MilliQ. Gel images were obtained using the Bio-Rad GS-800 gel imaging dock.

2.2.9 Starvation of cells:

Overnight cultures were diluted 1:100 times to get a working culture of 25 ml. At a cell density corresponding to an OD_{600} of 0.3-0.4, production of the proteorhodopsin was induced by the addition of IPTG to a final concentration of 1 mM and of the selected retinal to a final concentration of 5 µM. The cultures were allowed to grow for a further 24 h at 30°C in the dark, and then harvested. The cells were washed twice in starvation buffer (SB) containing 250 mM KCl, 10 mM NaCl, 10 mM $MgSO_4$, 100 µM $CaCl_2$, 10 mM Tris-HCl pH 7 and were starved by incubation with continuous mixing for 4 days at RT. The cells were washed another 3 times and resuspended in 5 ml SB supplemented with 40 µM final concentration of valinomycin. The cell suspension was incubated for 30 min in the dark at RT.

2.2.10 Proton pumping assay:

The cell suspension was illuminated through a bandpass filter in the range of 300-800 nm (BG-18, Schott) using a halogen light source with fibre optics (Euromex, LE.5211). A photon flux of 40 $\mu mol.m^{-2}.s^{-1}$ was used

throughout. Light-induced pH changes were measured with a pH microelectrode (SenTix MIC, WTW) and the readout was monitored by a pH meter (Inolab pH 7310, WTW) fed into a computer. The following light regime was used: 1 min dark, 1 min light, 2 min dark, 1 min light, 2 min dark. Pumping rates were calculated for 5 mL of the cell suspension using two independent trials. Finally, CCCP was added to a final concentration of 40 µM and the suspension was incubated at RT for half an hour in the dark. Light induced pH changes were then measured again using the same light regime. This system was calibrated using 0.1 M oxalic acid and 0.1 M HCl. Pumping rates were calculated as protons/sec from the initial rate of the light-induced pH change, if required corrected for baseline drift in controls (starved cells without expression of proteo-opsin or without retinal). Molecular pumping rates could subsequently be calculated after assay of the proteorhodopsin level (see below).

2.2.11 Determination of proteorhodopsin levels:

The above cell suspension from the proton pumping assay was rinsed with starvation buffer (2.2.9) and the pellet was resuspended in 10 ml buffer B (10mM Tris-Cl, 150 mm NaCl, pH 7). The cell suspension was sonicated as mentioned above and the membrane vesicles and cell debris were pelleted together (147,000xg, 4°C, 1 h). The pellet was resuspended in 1.5 ml of 150 mM NaCl. DDM was added to a final concentration of 2.5% and incubated at RT with mixing overnight. Under these conditions, maximal extraction of proteorhodopsin was achieved without significant losses. The following day, the insoluble material was removed by centrifugation (16,000xg, 4°C, 20 min). The supernatant was used to measure an absorbance spectrum before and after bleaching with hydroxylamine as described above. The optical density value at the absorbance maximum was used to calculate the original proteorhodopsin level in the cell suspension using a molar absorbance of 45000 $M^{-1}cm^{-1}$[14].

2.2.12 Construction of homology models:

A homology model for PR was built using the structure of sensory rhodopsin II (SRII) as a template (PDB 1H2S) [15], with which it has the highest sequence identity out of the retinal proteins for which structural information was available at that time (24% sequence identity). For GR, we built a model using the structure of XR as a template (PDB 3DDL, 56% sequence identity) [16]. Model building and subsequent analysis was performed using the WHAT IF (PMID:2268628) & YASARA (PMID:11948792) Twinset with standard parameters.

2.3 Results

2.3.1 Reconstitution of proteorhodopsins with retinal analogs:

Production of proteorhodopsins following induction with IPTG and simultaneous addition of A1 to the UT5600 cells could be easily verified by the red coloration of the pelleted cells or membrane vesicle preparation. However, this requires substantial amounts of retinal (up to 0.5 mg/100 mL culture) and in view of the limited quantities of retinal analogs available, we investigated other options. It turned out that the apoproteins produced *in vivo* would still readily bind A1 after harvesting the cells and preparation of membrane vesicles. We observed that incubation of these vesicles with A1 resulted in at least the same yield of pigment as when A1 was supplied to the cell culture, but required 5-10 fold less retinal. Incorporation of A1 or the analogs could be detected visually from the development of a red or purple color (Figure 2.2) and was subsequently characterized by spectroscopy after solubilization in 2% (w/v) DDM. Since the spectra also have contributions from other membrane components (cytochromes, excess retinal), the specific absorbance band of the proteo-rhodopsin was isolated by incubation with 50 mM hydroxylamine (Figure 2.2). This procedure works well for all proteorhodopsins tested. We

observed that the PRs were much more sensitive to bleaching with hydroxylamine than GR, which may be related to the slower photocycle kinetics of PR [17-19]. The absorbance maxima obtained with A1 at neutral pH for PR, PR-DNFS, and GR lie at 526 nm, 545 nm and 540 nm respectively, and are in good agreement with those reported in the literature [1, 18, 20].

Upon incubation of the three proteo-opsin species with the retinal analogs we observed that all three analogs regenerate the PR opsins with distinct absorbance maxima, while only two of the analogs regenerate the GR opsin (Figure 2.3). A2 and ALL-E were rapidly incorporated within 30-60 min at RT. Incorporation of PHE was much slower, requiring additional overnight incubation at 4°C. Incorporation of A2 induces an appreciable red-shift of about 30 nm relative to A1 in the absorbance band of all species tested. Incorporation of PHE on the other hand causes a significant blue-shift of about 30 nm in PR, while it does not seem to generate a stable pigment with GR. This was further corroborated by the lack of a distinct negative peak after hydroxylamine treatment of GR-opsin vesicles, incubated with PHE (data not shown). ALL-E can be incorporated in all three opsins, and produces only a small red-shift in their absorbance band, relative to A1.

The position of the absorbance band of PR and reported mutants is pH-dependent, probably because of protonation of D97 [14, 21], which induces a red-shift of 25-30 nm. The corresponding pKa values for PR and PR-DNFS are reported to be 7.3 and 8.0, respectively [1]. This strong pH dependence has not yet been observed for GR [18, 22, 23]. We were interested in whether the analog pigments would show a similar behaviour, and recorded the absorbance spectra of the corresponding solubilized membrane vesicles at pH 5, 6.5 and 9.5 (Table 2.1).

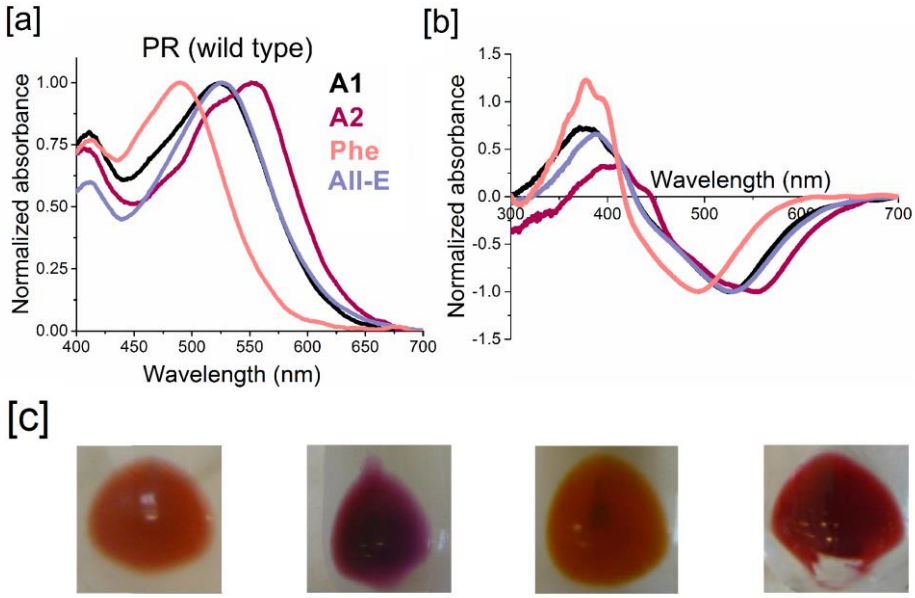

Figure 2.2 [a] Absorbance spectra of solubilized membrane vesicles containing PR reconstituted with the indicated retinals [b]. Difference spectra of the same obtained after incubation of with 50 mM hydroxylamine. Negative bands correspond to the original holoprotein absorbance band. [c] Coloured membrane vesicle pellets of A1, A2, PHE and ALL-E respectively.

All PR-based analog pigments showed a clear pH dependence of their visible absorbance band. The largest red shift upon going from pH 9.5 to 5 of around 25 nm was observed for the ALL-E analog of PR. The magnitude of the shift between pH 9.5 and 5 will also depend on the value of the pKa. On the other hand, we did not observe a significant pH effect in this range on the absorbance profile of GR nor of the GR-based analog pigments.

2.3.2 Purification of the proteorhodopsins:

Following their characterization in membrane vesicles, we aimed for optimal spectral characterization of the native and analog pigments by purification over a Ni^{2+}-NTA resin exploiting their C-terminal 6-His tag.

Species	Retinal analog	λmax (nm)		
		pH 9.5	pH 6.5	pH 5
PR	A1	516	526	531
	A2	551	553	570
	ALL-E	522	525	547
	PHE	478	490	495
PR-DNFS	A1	535	542	553
	A2	560	565	582
	ALL-E	541	547	560
	PHE	492	497	510
GR	A1	537	533	536
	A2	564	569	572
	ALL-E	541	538	546

Table 2.1 λ_{max} values of the pigments at pH 9.5, 6.5 and 5, in solubilised membrane vesicles. Accuracy of the λ_{max} values $\pm$ 5 nm. All PR derived pigments display a strong red-shift upon acidifcation. The pKa of this shift seems to depend on the chromophore, and required further investigation. We did not find a significant effect of the pH in this range on the absorbance band of the GR derived pigments.

According to the ratio A280/A5xx in the absorbance spectra, which varied between 1.5 and 2.5 for all pigments, and the strong band at ~25 kDa for PR (Figure 2.3) and at ~27 kDa for GR (data not shown) observed upon SDS-PAGE analysis, we conclude that a high degree of purification was achieved for all pigments. The purified fractions remained spectrally stable for several weeks at 4°C. Purified PR, PR-DNFS and GR show λ_{max} values of 522 nm, 540 nm and 543 nm with retinal A1 respectively (Figure 2.3), in excellent agreement with literature data and in close agreement with the vesicle data.

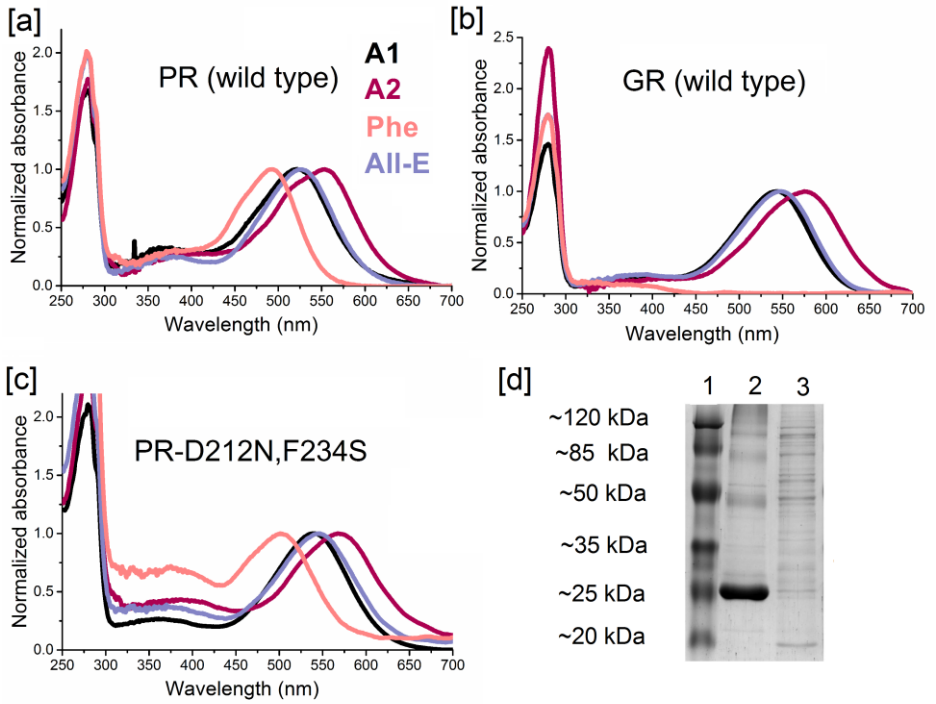

Figure 2.3 Absorbance spectra of purified analog pigments of [a] PR [b] GR and [c] PR-DNFS. No specific peak around 500 nm was obtained for GR with PHE. Spectra are taken at pH 8. Accuracy of the λ_{max} values $\pm$ 2 nm. A1 (black), A2 (magenta), ALL-E (violet) and PHE (pink). [d] Coomassie Blue stained SDS-PAGE gel. The lanes contain (1) protein ladder (2) fraction with purified PR (3) membrane vesicles containing PR. The strong band in lane-2 at ~25 kDa corresponds to the PR monomer.

Incorporation of A2 induces a large red-shift of about 30 nm in the specific absorbance band of all three proteorhodopsins to λ_{max} values of 554 nm, 568 nm and 575 nm for PR, PR-DNFS and GR respectively. In contrast, PHE induces a blue-shift of at least 30 nm in PR and PR-DNFS to 493 nm and 501 nm, respectively. No specific absorbance band was seen for GR purified after incubation with this analog. SDS-PAGE analysis revealed that the opsin was purified successfully, which strengthens our conclusion that the GR opsin is not able to stably bind PHE, or this analog pigment is not stable under our experimental conditions. Incorporation of ALL-E induces a small

red-shift of ~5 nm in all analog pigments to 526 nm, 545 nm and 548 nm for PR, PR-DNFS and GR, respectively. These data are compiled in table 2.2.

2.3.3 Proton pump activity of proteorhodopsins:

While membrane vesicles are economical with respect to ligand usage, we find them less suitable for a quantitative proton-pumping assay. We were not able to isolate vesicle preparations with largely right-side out or inside-out oriented proteorhodopsin. In addition, isolated vesicles can be leaky. Hence, we opted to use intact *E. coli* cells. However, the activity of proteorhodopsins is not easily assayed reproducibly in viable *E. coli* cells. The proton electromotive force is used to drive metabolic processes (e.g. ATP synthesis by ATP synthase) and may trigger the opening of voltage-gated proton channels in the *E. coli* membrane [24]. To avoid such complications, the cells were starved for a few days, with most reproducible results obtained after 4-5 days of starvation. The proton pump activity of the native proteorhodopsins and their analog pigments was measured in starved cell suspensions in the presence of the K^+ ionophore valinomycin and potassium ions, which eliminates the electrical component of the electrochemical proton gradient. This allows quantification of the proton efflux mediated by the proteorhodopsins, without interference from any possible back-pressure effects of the transmembrane electrical potential gradient. For the cells producing proteorhodopsin, this was seen as a decrease in pH upon illumination, which slowly returned to the baseline value in darkness. We did not try to optimize conditions to achieve maximal pumping rates (spectral range, photon intensity, vesicle density). Instead, for mutual comparison, the calculated rates were normalized relative to the most active A1 rhodopsin (GR).

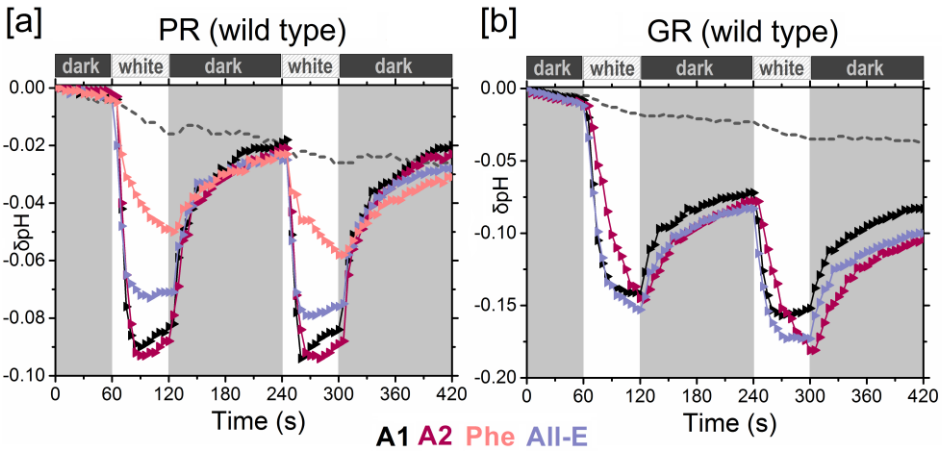

Figure 2.4 Proton pumping traces of starved *E. coli* UT5600 cell suspensions containing PR/GR or one of its analogs. A1 (black), A2 (magenta), ALL-E (violet) and PHE (pink). Dotted black line represents the control opsin without a retinal.

Representative traces for PR and GR and their analog pigments are shown in Figure 2.4, and the normalized pumping rates in Table 2.2. The highest pumping rates obtained with A1 were observed for GR (4-5 protons mol^{-1} s^{-1}), which corroborates findings from previous studies [18, 22, 25]. The lowest pumping activity of was observed for PR-DNFS, which retains 40-60% pumping activity of the wild type. This is consistent with previous data using sphaeroplast suspensions [1]. Interestingly, with A2 or ALL-E, all three proteorhodopsins presented proton pump activity very similar to that with A1, indicating that these analogs hardly perturb the proton translocation mechanism. Also, PHE retains significant proton pump activity for both PR and PR-DNFS. Light induced pH changes were largely prevented by the addition of 40 µM of the protonophorous uncoupler CCCP. In addition, no light induced pH changes were observed for the control situation, where the opsin-expression was not induced but retinal was present (data not shown), or the converse, i.e. when the opsin was expressed but retinal not added (Figure 2.4).

Species	Retinal analog	λmax (nm)	Spectral shift (nm)	Spectral shift (cm^{-1})	Pump rate
PR	A1	522	NA	NA	++
	A2	554	+32	1106	++
	ALL-E	526	+4	146	++
	PHE	493	-29	1127	++
PR-DNFS	A1	540	NA	NA	+
	A2	568	+28	913	+
	ALL-E	545	+5	170	+
	PHE	501	-39	1442	+
GR	A1	543	NA	NA	+++
	A2	575	+32	1025	+++
	ALL-E	548	+5	168	+++

Table 2.2 Proton pumping scores and absorbance maximum values of PR, PR-DNFS, GR and their analogs. GR does not form a stable pigment with PHE. The λ_{max} of the purified proteins were measured at pH 8, with an accuracy of $\pm$ 2 nm (n=3). The spectral shift relative to A1 is given in wavelength (nm) and energy (cm^{-1}). Proton pumping rates were normalized with respect to GR with retinal A1. +++ pumping rate 70-120 % of that of A1-GR ; ++ pumping rate 40-70 % of that of A1-GR; + pumping rate 20-40 % of that of A1-GR

2.3.4 Homology models of PR and GR:

In order to evaluate the effect of retinal analogs and mutations, a 3D structure of PR and GR would be very useful. However, a crystal structure is not available for these retinal proteins and the PR structure solved using NMR spectroscopy [26] significantly deviates even in the transmembrane domain from the crystal structures of other microbial retinal proteins [27, 28] and from earlier PR homology models based on the bR structure [29, 30]. Hence, we decided to generate homology models for GR and PR, based upon the crystal structures of retinal proteins with which they had the highest sequence identity at that time (XR and SRII respectively).

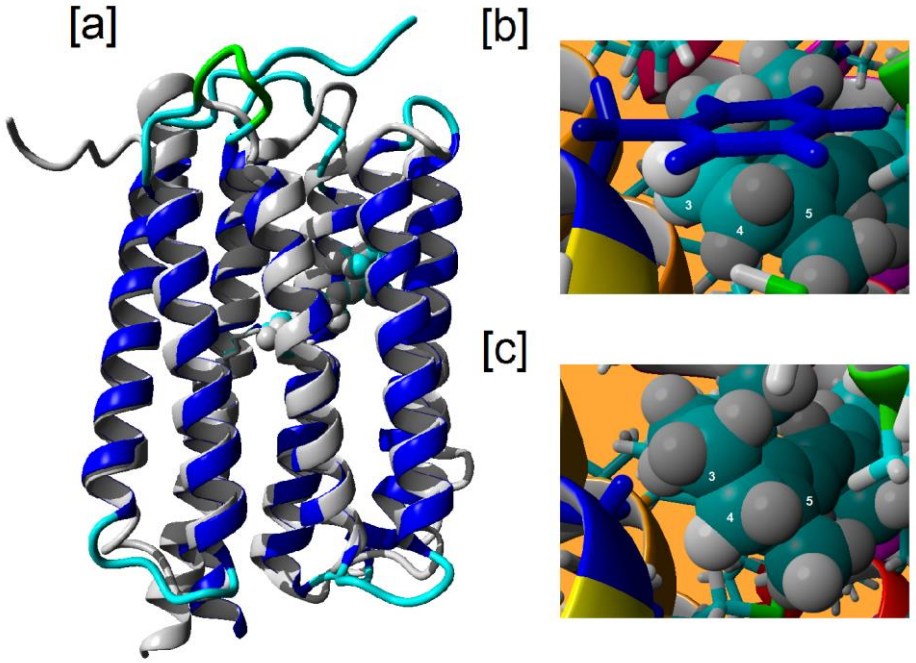

Figure 2.5 Homology models of PR and GR. [a] Overlay of the backbone of the PR homology model (blue) with that of the BPR structure [23] (PDB: 4KNF; grey). Retinal is represented in cyan as a space filled residue. [b] and [c] Enlarged view of the binding pocket in the PR [b] and GR [c] homology models showing the sites Phe152 (PR) and Gly172 (GR) in dark blue. Retinal is represented as in [a] with some ring carbons numbered.

The resulting models for PR and GR show high similarity in the structure of the transmembrane domain and the binding pocket, but, as expected, show variation in the loop regions. Recently, a crystal structure was published for BPR having 83% sequence identity with PR [27]; (PDB 4KNF). A comparison of this structure with our homology model for PR, presented in Figure 2.5, shows excellent conformity in the α-helical domain, and a root-mean-square deviation of only 1.8 Å over all identical residues.

2.4 Discussion

2.4.1 Proteorhodopsin selection

PR, and to a smaller extent GR have been extensively characterized with their native ligand A1. We obtained good expression levels in the *E. coli* strain UT5600 (at least 10 mg/L for PR and 4 mg/L for GR). The produced proteorhodopsins could be purified to a high degree. Furthermore, we obtained good agreement between the λ_{max} values obtained from the absorbance spectra of the purified protein, and the difference spectrum obtained after bleaching the solubilized membrane vesicles with hydroxylamine.

The spectral characteristics of a retinylidene chromophore are strongly affected by its interaction with protein residues lining its binding pocket. However, residues can also exert their effect on the chromophore from a distance, via their involvement in the secondary structure of the protein or their contribution to the local electrostatic field. This is exemplified in the D212N,F234S double mutant of PR, which has been previously described [1]. The authors report that mutation of the binding pocket residue Phe234 to Ser causes a red-shift of the main absorbance band and strongly reduces proton pump activity. According to our homology model, residue Asp212 is located in interhelical loop E-3 and it is not surprising that the single mutation D212N does not change the absorbance or pumping activity of PR (data not shown). However, when these mutations are combined, this yields a red-shifted PR-DNFS that retains significant proton pump activity. We could fully reproduce these characteristics and included this double mutant in our study to test whether spectral shifts induced by a mutation are complementary to those implemented by retinal analogs. With PR-DNFS, expression yields of at least 6 mg/L culture were obtained.

2.4.2 Analog pigments

To our knowledge no detailed study has been reported to date on the effect of retinal analogs on molecular properties of PR or GR. In the context of a wide-angle X-ray scattering study of PR, the 13-desmethyl,13-iodo retinal A1 analog was tested and shown to induce a 23 nm red-shift [30]. In the current study, we focus on ring modifications.

Incorporation of A2 is expected to red-shift the absorbance band relative to A1. This has been demonstrated previously in archaeal and channel rhodopsins (ChR), where red-shifts of about 30 nm are reported, with only a small effect on proton pumping or channel functionality [2-5], as well as in XR with a 23 nm red-shift [9]. As anticipated, this analog rapidly reacted to completeness with all three proteo-opsins and induced comparable red-shifts of about 30 nm corresponding to an energy difference of about 1100 cm^{-1} (Table 2.1). The resulting A2 analog pigments were quite stable in detergent solution and could be purified to a high degree. The A2 analog pigments also present a slightly broadened absorbance band with a small shoulder at the hypsochromic wing of the spectrum (at about 510 nm for PR and about 530 nm for the other two analog pigments). Such a shoulder was previously observed in the A2 analogs of bR [26], ChR and AR3 [29]. Most likely, this shoulder represents fine structure of vibronic origin, possibly due to a more rigid conformation [6], e.g. also evident in the spectrum of ALL-E (see Appendix). An important observation is that A2 is largely equivalent to A1 in maintaining proton pump activity in all three proteorhodopsins (Figure 2.4, Table 2.2).

In ALL-E, the polyene system is locked in the 6-s-*trans* configuration effectuating optimal conjugation. This analog was previously tested on bacterio-opsin and xantho-opsin, to study the effect of the configuration about the C6-C7 single bond [6, 11]. It was observed that the 6-s-*trans* form

of this compound smoothly reacted with both opsins, but the 6-s-*cis* form did not. The 6-s-*trans* analog provided spectral properties very similar to native bR and XR, and retained 90% of the bR pumping activity. This corroborated previous solid-state NMR studies indicating that retinal A1 has taken up a 6-s *trans* configuration upon binding to bacterio-opsin [31]. The transition from the twisted 6-s-*cis* in the free retinal A1 to the planar 6-s-*trans* form in the binding pocket of the protein accounts for a part of the spectral shift in the binding site. In ALL-E , the 6-s-*trans* form already has been enforced, which explains its red-shifted absorbance band relative to free retinal A1 (Appendix A.2) and its small effect on the absorbance band when bound in bR or XR. ALL-E was not tested before on PR or GR. This analog reacted with all three proteo-opsins, reaching completion in 30-60 min at RT. The resulting analog pigments exhibit only small red-shifts relative to the native pigments (4-5 nm). These data present strong evidence that in eubacterial rhodopsins, the retinal is bound in the 6-s-*trans* configuration, as well. This implies that the bathochromic shift of the absorbance band in XR and archaerhodopsins, relative to these eubacterial rhodopsins, is largely induced by the protein environment. All three proteorhodopsin analogs containing ALL-E retained 70-100% proton pump activity (Table 2.2). This would render this retinal analog interesting for optogenetic applications. It can be supplied directly or in precursor form in the diet and will hardly interfere with the visual system. In addition, it may be less prone to generate metabolic products like retinoic acids with strong signalling function.

PHE was previously reported to react very slowly with bacterio-opsin yielding a strongly blue-shifted analog pigment [7, 8]. In case of the eubacterial opsins, PHE behaves quite differently from the other two analogs. It forms a stable pigment with the PR and PR-DNFS opsins, but not with the GR opsin. Furthermore, it regenerates the PR opsins slowly, with only partial regeneration after 60 min incubation at RT, requiring

additional overnight incubation at 4°C. Finally, it induced a significant blue-shift in absorbance, compared to A1. The slow regeneration is most likely due to a poor fit in the opsin binding pocket because of the absence of the methyl groups on the ring element, which sterically contribute to correct positioning and stabilization of the ring and to its interaction with its protein environment [6, 32]. Nevertheless, the resulting analog pigments maintained significant proton pump activity and could be successfully purified.

The structural models we generated for GR and PR may present a clue for their different reactivity with PHE. Figure 2.5 shows the models for the rear end of the binding pockets. The most striking difference is seen at the position of Phe152 in PR, where GR has a glycine residue (Gly178). This difference is physiologically relevant, since it was demonstrated that mutating Gly178 in GR to a bulkier Trp abolished strong binding of the carotenoid echinenone, which is involved in energy transfer to the retinal [18, 33, 34], and eliminated this energy transfer. The smaller Gly residue at position 178 apparently is required to allow enough space for immobilizing the carotenoid ring [6, 16], thereby allowing energy transfer and increasing the cross section for photo-activation of retinal. We surmise that the aromatic ring of Phe152 in PR, which is positioned right above the ring element of retinal, would contribute significant π-π stacking interaction. Together with the methyl groups on the polyene chain, this may sufficiently stabilize PHE in the binding pocket. GR cannot provide this stacking interaction, and thus may not provide sufficient interaction energy or too much motional freedom for the PHE to form a stable protonated Schiff base. This hypothesis can be verified by testing whether the G178F mutant of GR will yield a stable pigment with PHE.

In this context, a comparison with XR, is appropriate, since XR also binds a carotenoid (salinixanthin, a derivative of echinenone) [35]. The position

equivalent to Gly178 in GR carries the same residue in XR (Gly156). Xantho-opsin is reported to slowly react with PHE in the presence of bound salinixanthin, generating a stable pigment [30]. Possibly, the presence of the carotenoid ring sufficiently stabilizes PHE in the binding pocket. Since there is no echinenone available in our *E. coli* expression system, it needs to be investigated whether complementation with echinenone would result in a stable analog pigment of GR with PHE. It has been suggested that carotenoid fixation is required for pigment formation in XR [6, 36]. Our results show that this is not the case for GR, which easily generates analog pigments that retain full proton pumping capacity.

2.5 Conclusion

Our results demonstrate that ring modification can affect the affinity of the analog for the retinal binding site and will usually modulate the spectral properties of the respective rhodopsin, but, importantly, can largely maintain proton pump activity. This presents good prospects for further modification trials in the ring and eventual biotechnological applications. The smooth reaction with ALL-E while implementing only a small red-shift, corroborates available evidence, that the retinal chromophore in eubacterial rhodopsins is also bound in the 6-s-*trans* configuration. We further show that the spectral shifts effectuated by the analogs can be additive to spectral shifts induced by mutagenesis. Hence, combining selected mutagenesis with ligand analogs offers promising prospects for further extending the wavelength range of rhodopsins.

References

[1] Kim, S. Y., Waschuk, S. A., Brown, L. S. and Jung, K. H. "Screening and characterization of proteorhodopsin color-tuning mutations in Escherichia coli with endogenous retinal synthesis", *Biochim Biophys Acta*, 2008. **1777**(6): p. 504-13.

[2] Tokunaga, F. and Ebrey, T. "The blue membrane: The 3-dehydroretinal-based artificial pigment of the purple membrane ", *Biochemistry*, 1978. **17**(10): p. 1915-1922.

[3] Spudich, J. L., McCain, D. A., Nakanishi, K., Okabe, M., Shimizu, N., Rodman, H., Honig, B. and Bogomolni, R. A. "Chromophore/protein interaction in bacterial sensory rhodopsin and bacteriorhodopsin ", *Biophys J*, 1986. **49**(2): p. 479-83.

[4] Iwasa, T. "Artificial pigments of halorhodopsin and their chloride pumping activities ", *Biochemistry*, 1992. **31**(4): p. 1190-5.

[5] Sineshchekov, O. A., Govorunova, E. G., Wang, J. and Spudich, J. L. "Enhancement of the long-wavelength sensitivity of optogenetic microbial rhodopsins by 3,4-dehydroretinal ", *Biochemistry*, 2012. **51**(22): p. 4499-506.

[6] Smolensky Koganov, E., Hirshfeld, A. and Sheves, M. "Retinal beta-ionone ring-salinixanthin interactions in xanthorhodopsin: a study using artificial pigments ", *Biochemistry*, 2013. **52**(7): p. 1290-301.

[7] Derguini, F., Bigge, C. F., Croteau, A. A., Balogh-Nair, V. and Nakanishi, K. "Visual pigments and bacteriorhodopsins formed from aromatic retinal analogs ", *Photochem Photobiol*, 1984. **39**(5): p. 661-5.

[8] Maeda, A., Asato, A. E., Liu, R. S. and Yoshizawa, T. "Interaction of aromatic retinal analogues with apopurple membranes of Halobacterium halobium ", *Biochemistry*, 1984. **23**(11): p. 2507-13.

[9] Smolensky, E. and Sheves, M. "Retinal-salinixanthin interactions in xanthorhodopsin: a circular dichroism (CD) spectroscopy study with artificial pigments ", *Biochemistry*, 2009. **48**(34): p. 8179-88.

[10] Steen, R. v. d., Biesheuvel, P. L., Mathies, R. A. and Lugtenburg, J. "Retinal analogs with locked 6-7 conformations show that bacteriorhodopsin requires the 6-s-*trans* conformation of the chromophore ", *J Am Chem Soc*, 1986. **108**(20): p. 6410-6411.

[11] van Wijk, Arjan A. C., van de Weerd, Michiel B. and Lugtenburg, J. "Synthetic scheme for the preparation of ^{13}C-labeled 3,4-didehydro-retinal, 3-hydroxyretinal, and 4-hydroxyretinal up to uniform ^{13}C-enrichment ", *E J Org Chem*, 2003. **2003**(5): p. 863--868.

[12] Hubbard, R., Brown, P. K. and Bownds, D. "243: Methodology of vitamin A and visual pigments ", *Methods Enzymol*, 1971. **18, Part C**: p. 615 - 653.

[13] Groenendijk, G. W., Jansen, P. A., Bonting, S. L. and Daemen, F. J. "Analysis of geometrically isomeric vitamin A compounds ", *Methods Enzymol*, 1980. **67**: p. 203-20.

[14] Friedrich, T., Geibel, S., Kalmbach, R., Chizhov, I., Ataka, K., Heberle, J., Engelhard, M. and Bamberg, E. "Proteorhodopsin is a light-driven proton pump with variable vectoriality ", *J Mol Biol*, 2002. **321**(5): p. 821-38.

[15] Gordeliy, V. I., Labahn, J., Moukhametzianov, R., Efremov, R., Granzin, J., Schlesinger, R., Buldt, G., Savopol, T., Scheidig, A. J., Klare, J. P. and Engelhard, M. "Molecular basis of transmembrane signalling by sensory rhodopsin II-transducer complex ", *Nature*, 2002. **419**(6906): p. 484-7.

[16] Luecke, H., Schobert, B., Stagno, J., Imasheva, E. S., Wang, J. M., Balashov, S. P. and Lanyi, J. K. "Crystallographic structure of xanthorhodopsin, the light-driven proton pump with a dual chromophore ", *Proc Natl Acad Sci U S A*, 2008. **105**(43): p. 16561-5.

[17] Dioumaev, A. K., Brown, L. S., Shih, J., Spudich, E. N., Spudich, J. L. and Lanyi, J. K. "Proton transfers in the photochemical reaction cycle of proteorhodopsin ", *Biochemistry*, 2002. **41**: p. 5348-5358.

[18] Miranda, M. R., Choi, A. R., Shi, L., Bezerra, A. G., Jr., Jung, K. H. and Brown, L. S. "The photocycle and proton translocation pathway in a cyanobacterial ion-pumping rhodopsin", *Biophys J*, 2009. **96**(4): p. 1471-81.

[19] Yaowu, X., Ranga, P., Richard, K. and and Mark, B. "Time-resolved FTIR spectroscopy of the photointermediates involved in fast transient H^+ release by Proteorhodopsin", *J Phys Chem B*, 2005. **109**(1): p. 634-641.

[20] Béjà, O., Aravind, L., Koonin, E. V., Suzuki, M. T., Hadd, A., Nguyen, L. P., Jovanovich, S. B., Gates, C. M., Feldman, R. A., Spudich, J. L., Spudich, E. N. and DeLong, E. F. "Bacterial rhodopsin: Evidence for a new type of phototrophy in the sea", *Science*, 2000. **289**(5486): p. 1902-1906.

[21] Dioumaev, A. K., Wang, J. M., Balint, Z., Varo, G. and Lanyi, J. K. "Proton transport by proteorhodopsin requires that the retinal Schiff base counterion Asp-97 be anionic", *Biochemistry*, 2003. **42**(21): p. 6582-7.

[22] Vogt, A., Wietek, J. and Hegemann, P. "Gloeobacter rhodopsin, limitation of proton pumping at high electrochemical load", *Biophys J*, 2013. **105**(9): p. 2055-63.

[23] Choi, A. R., Shi, L., Brown, L. S. and Jung, K. H. "Cyanobacterial light-driven proton pump, Gloeobacter rhodopsin: complementarity between rhodopsin-based energy production and photosynthesis", *PLoS One*, 2014. **9**(10): p. e110643.

[24] Wang, W. W., Sineshchekov, O. A., Spudich, E. N. and Spudich, J. L. "Spectroscopic and photochemical characterization of a deep ocean proteorhodopsin", *J Biol Chem*, 2003. **278**(36): p. 33985-91.

[25] Lee, K. A. and Jung, K.-H. "ATP regeneration system using *E. coli* ATP synthase and *Gloeobacter* rhodopsin and its stability", *J Nanosci Nanotechnol*, 2011. **11**(5): p. 4261-4264.

[26] Reckel, S., Gottstein, D., Stehle, J., Lohr, F., Verhoefen, M. K., Takeda, M., Silvers, R., Kainosho, M., Glaubitz, C., Wachtveitl, J., Bernhard, F., Schwalbe, H., Guntert, P. and Dotsch, V. "Solution NMR structure of proteorhodopsin", *Angew Chem Int Ed Engl*, 2011. **50**(50): p. 11942-6.

[27] Ran, T., Ozorowski, G., Gao, Y., Sineshchekov, O. A., Wang, W., Spudich, J. L. and Luecke, H. "Cross-protomer interaction with the photoactive site in oligomeric proteorhodopsin complexes", *Acta Crystallogr D Biol Crystallogr*, 2013. **69**(10): p. 1965-80.

[28] Bamann, C., Bamberg, E., Wachtveitl, J. and Glaubitz, C. "Proteorhodopsin", *Biochim Biophys Acta*, 2014. **1837**(5): p. 614-25.

[29] Rupenyan, A., van Stokkum, I. H., Arents, J. C., van Grondelle, R., Hellingwerf, K. and Groot, M. L. "Characterization of the primary photochemistry of proteorhodopsin with femtosecond spectroscopy", *Biophys J*, 2008. **94**(10): p. 4020-30.

[30] Malmerberg, E., Omran, Z., Hub, J. S., Li, X., Katona, G., Westenhoff, S., Johansson, L. C., Andersson, M., Cammarata, M., Wulff, M., van der Spoel, D., Davidsson, J., Specht, A. and Neutze, R. "Time-resolved WAXS reveals accelerated conformational changes in iodoretinal-substituted proteorhodopsin", *Biophys J*, 2011. **101**(6): p. 1345-53.

[31] Harbison, G. S., Smith, S. O., Pardoen, J. A., Courtin, J. M., Lugtenburg, J., Herzfeld, J., Mathies, R. A. and Griffin, R. G. "Solid-state ^{13}C NMR detection of a perturbed 6-s-*trans* chromophore in bacteriorhodopsin", *Biochemistry*, 1985. **24**(24): p. 6955-62.

[32] Sheves, M., Friedman, N., Rosenbach, V. and Ottolenghi, M. "Preparation of (1,1,5-tri-demetyl)bacteriorhodopsin pigment and its photocycle study", *FEBS Letters*, 1984. **166**(2): p. 245--247.

[33] Imasheva, E. S., Balashov, S. P., Choi, A. R., Jung, K. H. and Lanyi, J. K. "Reconstitution of *Gloeobacter violaceus* rhodopsin with a light-harvesting carotenoid antenna", *Biochemistry*, 2009. **48**(46): p. 10948-55.

[34] Balashov, S. P., Imasheva, E. S., Choi, A. R., Jung, K. H., Liaaen-Jensen, S. and Lanyi, J. K. "Reconstitution of gloeobacter rhodopsin with echinenone: role of the 4-keto group", *Biochemistry*, 2010. **49**(45): p. 9792-9.

[35] Balashov, S. P., Imasheva, E. S., Boichenko, V. A., Anton, J., Wang, J. M. and Lanyi, J. K. "Xanthorhodopsin: a proton pump with a light-harvesting carotenoid antenna", *Science*, 2005. **309**(5743): p. 2061-4.

[36] Imasheva, E. S., Balashov, S. P., Wang, J. M., Smolensky, E., Sheves, M. and Lanyi, J. K. "Chromophore interaction in xanthorhodopsin--retinal dependence of salinixanthin binding", *Photochem Photobiol*, 2008. **84**(4): p. 977-84.

Chapter 3

Retinal based proton pumping in the near-infrared

Shifting the action spectra of rhodopsin proton-pumps beyond 700 nm would generate many new prospects in optogenetics, membrane sensor technology, and complementation of oxygenic phototrophy. We thereby studied the effect of red-shifting analogs of retinal, combined with red-shifting mutations, on the spectral properties and pump activity of proteorhodopsins. We investigated a variety of analogs, of which the novel analog 3-methylamino-16-nor-1,2,3,4-didehydroretinal (MMAR), produced exciting results. This analog red-shifted all rhodopsin variants tested, accompanied by a strong broadening of the absorbance band, tailing out to 850-950 nm. In particular, MMAR showed a strong synergistic effect with the PR-D212N,F234S double mutant, inducing an astonishing 200 nm red-shift in the absorbance maximum, which is by far the largest red-shift reported for any retinal protein. Very importantly, all MMAR containing holoproteins are the first rhodopsins retaining significant pump activity under near-infrared illumination (730 nm). Such MMAR-based rhodopsin variants present very promising opportunities for further synthetic biology modification and for a variety of biotechnological and biophysical applications.

This chapter has been published as: S. Ganapathy, H. Venselaar, Q. Chen, H. J. M. de Groot, K. J. Hellingwerf, W. J. de Grip **(2017)** *Journal of the American Chemical Society* 139 (6): 2338-2344

3.1 Introduction

In chapter 2 we confirm that PR and GR can be easily expressed in good yields in a non-native host like *Escherichia coli.* We further show that they can be readily combined with retinal analogs to generate analog pigments with different spectral properties, while maintaining pump activity. In addition, retinal analog induced spectral shifts can be additive to spectral shifts induced by mutagenesis. Such features make PR and GR attractive model systems for synthetic biology applications. A challenge in many of these applications is to extend the action spectrum of rhodopsins into the far-red and near-infrared (NIR) range of the electromagnetic spectrum (≥700 nm), which is relatively unexplored and has many advantages [1]. In chapter 2, the retinal analog A2 (Figure 3.1) was identified as a red-shifting analog, which retained significant activity of the corresponding pigments. In this chapter, we specifically focus on red-shifting retinal analogs containing more extensive ring modifications. We extend the conjugation of A2 by adding electron withdrawing substituents at the C3 position on the β-ionone ring. Here, we report on the ring-modified analogs: all-*trans*-3-methoxy-3,4-dehydroretinal (MOA2), all-*trans*-3-dimethylamino-16-nor-1,2,3,4-didehydroretinal (DMAR) and all-*trans*-3-methylamino-16-nor-1,2,3,4-didehydro retinal (MMAR) (Figure 3.1). MOA2 was shown before to red-shift visual rhodopsins up to 130 nm with retention of activity [2]. DMAR was based upon a 3-dimethylaminophenyl derivative of retinal, lacking methyl groups in the aromatic ring, which red-shifted channelrhodopsin 2 by 40 nm, while maintaining a retarded photocycle [3]. MMAR we devised on the basis of the results we obtained with DMAR. These analogs were combined with WT PR and GR as well as with the red-shifted mutants PR-D212N, F234S (PR-DNFS), PR-T101A (PR-TA) and GR-F260S (GR-FS) (Figure 3.2).

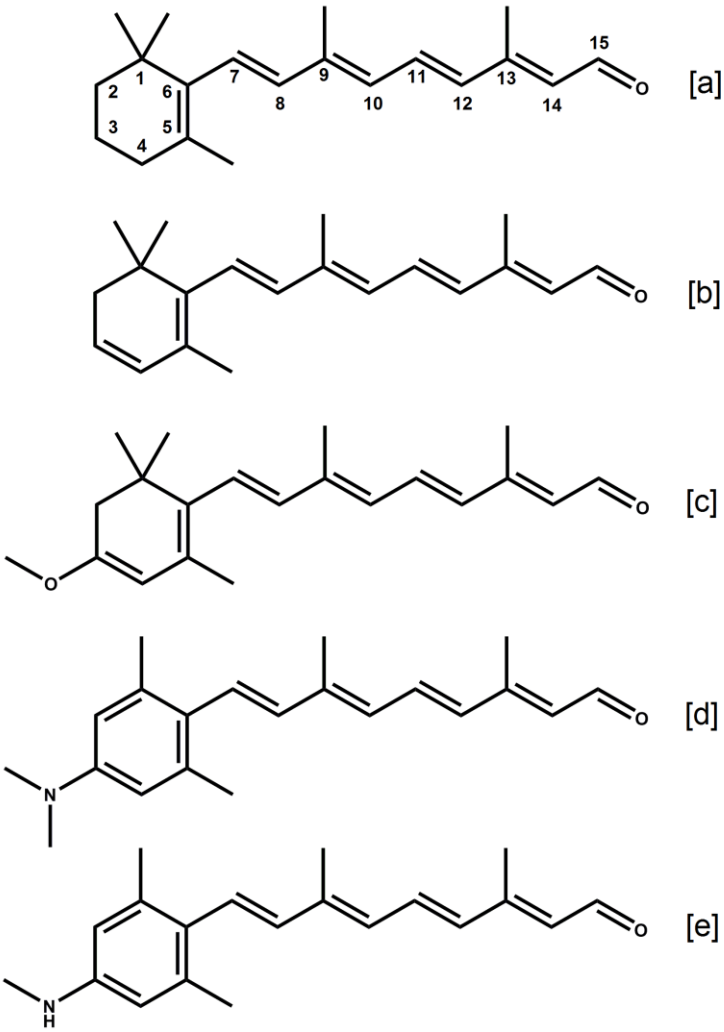

Figure 3.1 Chemical structures of retinal analogs used in this chapter [a] A1 [b] A2 [c] MOA2 [d] DMAR [e] MMAR. For nomenclature and spectral properties see Introduction and Appendix (Figure A2.1).

While all analogs tested yielded red-shifted pigments, MMAR was finally identified as the most promising analog from our study, inducing bathochromic shifts up to an astonishing 200 nm, while retaining activity in near-infra red light. MMAR pigments have broad potential for a variety of biotechnological, optogenetic and oxyphototrophic applications.

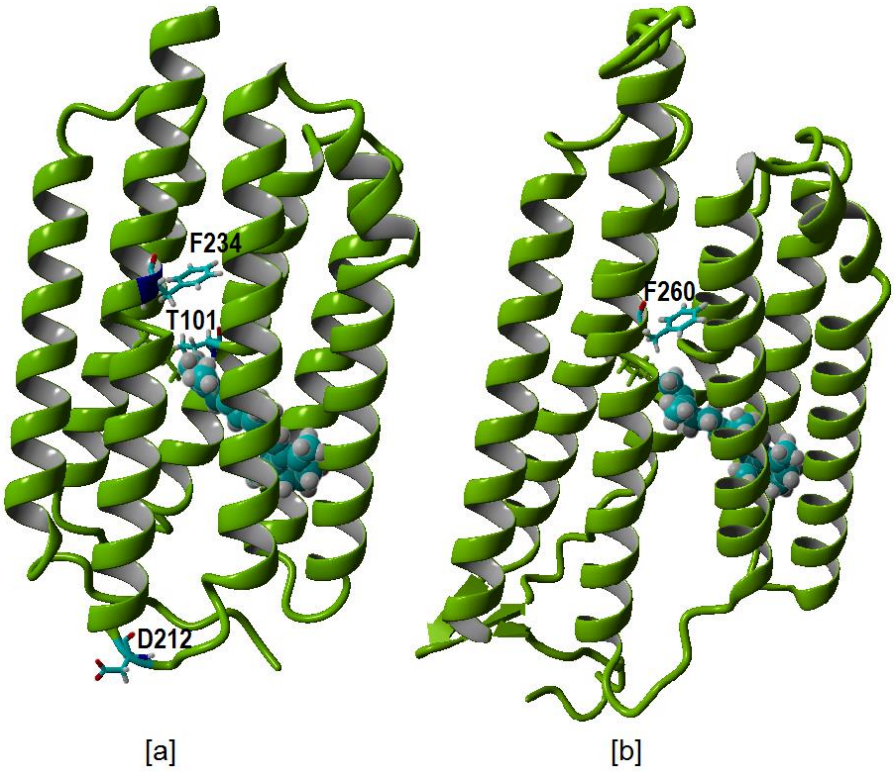

Figure 3.2 [a] Homology model of PR selectively displaying the mutation sites in cyan: F234 and T101 near the retinal binding pockets; and D212 in the loop region. [b] Homology model for GR selectively displaying the mutation site F260 in cyan, in the retinal binding pocket. The retinylidene chromophore is represented in cyan as a space-filled residue.

3.2 Experimental section

Next to the materials and methods already described in Chapter 2, the following materials and methods were used in this chapter.

3.2.1 Materials

All-*trans*-3,4-dehydroretinal (A2) was a generous gift from Hoffman-LaRoche. All-*trans*-3-methoxy-3,4-dehydroretinal (MOA2; purity 97.8% according to the manufacturer's certificate of analysis), all-*trans*-3-dimethylamino-16-nor-1,2,3,4-didehydroretinal (DMAR; purity 99.9%)

and all-*trans*-3-methylamino-16-nor-1,2,3,4-didehydroretinal (MMAR; purity > 99.9%) were synthesized on order by Buchem, B.V. (Apeldoorn, The Netherlands).

3.2.2 Spectroscopy of membrane vesicles:

The spectral properties of the pigments were measured in intact membrane vesicle suspensions using the end-on spectrophotometer SPECORD 210 PLUS (Analytik Jena). The end-window configuration of the photomultiplier and a close distance to the cuvette reduces the loss of light due to scattering by the vesicles. To isolate the major absorbance band of the proteorhodopsin out of the composite spectrum of membrane vesicles, hydroxylamine was added from a 1 M stock solution, pH 7, to a final concentration of 50 mM, followed by illumination with white light for 10 minutes. Hydroxylamine attacks the Schiff base and releases the retinal from the opsin binding pocket as retinaloxime. A difference spectrum then reveals the major absorbance band of the proteorhodopsin present. The same protocol was also used after solubilization of membrane vesicles with DDM. The vesicle protocol and DDM protocol were compared with pigments that were stable in DDM, and yielded equivalent results ($\pm$ <5%).

3.2.3 Spectroscopy of purified protein:

In order to test the pH-dependence of the main absorbance band of the PR based pigments, the purified proteins were analysed at different pH values by diluting the samples 1:1 with buffers containing either 100 mM bis-tris-propane at pH 9, 8.5, 8, 7.5, 7, 6.5, 6 or 100 mM MES at pH 5.5 or 5. For determination of molar absorbance values the purified pigments based upon WT PR and GR were illuminated in DDM (pH 7) in the presence of hydroxylamine as described in Chapter 2. The maximum absorbance of the generated oxime derivatives was measured, and was used to calculate the molar absorbance values of the corresponding WT PR and GR pigments.

3.2.4 Molar absorbance of retinals and corresponding pigments:

The λ_{max} (nm) and molar absorbance ε ($M^{-1}.cm^{-1}$) for A1, A2, MOA2, DMAR and MMAR and their corresponding oximes are listed in the appendix (Table A.2.2). In order to calculate the ε values, a stock solution of the retinals was made containing 1 mg of the crystalline powder dissolved in 1 ml of DMF, and its absorbance was measured using appropriate dilutions. Beer-Lambert's law was used to calculate the ε of the analogs in DMF. An aliquot of this stock was diluted 1:100 with a solution containing 1% DDM in 10 mM Tris pH 7, to determine the corresponding ε of the analogs in DDM. Hydroxylamine was then added to the DMF and DDM solutions to a final concentration of 50 mM and the solution was illuminated. The absorbance spectra of the resulting retinal oximes were measured and used to calculate the ε in DMF and DDM. These measurements were done in duplicate, resulting in a S.D. ≤ 8%. The ε of the oximes of A1 and A2 were previously calculated to be 51700 $M^{-1}.cm^{-1}$ at λ_{max}=367 nm and 45400 $M^{-1}.cm^{-1}$ at λ_{max}=386 nm respectively in 1% digitonin solution [4-6]. Based on our measurements, we calculated ε of 52500 $M^{-1}.cm^{-1}$ at λ_{max}=368 nm and 44000 $M^{-1}.cm^{-1}$ at λ_{max}=385 nm for A1 and A2 oximes in 1% DDM, respectively, in good agreement with the literature values. The ε values for the WT PR and GR pigments, calculated from the corresponding oxime absorbance, are also listed in Table A.2.2. The molar absorbances of PR:A1 and GR:A1 in detergent solution were estimated before. Our ε=55500 $M^{-1}.cm^{-1}$ for GR:A1 is not significantly different from the reported value of 50000 [7]. Our ε=54200 $M^{-1}.cm^{-1}$ for PR:A1 is however significantly larger than the earlier reported ε=44000 $M^{-1}.cm^{-1}$ [8]. Considering the reported molar absorbances for bacteriorhodopsin (54000 [9] and 63000 $M^{-1}.cm^{-1}$ [10]), we decided to keep to our own higher values for both PR and GR.

3.2.5 Proton pumping assay:

Suspensions of starved cells were generated as described in Chapter 2, section 2.2.9. The following light sources were used: white light (DLED9-T,

DEDOLIGHT; 800 $\mu E.m^{-2}.s^{-1}$); 617 nm LED (M617L3, Thorlabs; 1500 $\mu E.m^{-2}.s^{-1}$); 660 nm LED (M660L4, Thorlabs; 800 $\mu E.m^{-2}.s^{-1}$); 730 nm LED (M730L4, Thorlabs; 150 $\mu E.m^{-2}.s^{-1}$). Light-induced pH changes were measured with a pH microelectrode (SenTix MIC, WTW) and the readout was monitored by a pH meter (Inolab pH 7310, WTW) connected to a computer. The following light regime was used: 1 min dark, 1 min light, 2 min dark, 1 min light, 2 min dark. For the 730 nm illumination of all species and 660 nm illumination for PR-DNFS, a longer illumination period of 1.5 min was used, along with a 2 x concentrated cell suspension (cells from 50 mL culture in 4 mL starvation buffer). Pumping rates were calculated using two independent trials. A calibration curve was measured using 0.1 M HCl and 0.1 M oxalic acid. Pumping rates were calculated as protons/sec from the initial rate of the light-induced pH change, if required corrected for baseline drift in controls (starved cells without expression of proteo-opsin or without retinal). Molecular pumping rates could subsequently be calculated after assay of the proteorhodopsin level.

3.2.6 Determination of proteorhodopsin levels:

The above cell suspension from the proton pumping assay was rinsed with starvation buffer and the pellet was resuspended in 10 mL buffer B (50 mM Tris-HCl, 150 mM NaCl, pH 7). The cell suspension was sonicated as mentioned above and the membrane vesicles and cell debris were pelleted together (147,000xg, 4°C, 1 h). The pellet was resuspended in 4 mL of buffer B. An aliquot of this membrane vesicle suspension was used to extract the main absorbance band of the analog pigments after bleaching with hydroxylamine, using the end-on spectrophotometer. This method was useful to estimate the concentration of analog pigments which were unstable in DDM, particularly GR:DMAR, GR:MMAR, GR-FS:MMAR and PR-TA:MMAR. To another aliquot of the membrane vesicle suspension, DDM was added to a final concentration of 2.5% and incubated at RT with mixing overnight. Under these conditions maximum extraction of all stable

pigment species was achieved without significant losses. The following day, the insoluble material was removed by centrifugation at 16,000xg, 4°C for 20 min. The supernatant was used to measure an absorbance spectrum before and after bleaching with hydroxylamine. The optical density at the absorbance maximum was used to calculate the original proteorhodopsin level in the cell suspension, using the calculated ε listed in the Appendix, Table A.2.2. Hereby we assumed that the molar absorbance of the mutants is not significantly different from the parent pigments.

3.3 Results

3.3.1 Selection and properties of retinal analogs

In Chapter 2, we observed that A2 induced significant red-shifts in all species tested while largely retaining pump activity. In this chapter, we elaborated the conjugation of A2 by adding different electron withdrawing substituents at the C3 position in the β-ionone ring and/or at C13 or C14 in the polyene chain. Analogs modified at C13 or C14, however, showed poor reactivity or low stability of the resulting holoprotein (see Appendix A.4). Here, we report on the ring-modified analogs MOA2, DMAR and MMAR (Figure 3.1).

MOA2 contains the strong electron withdrawing methoxy group at the C3 position on the β-ionone ring. An extensive π-system is delocalized over the lone pairs of electrons on the oxygen atom of MOA2, resulting in a large red-shift of 52 nm relative to A1 (λ_{max} 434 nm vs 378 nm in DMF) along with a broadening of the main absorbance band (see Appendix, Figure A.2.1). DMAR contains an aromatized β-ionone ring with a bulky dimethylamino group at the C3 position. This analog was modelled on a variant lacking methyl groups on the β-ionone ring [3]. In Chapter 2, we showed that the aromatic PHE, which lacked methyl groups on the ring, did not form a stable pigment with GR [11]. Therefore, we decided to position

methyl groups, which are known to stabilize the retinal inside the binding pocket [12, 13], at the C1 and C5 positions, resulting in DMAR.

However, during the course of our study, we discovered that DMAR formed unstable pigments, which had low pumping activity. We surmised that the bulky dimethylamino group probably sterically hindered the fit and stability of DMAR in the retinal binding pocket. Considering that MOA2 containing a methyl-oxo substitution at C3 smoothly incorporates in all opsins, we therefore conceived MMAR, which contains only a single methyl group on the C3-amino substituent. This modification does not affect the absorbance of the free retinal analog in DMF, as both DMAR and MMAR display a similar complex absorbance band with a λ_{max} at ~434 nm, and an electronic side band at 360 nm (see Appendix, Figure A.2.1). However, when bound to the proteo-opsins, MMAR provides a definite increase in stability and proton pumping activity, compared to DMAR.

3.3.2 Expression and characterization of pigments

In the previous chapter we also described the generation of the PR double mutant PR-DNFS using mis-match PCR. Analogous to the single mutation in F234S in PR, we introduced the equivalent mutation in GR (F260S), based upon homology modeling (Figure 3.2). GR-FS only shows a small red-shift (9 nm), but in contrast to PR-DNFS retains full activity. We further generated PR-TA (T101A, Figure 3.2) [14]. This mutation introduces a 16 nm red-shift while maintaining significant pump activity. Several other single mutations and combinations were generated, but these displayed relatively smaller additional red-shifts with strong loss of pumping activity (Appendix A.5).

PR, GR and the mutants PR-DNFS, PR-TA and GR-FS were recombinantly expressed in *E. coli* strain UT5600 as described in Chapter 2. All opsins could be fully regenerated with A1 and A2, either upon addition of retinal

to the cell culture, or in isolated membrane vesicles. Good regeneration rates were also observed with MOA2 and MMAR, but complete regeneration with DMAR was difficult to achieve. The pigments were further purified using the C-terminal 6x-His tag to a high degree of purity in DDM. However, all the DMAR species and certain MMAR pigments (namely GR, GR-FS, and PR-TA) were not very stable in DDM, which was problematic for the estimation of expression levels. We found a way around this, by measuring the pigment absorbance in intact membrane vesicles.

The main absorbance bands of the pigments in membrane vesicles or in a solubilized state were extracted by reaction with hydroxylamine during illumination to liberate the bound retinal by converting it into the corresponding oxime. This reaction in membrane vesicles was particularly useful to extract the absorbance bands of pigments which were not sufficiently stable in DDM, or which could not survive the purification process. Furthermore, the oxime production was used to determine the molar absorbance values of the various analog species. This allowed quantification of expression levels, and thereby molecular pumping rates for all species generated.

The proton pumping activity of all analog species was measured using four different illumination conditions, namely white light (spectral range 300-900 nm), 617 nm LED (600-640 nm), 660 nm LED (620-680 nm) and 730 nm LED (690-760 nm) illumination. We used intact *E. coli* cells which were starved for an optimum duration of 4 days in a minimal buffer, and further incubated in the presence of valinomycin. The rates obtained probably do not yet reflect the maximally attainable ones, since the applied light intensities are still limiting. Hence, due to the variation in the photon flux of the illumination sources used, the pumping rates were normalized within a set of light conditions to the highest pumping activity obtained (Table 3.1). For instance, GR-FS:A1 has the highest pumping rate with white light (9.4

$H^+.s^{-1}$ per protein); hence white light pumping rates of all pigments are normalised to 9.4. For a comparison between the different light regimes, we can further normalize the highest pumping rates obtained in each light regime, to the highest pumping rate under white light illumination. For reference, these values are: White light (GR-FS:A1, 100%); 617 nm (GR-FS:A1, 80% of white light); 660 nm (GR:A2, 15% of white light) and 730 nm (GR-FS:MMAR, 2% of white light).

3.3.3 Properties of A2, MOA2 and DMAR pigments

In chapter 2, we demonstrated a 26-32 nm red shift in the absorbance bands of the A2 pigments of PR, GR and PR-DNFS. This red-shift was also observed with the PR-TA and GR-FS mutants tested in the present chapter (Table 3.1). All A2 species retained strong proton pumping activity upon white light illumination (50-100% of A1), except for PR-DNFS (23%), corroborating the results reported before [11] (Table 3.1). However, under 730 nm illumination, very low but measurable activity was only observed for the A2 pigments of GR and GR-FS (Figures 3.5, 3.6; Table 3.1). MOA2 was previously shown to induce large spectral shifts of up to 130 nm in visual rhodopsins, while retaining their activity [15]. When bound to the various proteo-opsins used in this study, MOA2 also shifts their absorbance bands to significantly longer wavelengths (55-80 nm, Table 3.1). All MOA2 pigments retain around 15-30% proton pumping activity upon white light illumination. However, negligible proton pumping activity of all these species was observed, when excited with lower energy light (617 nm), despite the high photon flux of the LED source used (1500 $\mu E.m^{-2}.s^{-1}$).

DMAR (Figure 3.1) was modelled after a recent publication [3] that employed a variant lacking methyl groups on the β-ionone ring. This resulted in a 40 nm red-shift in the action spectrum of ChR2 accompanied by a slower photocycle. We inferred that additional methyl groups at the ring would improve the stability and activity of such analog pigments.

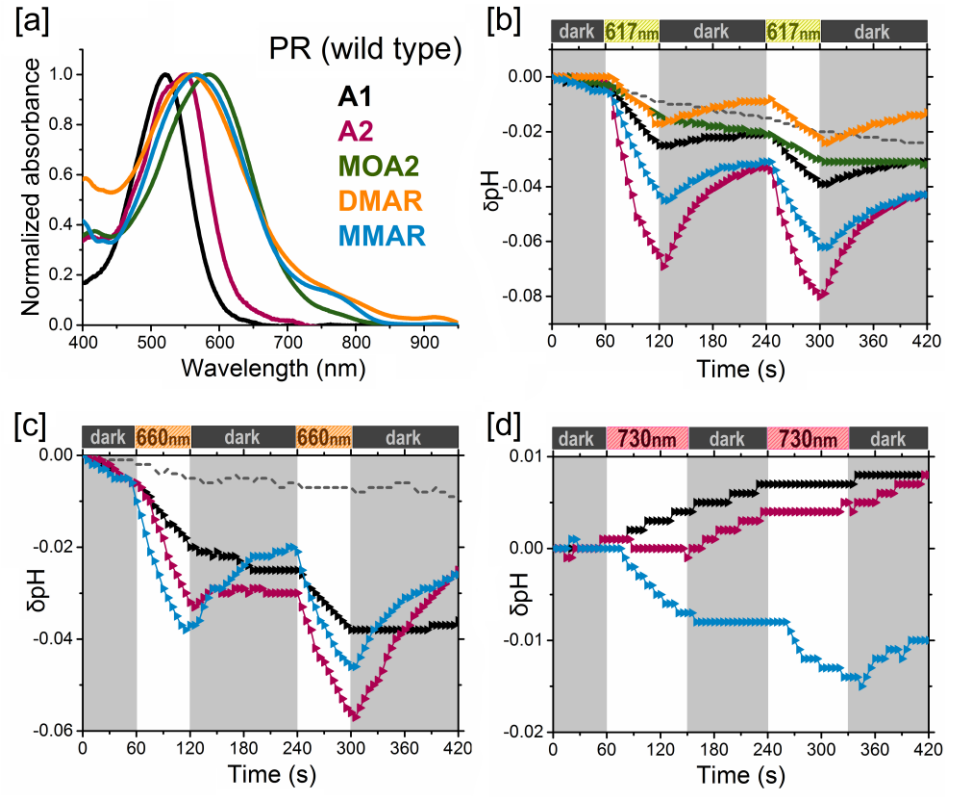

Figure 3.3 Analog pigments of PR. [a] Normalized absorbance spectra of purified pigments in DDM containing A1 (black), A2 (pink), MOA2 (green), DMAR (orange) or MMAR (blue). [b-d] Proton pumping activity of the pigments (same colors) in starved *E. coli* UT5600 cells upon illumination with 617 nm [b], 660 nm [c], and 730 nm [d]. Controls without retinal are represented as a dashed line.

DMAR, however, did not react very smoothly with any of the opsins and a significant red-shift was observed only with PR (38 nm; Table 3.1). Furthermore, DMAR pigments, in particular with GR and GR-FS, were quite unstable in detergent solution. No intact pigment could be isolated for these pigments in DDM, even upon rapid solubilization in the cold (data not shown). The DMAR pigments showed relatively low pumping rates under white light illumination (<10% of A1; Table 3.1, Figure 3.3, 3.5). On the other hand, they could still be activated by 617 nm illumination.

We did not extensively investigate the MOA2 pigments (no pump activity in red light) or the DMAR pigments (poor reactivity and thermal stability). However, the persistent pump activity of DMAR pigments in red light (Table 3.1) led us to elaborate upon this concept and test a variant, MMAR (Figure 3.1). This analog produced exciting results.

3.3.4 Properties of MMAR pigments

MMAR induced a 47 nm red-shift in the λ_{max} of PR and a 23-30 nm red-shift in the λ_{max} of PR-TA, GR and GR-FS (Table 3.1), accompanied with extensive spectral broadening and tailing up to 850-950 nm (Figure 3.3, 3.4, 3.5, 3.6). PR:MMAR also displayed a composite band around 770 nm (Figure 3.3). All PR based pigments exhibited the slight red-shift in the main absorbance band upon acidification (Figure 3.8, panel a). However, in PR:MMAR this was accompanied by an unusual enhancement of the absorbance around 770 nm (Figure 3.8, panel b). In the PR-DNFS:MMAR pigment this enhancement of the lower-energy bands was already induced by the mutation, resulting in an extraordinary red-shift of the absorbance band to ca 740 nm (Figure 3.4). Even then, acidification induced a congruent red-shift with some further enhancement of the 740 band (Appendix, Figure A.5).

All MMAR pigments displayed relatively low proton pumping activity under white light (5-10 % of A1 and A2). However, significant activity was retained with 730 LED illumination, in fact strongly surpassing that of any remaining A2 activity (Figures 3.3, 3.4, 3.5, 3.6; Table 3.1). Because of the low intensity of the 730 LED, an absolute comparison cannot yet be made, but we estimate that under equal intensity light the pumping activity with the 730 LED would be at least as high as under white light. Even the PR-DNFS mutant, which is quite impaired in its pump function (with A1, 30 – 40 % of WT in white light), with MMAR clearly displays pumping activity under 730 LED illumination (Figure 3.4).

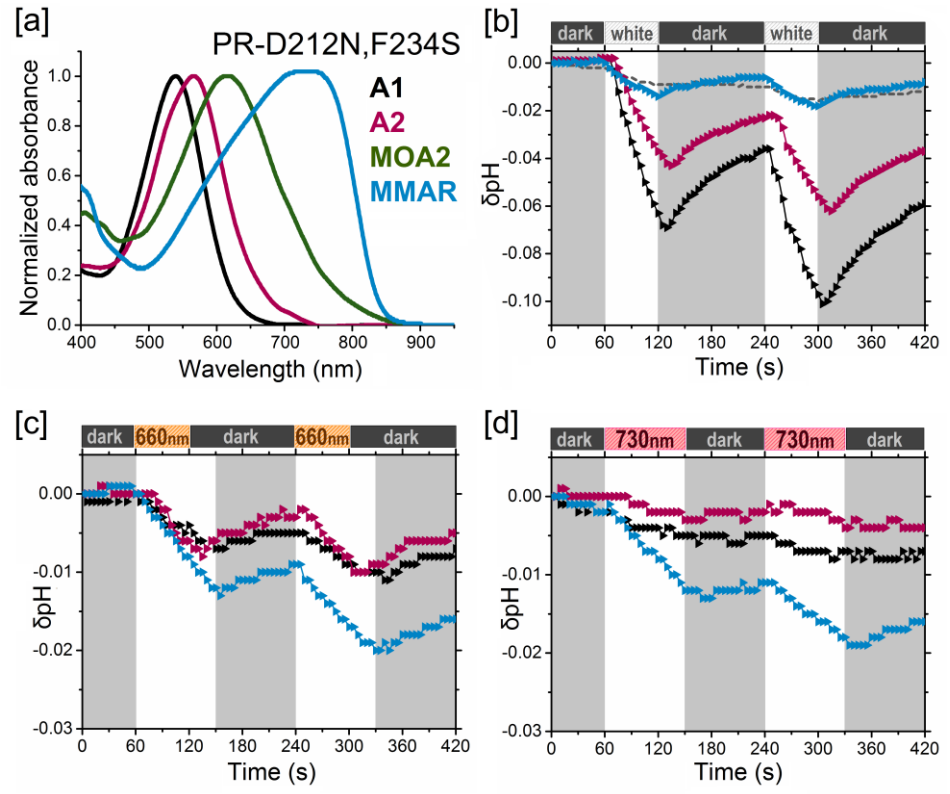

Figure 3.4 Analog pigments of PR-D212N,F234S. [a] Normalized absorbance spectra of purified pigments in DDM containing A1 (black), A2 (pink), MOA2 (green) or MMAR (blue). [b-d] Proton pumping activity of the pigments (same colors) in starved *E. coli* UT5600 cells upon illumination with white light [b], 660 nm [c] and 730 nm [d]. Controls are represented as a dashed line.

The highest activity under this NIR light was observed for the GR-FS:MMAR combination (0.2 $H^+.s^{-1}$ per protein), but this will still increase considerably at higher light intensity and broad frequency-range illumination.

3.4 Discussion

3.4.1 A2, MOA2 and DMAR pigments

All opsin variants tested with MOA2 reacted smoothly forming stable pigments in DDM, allowing extensive purification. MOA2 not only induced very large red-shifts in λ_{max} (55-81 nm, depending on the opsin, Table 3.1), but also increased the half-width of the spectra. As a result, all the spectra tail out clearly beyond 700 nm, up to 800-850 nm (Figures 3.3, 3.4, 3.5, 3.6). Under white light illumination, all MOA2 pigments tested showed low proton-pump activity (15-30% of the corresponding A1 pigments). We expected this ratio to increase in red light, in view of the red-shifted absorbance bands of the MOA2 pigments. However, hardly any pump activity could be detected with 617 nm LED illumination (Table 3.1, Figures 3.3, 3.5). This was a surprising result, since the emission band of the LED overlaps with a significant portion of the main absorbance bands of all MOA2 pigments. The low energy light with $\lambda>600$ nm is apparently insufficient to drive a complete photocycle, and the strong electronegative character of the methoxy substituent may effectively suppresses the pump mechanism. We are currently investigating this phenomenon further by femtosecond spectroscopy and a computational investigation of the energetic constraints involved in photoexcitation of MOA2 pigments.

Subsequently, we turned to the 3-dimethylaminophenyl derivative that maintained activity in the channelrhodopsin ChR2 [3], but decided to add a methyl group at position 1 and 5 to increase fit and stability in the binding site [12]. This resulted in the novel derivative DMAR (Figure 3.1). DMAR, however, showed low reactivity with most opsins and very low stability of the resulting pigments in DDM, especially for GR and GR-FS. Of all pigments tested, only PR:DMAR could be successfully purified (Figure 3.3), showing a broad absorbance band peaking at 558 nm (38 nm red-shift) and extending out to 850 nm. A clue for this discriminatory behaviour can be

extracted from the homology models of PR and GR (Figure 2.5). PR contains a Phe 152 group in the retinal binding pocket, which might stabilize the aromatic ring in DMAR via π-π stacking interactions. GR however contains a G178 in this location and would lack this stabilizing effect.Moreover, the bulky dimethylamino group probably sterically hinders the fit and reactivity of DMAR in the retinal binding pocket. While low pumping rates (<10% of A1) were observed under white light illumination for both PR:DMAR and GR:DMAR, it was inspiring to notice that now pumping persisted under 617 nm illumination (Figures 3.3 and 3.5). Hence, we decided to improve reactivity of this analog and stability of the resulting pigments, by replacing the larger dimethylamino group in DMAR with the smaller monomethylamino group. This group is similar in size to the methoxy group in MOA2, an analog that yields very stable pigments. This strategy resulted in MMAR (Figure 3.1).

3.4.2 MMAR pigments

MMAR indeed rapidly incorporated in all opsins and the resulting pigments showed a clear increase in stability and proton pumping activity, compared to DMAR. MMAR thus came out as the most promising analog identified from our study. MMAR induced bathochromic shifts in all opsins tested, along with broadening of the absorbance bands. However, the unprecedented ~200 nm shift (equivalent to 5005 cm^{-1}) in the absorbance of PR-DNFS:MMAR relative to the A1 pigment is a spectacular result from this chapter, which is discussed in more detail, below.

PR-derived pigments exhibit a 20-30 nm red-shift in the main absorbance band (Figure 3.8) upon protonation of the counterion (D97; pKa ~6.5). Of all PR pigments, only PR:MMAR displayed a complex absorbance band with a λ_{max} at 567 nm containing a 770 nm composite band, which extends to 850 nm (Figure 3.3).

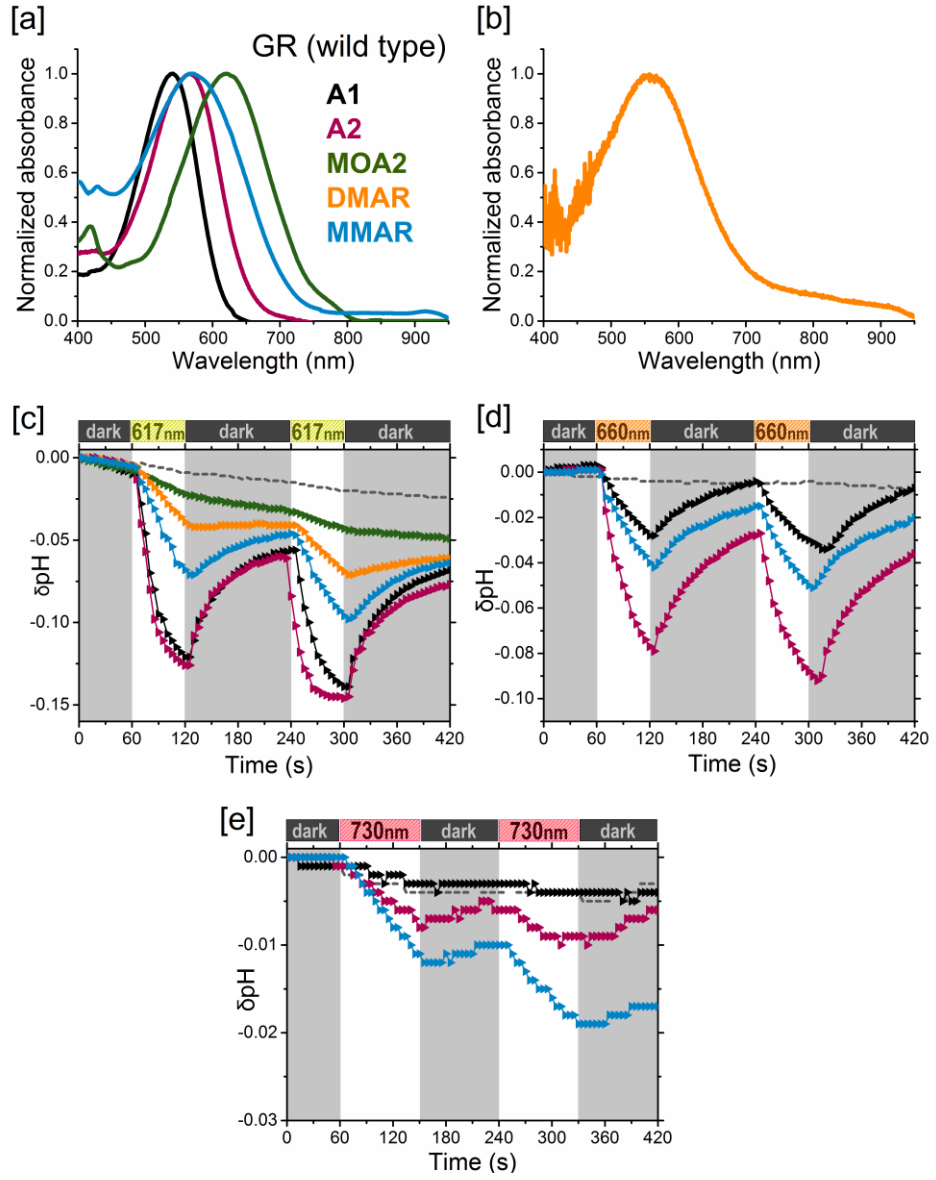

Figure 3.5 Analog pigments of GR [a] Normalized absorbance spectra of His-tag purified pigments in DDM containing A1 (black), A2 (pink), MOA2 (green) or MMAR (blue). [b] Hydroxylamine difference spectra of the DMAR pigment (orange) in membrane vesicles. [c-e] Proton pumping activity of the pigments (same colors) in starved *E. coli* UT5600 cells upon illumination with 617 nm [c], 660 nm [d], and 730 nm [e]. Controls are represented as a dashed line.

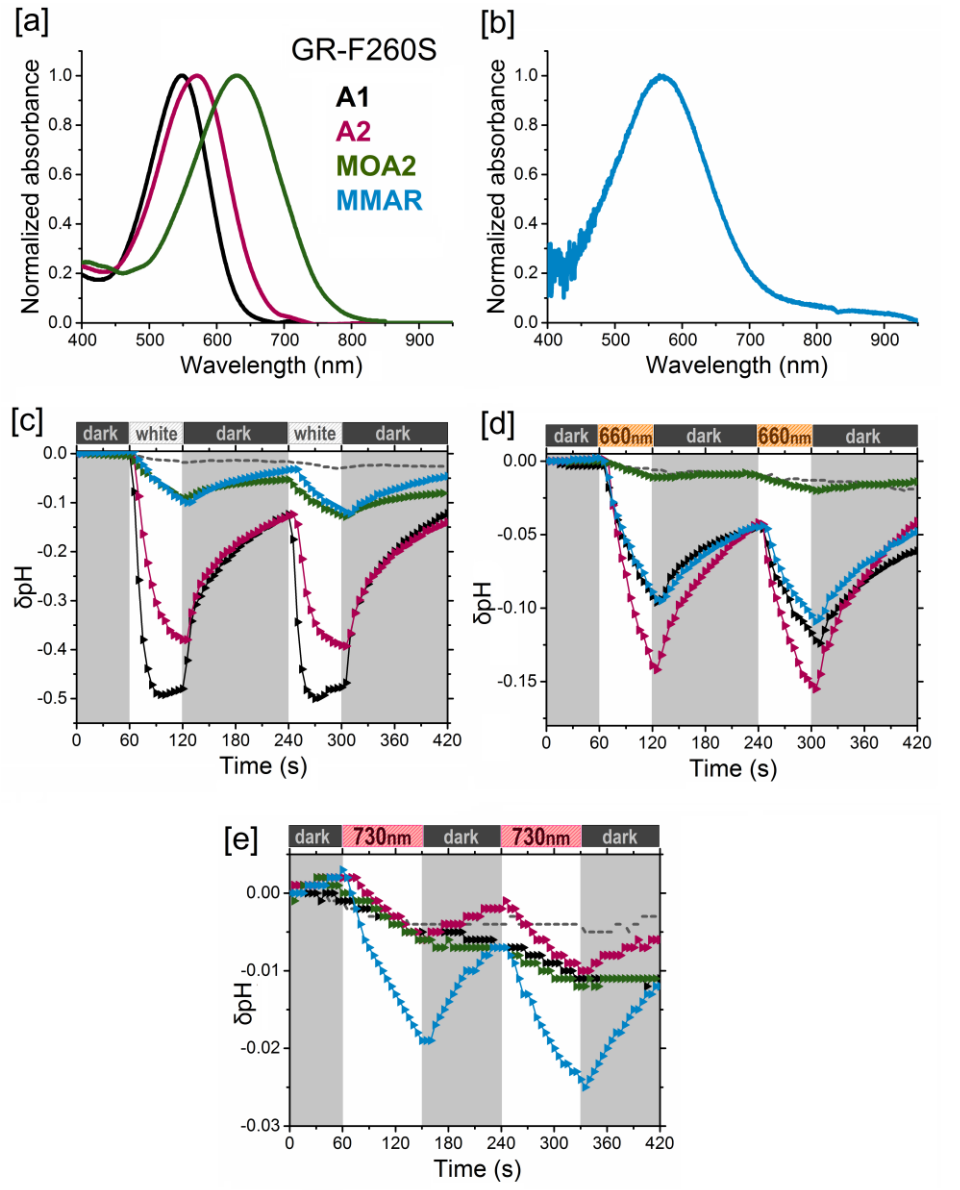

Figure 3.6 Analog pigments of GR-F260S [a] Normalized absorbance spectra of His-tag purified pigments in DDM containing A1 (black), A2 (pink) and MOA2 (green). [b] Hydroxylamine difference spectrum of the MMAR pigment (blue) in membrane vesicles. [c-e] Proton pumping activity of the pigments (same colors) in starved E. coli UT5600 cells upon illumination with white light [c], 660 nm LED [d] and 730 nm LED [e]. Controls are represented as a dashed line.

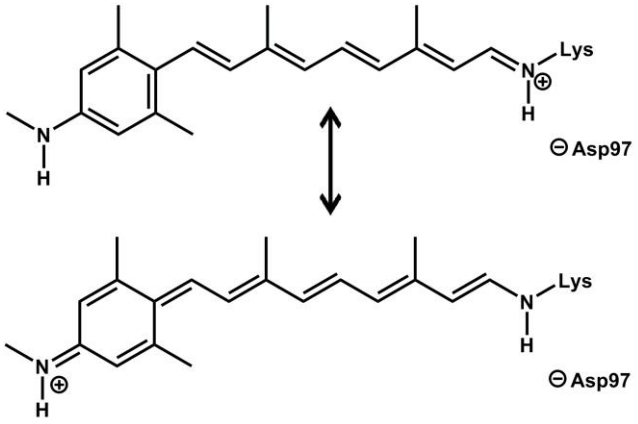

Figure 3.7 Resonance structures of MMAR showing the delocalization of the positive charge from the Schiff-base to the secondary amine. These resonance structures are in a dynamic equilibrium, where the positive charge oscillates between the two nitrogens. Upon averaging over time, this leads to a complex absorption profile with an effective delocalization towards the ring.

Surprisingly, the entire band-shape of this pigment is very sensitive to protonation, presumably of the counterion D97, since acidification led to a strong enhancement of the lower energy bands (Figure 3.8). While MMAR does not appear to have a significant effect on the pKa of the counterion, the charge distribution and electrostatic interactions in the retinal-binding pocket apparently have a strong influence on its spectral properties. For the PR-T101A mutation which is located in the binding pocket, MMAR also induced a red-shift (25 nm), but much smaller than for PR (47 nm), as well as a broad absorbance band extending out to 850 nm, but without the wings observed in PR:MMAR (not shown). We surmise that the exceptional spectral broadening seen in the MMAR pigments may originate from a population of near-degenerate electronic or vibronic transitions, the absorbance cross-section of which apparently strongly depends on the local charge distribution.

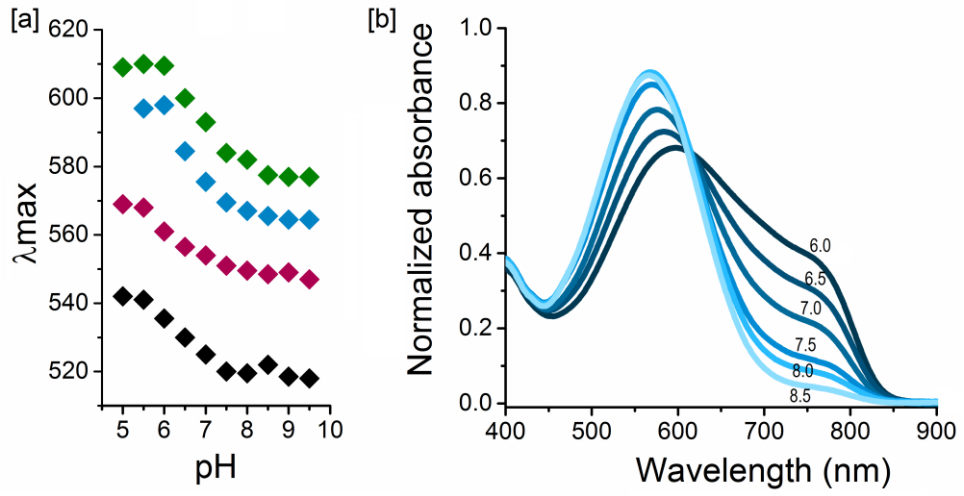

Figure 3.8 Spectral properties of PR pigments depend on pH. [a] Protonation of the counterion D97 in PR red-shifts the absorbance band by 20-30 nm in all pigments tested. PR containing A1 (black), A2 (pink), MOA2 (green) and MMAR (blue). For all pigments the pKa of this transition lies between 6.5 and 7.0. [b] Normalized absorbance spectra of His-tag purified PR:MMAR in DDM solution at pH 6, 6.5, 7, 7.5, 8, 8.5. pH values are indicated next to the corresponding spectrum in the graph. Spectra represent separate samples, not a titration of a single sample.

One distinct possibility is that resonance structures are involved in a dynamic equilibrium, where the positive charge of the Schiff base is more distributed over the π-electron system. An example of potential boundary structures is given in Figure 3.7. Such compounds can exhibit absorbance bands in the deep red to NIR spectral range [16], which can be strongly modulated by the charge distribution in their microenvironment.

The spectral broadening is most strikingly seen in PR-DNFS, where binding of MMAR induced a very large red-shift of about 200 nm, creating a complex modulation of the absorbance band with a broad maximum around 740 nm (Figure 3.4). The band shape here is in fact a mirror image of the one of PR:MMAR, since now the lower energy transitions contribute most strongly to the absorbance band (Figs 3.3, 3.4). The band-shape of PR-DNFS:MMAR also shows some pH dependence, with the hypsochromic

shoulder presenting a congruent red-shift upon acidification and the 740 band somewhat increasing (Appendix A.6). Apparently, the F234S mutation has strongly facilitated this change in band-shape, which can still be further enhanced by acidification. To our knowledge, this is the first report of such a large synergistic spectral shift induced by a retinal analog in an opsin mutant.

The extremely large red-shift in PR-DNFS:MMAR, in combination with the broad trilobal absorbance band, is impressive and unexplained as of yet. However, it is clear that the electronic transitions involved in shaping the PR:MMAR absorbance band are particularly sensitive to the local charge distribution. This was revealed upon counterion protonation in the WT, as well as in the F234S mutant, where both sites are situated in or near the binding pocket (Figures 3.2, 3.4, 3.8). This effect is then expected to be protein-dependent, and in fact the equivalent GR mutant GR-FS:MMAR only displays a moderate 23 nm red shift in λ_{max} with just a long spectral tail extending to 950 nm (Figure 3.6). As mentioned above, a major difference in the binding site between PR and GR is the presence of the F152 near the retinal ring in PR. The Phe-ring may fixate or interact with the aromatic ring of MMAR in such a way as to select or enhance low-energy electronic transitions.

The influence of the local charge environment on its absorbance band thus renders MMAR an excellent candidate for the spectral modulation of microbial rhodopsins. Considering the pumping activity of GR-FS:MMAR and the unique spectral properties of PR-DNFS:MMAR, these analog pigments would make very promising starting materials for further engineering strategies. For instance, the PR-DNFS:MMAR combination may be a good starting point for directed evolution and computational studies so as to improve the pump function or to further red-shift the absorbance band.

Opsin	Retinal analog	λ_{max} nm[a]	H^+ white[c]	H^+ 617 nm[c]	H^+ 660 nm[c]	H^+ 730 nm[c]
PR	A1	520	+++	+	-	-
	A2	552	+++	+++	+	-
	MOA2	585	++	-	nd	nd
	DMAR	558	-	+	nd	nd
	MMAR	567	-	+	+	++
PR-DNFS	A1	540	++	nd	-	-
	A2	566	+	nd	-	+
	MMAR	~740	-	nd	-	++
PR-TA	A1	536	+	nd	+	-
	A2	563	+	nd	+	+
	MMAR	561[b]	-	nd	+	++
GR	A1	540	++++	+++	++	-
	A2	566	++++	++++	**++++**	+
	MOA2	620	++	-	nd	nd
	DMAR	538[b]	+	+	nd	nd
	MMAR	570	+	+	++	++
GR-FS	A1	549	**++++**	**++++**	+++	-
	A2	571	+++	nd	++++	++
	MOA2	630	++	-	-	-
	MMAR	571[b]	+	+	++	**++++**

Table 3.1 Absorbance maxima λ_{max} and proton pumping scores of the analog pigments generated in this study. [a] λ_{max} of purified protein [b] λ_{max} from hydroxylamine difference spectrum in vesicles. [c] proton pumping activity normalized within each light condition to the highest pumping rate measured under that condition (indicated in bold): ++++ : 100-70% ; +++ : 70-40% ; ++ : 40-20% ; + : 20-5% ; - : < 5% ; nd = not determined.

Next to the proton pump function, the MMAR pigments could have an interesting alternative function as a voltage sensor. The D97N mutant of PR:A1 was shown to be a sensitive sensor of the membrane voltage, exhibiting strongly voltage-dependent fluorescence emission that peaks around 700 nm [17]. In preliminary experiments, we observed very strong red-shifted fluorescence of PR-D97N:MMAR peaking around 800 nm (Appendix, Figure A.7). This spectral range would be quite useful for biotechnological and optogenetic applications [18].

3.5 Conclusion

In summary, we have utilized a novel exciting retinal analog in combination with site-directed mutagenesis to generate unique rhodopsin proton-pump variants, which for the first time can be activated by near-infrared light. We thus provide proof of principle for modifying the functionality of such systems beyond their natural paradigm. These novel pigments are suitable starting points for additional modification using directed evolution based methods. Ultimately, this research has important implications for synthetic biology strategies to complement oxygenic photosynthesis [19], and towards (near-infra-)red light activation of biotechnological and optogenetic tools and membrane sensors [17, 20-22].

References

[1] Ort, D. R., et al. "Redesigning photosynthesis to sustainably meet global food and bioenergy demand ", *Proc Natl Acad Sci U S A*, 2015. **112**(28): p. 8529-8536.

[2] Imai, H., Hirano, T., Terakita, A., Shichida, Y., Muthyala, R. S., Chen, R. L., Colmenares, L. U. and Liu, R. S. "Probing for the threshold energy for visual transduction: red-shifted visual pigment analogs from 3-methoxy-3-dehydroretinal and related compounds ", *Photochem Photobiol*, 1999. **70**(1): p. 111-5.

[3] AzimiHashemi, N., et al. "Synthetic retinal analogues modify the spectral and kinetic characteristics of microbial rhodopsin optogenetic tools ", *Nat Commun*, 2014. **5**: p. 5810.

[4] Hubbard, R. "The stereoisomerization of 11-*cis*-retinal ", *J Biol Chem*, 1966. **241**(8): p. 1814-8.

[5] Groenendijk, G. W., Jansen, P. A., Bonting, S. L. and Daemen, F. J. "Analysis of geometrically isomeric vitamin A compounds ", *Methods Enzymol*, 1980. **67**: p. 203-20.

[6] Hubbard, R., Brown, P. K. and Bownds, D. "243 Methodology of vitamin A and visual pigments ", *Methods Enzymol*, 1971. **18, Part C**: p. 615 - 653.

[7] Imasheva, E. S., Balashov, S. P., Choi, A. R., Jung, K. H. and Lanyi, J. K. "Reconstitution of *Gloeobacter violaceus* rhodopsin with a light-harvesting carotenoid antenna ", *Biochemistry*, 2009. **48**(46): p. 10948-55.

[8] Friedrich, T., Geibel, S., Kalmbach, R., Chizhov, I., Ataka, K., Heberle, J., Engelhard, M. and Bamberg, E. "Proteorhodopsin is a light-driven proton pump with variable vectoriality ", *J Mol Biol*, 2002. **321**(5): p. 821-38.

[9] Oesterhelt, D. and Stoeckenius, W. "Rhodopsin-like protein from the purple membrane of Halobacterium halobium ", *Nat New Biol*, 1971. **233**(39): p. 149-52.

[10] Oesterhelt, D. and Hess, B. "Reversible photolysis of the purple complex in the purple membrane of *Halobacterium halobium* ", *Eur J Biochem*, 1973. **37**(2): p. 316-26.

[11] Ganapathy, S., Bécheau, O., Venselaar, H., Frölich, S., van der Steen, J. B., Chen, Q., Radwan, S., Lugtenburg, J., Hellingwerf, K. J., de Groot, H. J. and de Grip, W. J. "Modulation of spectral properties and pump activity of proteorhodopsins by retinal analogues ", *Biochem J*, 2015. **467**(2): p. 333-43.

[12] Smolensky Koganov, E., Hirshfeld, A. and Sheves, M. "Retinal beta-ionone ring-salinixanthin interactions in xanthorhodopsin: a study using artificial pigments ", *Biochemistry*, 2013. **52**(7): p. 1290-301.

[13] Sheves, M., Friedman, N., Rosenbach, V. and Ottolenghi, M. "Preparation of (1,1,5-tri-demetyl)bacteriorhodopsin pigment and its photocycle study ", *FEBS Letters*, 1984. **166**(2): p. 245--247.

[14] Kim, S. Y., Waschuk, S. A., Brown, L. S. and Jung, K. H. "Screening and characterization of proteorhodopsin color-tuning mutations in *Escherichia coli* with endogenous retinal synthesis ", *Biochim Biophys Acta*, 2008. **1777**(6): p. 504-13.

[15] Imai, H., Hirano, T., Terakita, A., Shichida, Y., Muthyala, R. S., Chen, R., Colmenares, L. U. and Liu, R. S. H. "Probing for the threshold energy for visual transducin: red-shifted visual pigment analogs from 3-methoxy-3-dehydroretinal and related compounds ", *Photochem Photobiol*, 1999. **70**(1): p. 111-115.

[16] Liu, R. S. H. and Asato, A. E. "Tuning the color and excited state properties of the azulenic chromophore: NIR absorbing pigments and materials ", *Journal of Photochemistry and Photobiology C: Photochemistry Reviews*, 2003. **4**(3): p. 179-194.

[17] Kralj, J. M., Hochbaum, D. R., Douglass, A. D. and Cohen, A. E. "Electrical spiking in *Escherichia coli* probed with a fluorescent voltage-indicating protein ", *Science*, 2011. **333**(6040): p. 345-8.

[18] Herwig, L., Rice, A. J., Bedbrook, C. N., Zhang, R. K., Lignell, A., Cahn, J. K., Renata, H., Dodani, S. C., Cho, I., Cai, L., Gradinaru, V. and Arnold, F. H. "Directed evolution of a bright near-infrared fluorescent rhodopsin using a synthetic chromophore ", *Cell Chem Biol*, 2017. **24**(3): p. 415-425.

[19] Chen, Q., van der Steen, J. B., Dekker, H. L., Ganapathy, S., de Grip, W. J. and Hellingwerf, K. J. "Expression of holo-proteorhodopsin in Synechocystis sp. PCC 6803 ", *Metab Eng*, 2016. **35**: p. 83-94.

[20] Zhang, F., Vierock, J., Yizhar, O., Fenno, L. E., Tsunoda, S., Kianianmomeni, A., Prigge, M., Berndt, A., Cushman, J., Polle, J., Magnuson, J., Hegemann, P. and Deisseroth, K. "The microbial opsin family of optogenetic tools *", Cell*, 2011. **147**(7): p. 1446-57.

[21] Kushibiki, T., Okawa, S., Hirasawa, T. and Ishihara, M. "Optogenetics: Novel tools for controlling mammalian cell functions with light *", Int J Photoenergy*, 2014. **2014**: p. 1-10.

[22] Ernst, O. P., Lodowski, D. T., Elstner, M., Hegemann, P., Brown, L. S. and Kandori, H. "Microbial and animal rhodopsins: structures, functions, and molecular mechanisms *", Chem Rev*, 2014. **114**(1): p. 126-63.

Chapter 4

A novel chemotaxis-based directed evolution assay

Rational design for protein engineering is difficult, due to a limited structure-function understanding of proteins. Moreover, standard laboratory mutagenesis methods require several days of cloning, culturing and characterization of the corresponding mutants. Directed evolution provides a rapid and efficient alternative to improve the function of specific proteins. Here, we describe the construction of a directed evolution assay to evolve PR and GR to absorb (near-infra) red wavelengths of lights. We use chemotaxis of transformed *Escherichia coli* cells as a screening method to simultaneously select for red-shifted absorbance bands and conserved proton-pumping function of the pigments.

This chapter is under preparation for a manuscript to be submitted for publication by: S. Ganapathy, A. Razumovski, J. B. van der Steen, Q. Chen, H.J.M. de Groot, K.J. Hellingwerf and W.J. de Grip

4.1 Introduction

Protein engineering involves the optimization of the function of a protein outside its native host organism. Though straightforward in aim, it is often challenging in execution. The prediction of amino acid substitutions to modify or improve a protein's function requires detailed structural information and an understanding of the structure-function relationship. Despite this information, it is often impossible to predict *de novo* how a specific protein mutation will affect the overall function of the system. In the case of proton-pumping rhodopsins, mutations will have an impact on both their spectral properties and proton-pumping function. In addition, difficulties inherent in heterologous expression, such as poor yields and thermal stability, often require additional optimization in the novel context. These limitations in rational design have paved the way for alternative high-throughput strategies based on directed evolution.

Directed evolution is a powerful emerging technique in synthetic biology for protein engineering, which mimics natural evolution on a laboratory scale [1]. It is used to rapidly evolve and select several desired properties of a protein, without requiring any prior structural information. There are four main stages in a typical directed evolution cycle (Figure 4.1): (1) generating a library of mutant genes, (2) translation of the mutant protein in a suitable host organism, (3) high throughput screening and selection of desired phenotypes, and (4) replication of the mutant library for further characterization or the next cycle of directed evolution [2]. The screening and characterization of mutants is typically the most time consuming step in standard mutagenesis methods. In a directed evolution approach, this is primarily accomplished by coupling a specific selection criterion or advantage displayed by the host to the desired protein function.

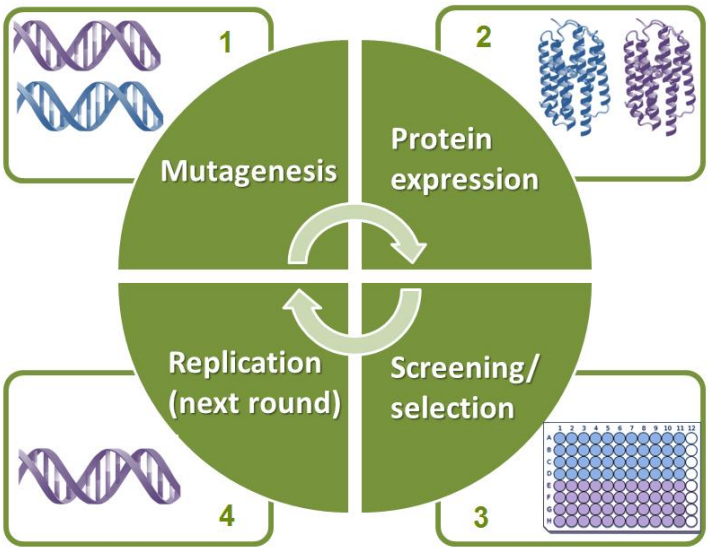

Figure 4.1 A simplified overview of the four main stages in a directed evolution cycle. All or most steps are performed in a suitable host organism.

The research aim of this chapter is the development of a directed evolution assay to rapidly evolve and select near-infra red absorbing functional variants of PR and GR. We utilized a mutagenesis plasmid [3] to generate an *in situ* library of mutations in the opsin, and further tested a number of screening strategies to simultaneously select for spectral shifts and proton-pumping activity of these mutants, using *E. coli* as a model organism for selection. Our results show that bacterial chemotaxis provides a reliable selection method when coupled with respiratory inhibition with better prospects than conventional growth or survival based assays. We thus present our design for a novel chemotaxis-based directed evolution assay for the laboratory scale evolution of rhodopsin proton-pumps.

4.2 Experimental section

The sources of special chemicals are presented in the Appendix (A.1). All chemicals are of the highest purity available.

4.2.1 Cell lines and constructs

E. coli K-12 strain MG1655 was used in this study, since it contains a deletion of the iscS gene. This deletion introduces a respiratory deficiency [4], which is explained later in this chapter. It was transformed with the plasmids pJBS1255 or pJBS1257 which encode a 6x-His tagged PR or GR opsin, respectively, driven by the inducible P_{trc} promoter, constructed as described elsewhere [5, 6]. This strain was further transformed with a mutagenesis plasmid (MUT) [3], which encodes the DNA polymerase double negative proofreading subunit dnaQ926 and error-prone repair DNA polymerase V, under control of the arabinose inducible promoter. The antibiotic resistance of the strains and plasmids used is as follows: chloramphenicol (ΔiscS), kanamycin (pJBS1255 and pJBS1257), spectinomycin (MUT).

4.2.2 Cell culturing

An overnight culture was grown in LB medium at 37 °C for 24-36 hours with appropriate antibiotic selection. The culture was diluted 1:50 times to obtain a 25 mL working culture in LB, which was grown till an OD_{600} of 0.3 and induced with 0.5 mM IPTG, 20 μM retinal and 0.1% arabinose. No retinal and arabinose were added to the controls. The cultures were further grown for 24-36 hours at 37°C and were finally spun down at 3700xg for 20 min. For the growth curve experiments, the OD_{600} of the culture was measured every hour with appropriate dilutions. The cultures were illuminated after induction with white light resulting in a photon flux of 300-400 μE.m-2.s-1.

4.2.3 Treatment with sodium azide

The cell pellet was washed once and resuspended in an equal volume of starvation buffer (SB) containing 250 mM KCl, 10 mM NaCl, 10 mM $MgSO_4$, 100 μM $CaCl_2$, 10 mM Tris-HCl at pH 7, and incubated overnight at RT with

continuous mixing. The following day, the cells were spun down at 3700xg for 20 minutes and washed once with an equal volume of SB. The cell pellet was finally resuspended in 25 mL of SB supplemented with 30 mM sodium azide (SBAz), and incubated at RT for 1 h with continuous mixing. The cells were diluted to an OD_{600} of 1.5 and directly used in the chemotaxis assay.

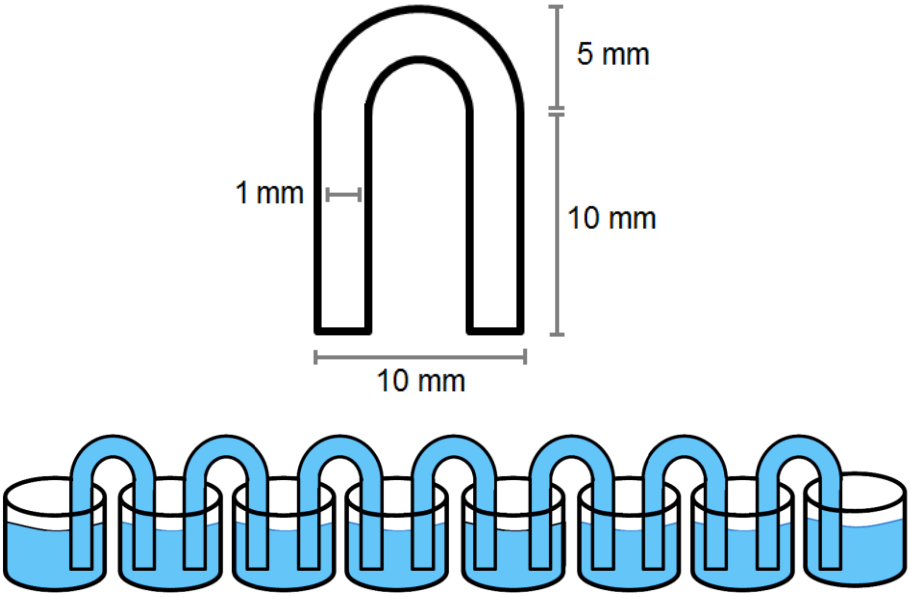

Figure 4.2 Dimensions of the U-shaped glass capillary tubes used for the chemotaxis assay and side-view of the capillaries connecting adjacent wells in a microplate.

4.2.4 Chemotaxis assay

The chemotaxis setup consists of a 96 well microplate where adjacent wells are bridged by U-shaped custom made glass capillary tubes, having an inner diameter of 1 mm, and the outer dimensions shown in figure 4.2. For initial testing and standardization of the assay, 5 wells were connected in tandem, as shown in figure 4.4. Then, 0.3 mL of the azide treated cells were loaded in well-1. Wells 2-5 were filled with 0.3 mL of 2.5, 10, 50 and 200 mM of L-serine in SBAz. The plates were sealed with a plastic cover

containing holes for the capillaries to pass through. Capillaries 1-4 were completely filled with 1, 5, 25 and 100 mM L-serine in SBAz and inserted into the wells to generate a gradient of serine, as shown in figure 4.4. The plate was illuminated for 6-10 hours from above and below with 300-800 nm white light having a photon flux of 1500 $\mu E.m^{-2}.s^{-1}$, either unfiltered or provided with 590 nm long-pass filters (OG590, Schott) resulting in a photon flux of 500 $\mu E.m^{-2}.s^{-1}$.

4.2.5 Plating of migrated colonies

After illumination, the entire content of wells 3-5 along with the previous capillary was mixed with 0.2 mL of LB medium and plated on separate LB-agar plates. The content of well-2 was diluted 10,000 times and a 0.1 mL aliquot was plated with 0.2 mL LB. The LB-agar plates were incubated at 37°C for 2-3 days, following which the number of single colonies obtained were counted as colony forming units (cfu).

4.2.6 Analysis of mutations

Individual colonies were picked using sterile toothpicks and inoculated into 5 ml LB with antibiotic selection, and grown at 37°C overnight. The following day the cultures were spun down and the total plasmid content was isolated using the QIAGEN miniprep plasmid isolation kit. The isolated plasmids were transformed into chemically competent *E. coli* XL10 to obtain a single copy of pJBS1255 or pJBS1257 per cell. The obtained colonies were cultured and used for sequencing and further characterization of the isolated mutants.

4.3 Results

4.3.1 Characterization of cell lines used and their growth rate

E. coli MG1655 Δ*isc*S, a respiratory restricted cell line, was co-transformed with two plasmids, (1) the arabinose inducible MUT which increases the error-rate during DNA replication, and (2) either pJBS1255 or pJBS1257, which encode for IPTG inducible PR or GR respectively. The controls PR_{CTRL} and GR_{CTRL} were induced with IPTG alone to generate the opsin. The wild type holo-proteins PR_{WT} and GR_{WT} were generated upon induction with IPTG and supplementation with retinal. Induction with IPTG, retinal and arabinose led to the generation of PR_{MUT} and GR_{MUT}, containing various random mutations in the opsin gene. These could be assessed by sequencing the pJBS plasmids, and could even be observed as a difference in the colour of the cell pellets (data not shown).

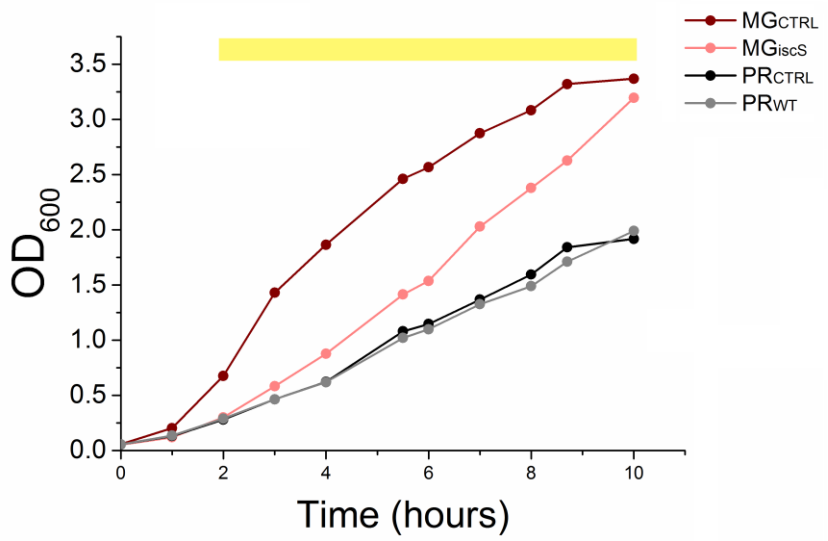

Figure 4.3 Representative growth curve of the following cell lines in LB medium at 37°C: *E. coli* MG1655 (MG_{CTRL}), *E. coli* MG1655 ΔiscS (MG_{ISCS}), *E. coli* MG1655 ΔiscS-pJBS1255-MUT induced with IPTG (PR_{CTRL}) or with IPTG and retinal A1 (PR_{WT}). The yellow bar indicates the start of induction and illumination with white light. Data is presented as an average of 3 trials; standard error is less than 1%.

We explored the possibility of using the growth of *E. coli* as a selection criterion, guided by the notion that cells can utilize the pmf generated by PR/GR for growth, especially during conditions of respiratory distress. The cells were grown in LB medium and their growth rate was assessed every hour by measuring the OD_{600} with appropriate dilutions. The doubling time of *E. coli* MG1655 Δ*isc*S was found to be around 40 minutes at 37°C, which is about twice the doubling time of WT MG1655 (Figure 4.3). In order to assess the impact of PR or GR expression upon their growth rate, the *E. coli* cultures were illuminated with white light after induction. However, no clear difference was observed between PR_{CTRL}/GR_{CTRL} and PR_{WT}/GR_{WT}, as shown in figure 4.3. We then utilized the respiratory inhibitor sodium azide, in combination with the Δ*isc*S mutation. The cells were strongly retarded in growth upon azide treatment, even at concentrations as low as 1 mM. Again, the growth rate of the controls and PR_{WT}/GR_{WT} were similar (data not shown). These data indicate that the pmf generated by PR/GR is insufficient to rescue the growth deficit prompted by respiratory inhibition. Since selection based on growth is clearly not an optimal strategy, we decided to pursue other alternatives.

We were prompted by a recent study, which showed that the pmf dependent rotation of the *E. coli* flagellar motor could be inhibited by azide treatment, but was rescued upon activation of PR [7]. The rotation of the flagellar motor enables the "swimming" of *E. coli* towards an attractant or away from a repellant, termed as bacterial chemotaxis. We thereby decided to test the possibility of using chemotaxis as a screening method in the directed evolution of PR and GR. The amino acid serine was selected as a potent chemo-attractant [8, 9].

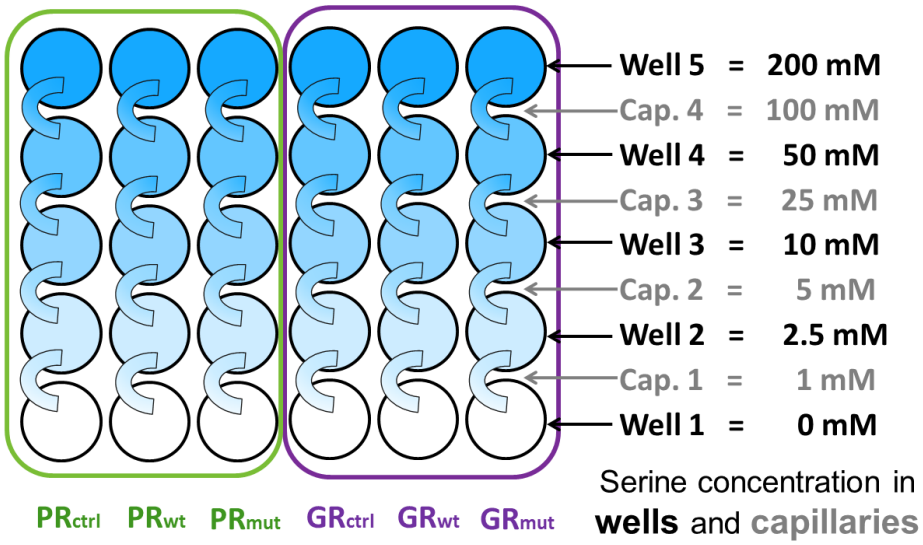

Figure 4.4 Illustration of a chemotaxis assay in which 5 adjacent wells are bridged with U-shaped capillary tubes, generating a continuous gradient of serine. The azide treated cells are loaded in well-1. *E. coli* MG1655 Δ*isc*S containing the plasmids MUT and pJBS1255 or pJBS1255, which encode for PR or GR respectively, were induced with IPTG (PR_{ctrl}, GR_{ctrl}), IPTG and retinal (PR_{wt}, GR_{wt}) or IPTG, retinal and arabinose (PR_{mut}, GR_{mut}).

4.3.2 Design of a novel chemotaxis assay

We applied a conventional 96-well microplate for the chemotaxis assay using glass capillaries to bridge adjacent wells, thereby maintaining a continuous liquid interface. These U-shaped glass capillary tubes containing an inner diameter of 1 mm were custom-made for this experiment (Figure 4.2). We first decided to test the feasibility of this assay on a small scale by bridging 5 microplate wells in tandem. This assay was optimized for the length of the capillary tubes, the serine gradient, duration of chemotaxis, duration of starvation and starting OD_{600} of cells used to achieve the maximum migration potential of PR_{WT} and GR_{WT}. The following protocol was developed under white-light illumination, and yielded consistent data providing good discrimination between control cells and cells containing active PR or GR.

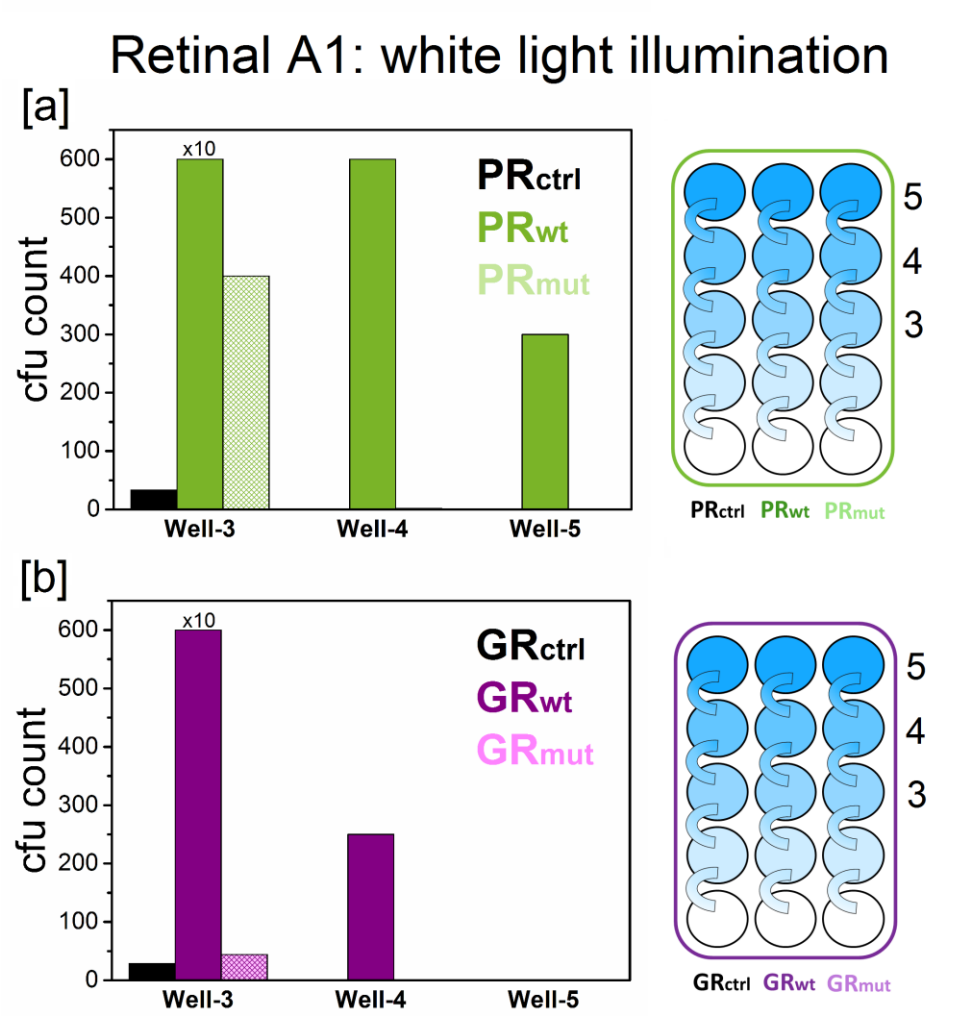

Figure 4.5 Cfu counts of migrated *E. coli* MG1655 Δ*iscS* cells expressing PR [a] or GR [b] from a representative 6 hours chemotaxis experiment under white light illumination (300-800 nm). The PR_{WT} and GR_{WT} bars for well-3 have been reduced tenfold to fit in the figure.

E. coli MG1655 Δ*iscS* cells expressing MUT and PR or GR were starved for a day in SB, followed by treatment with 30 mM azide for an hour, in order to thoroughly disrupt cellular pmf. These cells were diluted to an OD_{600} of 1.5 using a dilution curve, and then pipetted into well-1. The remaining wells and capillaries were filled with different concentrations of serine, to

generate a gradient over 5 wells, as shown in figure 4.4. The setup was illuminated for 6-10 hours and the contents of the wells were immediately plated on LB-agar. The individual colony forming units (cfu) were counted, which each represent a single migrated *E. coli* cell.

We found that PR_{WT} migrated significantly further along the serine gradient than PR_{CTRL} all the way to well-5, as seen from the cfu counts in figure 4.5. This trend was also seen to a smaller extent with GR_{WT}, which migrated till well-4. These findings were mirrored across all trials with white light illumination, indicating that the azide inhibition of chemotaxis can indeed be rescued by the pmf generated by PR and GR. However varying results were obtained for PR_{MUT} and GR_{MUT} across several trials. Overall, the mutant population was not able to migrate as far as the population with wild type. In the representative experiment shown in figure 4.5, very little migration was seen beyond well-3 for GR_{MUT} and PR_{MUT}, though their cfu counts were still higher than the controls. This is not unexpected, since the random mutagenesis process will reduce the viability of a significant part of the cell population under white-light illumination. Therefore, we decided to further test the feasibility of this assay with retinal analogs and selection with progressively red-shifted light regimes in order to confer a better selection advantage towards mutants with red-shifted rhodopsins.

4.3.3 Selection for red-shifting mutations

Retinal A2 is a promising retinal analog investigated in chapters 2 and 3 of this thesis, which generated ~40 nm bathochromic shifts in the action spectrum of both PR and GR. We thereby generated A2 pigments of PR and GR and tested them in the chemotaxis assay using illumination through 590 nm long-pass filters (590-800 nm light regime). In this case the light intensity is roughly three times lower than with the white light illumination trials, due to which the overall migration rates are lower. A representative trial is displayed in figure 4.6.

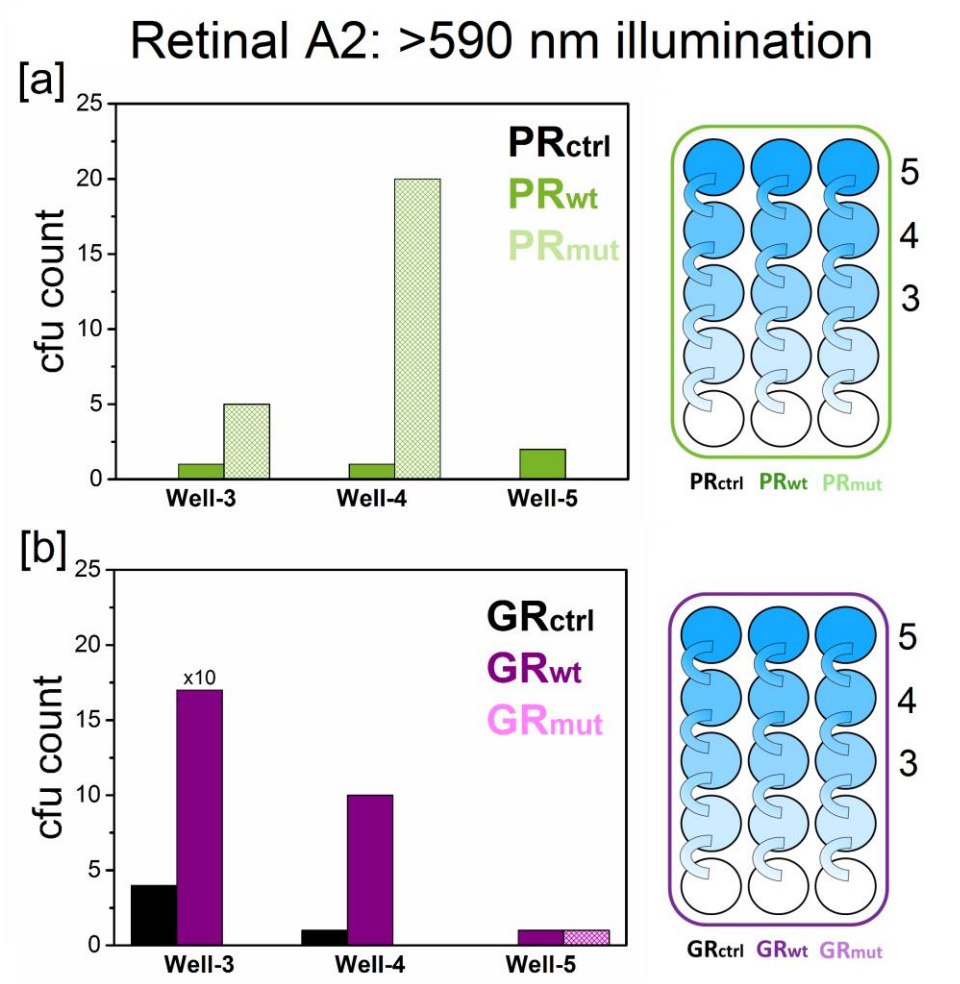

Figure 4.6 Cfu counts of migrated *E. coli* MG1655 ΔiscS cells expressing A2 pigments of PR [a] or GR [b] from a representative chemotaxis experiment, after 10 hours of 590-800 nm illumination. The GR_{WT} bar for well-3 has been reduced tenfold to fit in the figure.

Under these red-light conditions the PR_{CTRL} cells even did not reach well-3, and PR_{WT} performed less well than under white-light. However, now PR_{MUT} migrated significantly better compared to PR_{WT}. On the other hand, GR showed a trend similar to the white light illumination trials, except that some GR_{MUT} cells now managed to migrate till well-5. The individual PR_{MUT} and GR_{MUT} colonies from wells-4 and 5 were cultured and analyzed. Initial

results indicate that some of these cells indeed have generated rhodopsins with red-shifted absorbance bands (data not shown), which require further characterization.

4.4 Discussion

4.4.1 Towards a directed evolution approach

Site-directed mutagenesis is the most common method used to introduce a desired mutation at a point of interest on a gene [10]. As described earlier in this thesis, we utilized mis-match PCR to generate several site-directed mutants of PR and GR listed in the Appendix A.6. However, this approach is painstaking, requiring several days of cloning to introduce, verify, and test a specific mutation. Faster techniques such as CRISPR have now become available, which are widely used for rapid *in situ* genome editing in host organisms [11]. Site-saturation mutagenesis is another popular approach, which has the advantage of sampling all possible amino-acid substitutions at a given site [12]. This method has been employed to spectrally modulate GR by targeting residues in the retinal-binding pocket [13]. Random mutagenesis using error prone PCR has also been used to generate red and blue shifted PR mutants [14]. These different *in vitro* mutagenesis protocols have been successful in generating a handful of PR and GR mutants with variable red-shifts (5-30 nm) in absorbance maximum [13-16]. However, a common drawback in all these methods is the substantial to complete loss in proton-pumping activity of the mutants. So far the F260S mutation in GR, described in chapter 3 (9 nm red-shift) is the only one retaining full activity. Hence, a directed evolution assay, including a random mutagenesis protocol and a tight screen on both spectral properties and pump activity would be very welcome. We reasoned that the additional pmf and ATP provided by an active proton pump could be a solid basis for such a screen, and should be combined with a plasmid inducibly suppressing DNA proofreading activity.

4.4.2. Testing growth as a selection criterion

Various studies have shown that the light-induced pmf generated by proteorhodopsins can drive ATP production *in vivo* [17, 18], and it was speculated that this ATP can utilized for the growth and survival of host organisms [19, 20]. Such a growth or survival advantage can be exploited as a convenient selection criterion in designing a directed evolution setup. However, in initial experiments, little stimulatory effect of PR expression was found upon the aerobic growth of *E. coli* (Figure 4.3). This finding was mirrored by previous studies both in *E. coli* [21] and native hosts [22]. These experiments indicate that the pmf induced by PR is largely overshadowed by the endogenous pmf generated by the *E. coli* respiratory chain. PR did, however, contribute towards the growth of *E. coli* [21] or its native host *Vibrio* sp. [23] under anaerobic conditions or nutrient limitation. We thereby decided to use a strain of *E. coli* with compromised respiration, namely *E. coli* MG16555 Δ*isc*S.

Deletion of the *isc*S gene was shown to affect the formation of Fe-S clusters, which in turn impacts electron transport and pmf generation via the respiratory complexes [24, 25]. We found that *E. coli* MG16555 Δ*isc*S grew slower than its WT counterpart showing an elongated lag phase and 40 minute doubling time in agreement with what was reported previously [25]. Another study reported that *E. coli* lacking *isc* displays a pmf-dependent gentamycin resistance phenotype, which could be reversed upon PR expression [4]. We hypothesized that activation of PR or GR would also be able to reverse the growth defect induced by Δ*isc*S. However, stimulation of PR_{WT} or GR_{WT} with white light illumination did not appear to confer any significant growth advantage to the cells, indicating that the respiratory inhibition of Δ*isc*S may be insufficient for PR/GR to provide a distinct advantage. Therefore, we exerted additional respiratory pressure on the cells using the poison sodium azide, which has multiple cellular effects, including inhibition of cytochrome oxidase and of the H^+-ATPase

complex [26, 27]. Azide is a very potent poison and indeed very little growth was observed in control cells at concentrations over 1 mM (not shown). This growth inhibition persisted upon expression and activation of PR/GR. These findings indicate that the pmf generated by PR/GR is insufficient to rescue growth defects due to severe respiratory distress. Consequently, we explored other options.

4.4.3.1 Chemotaxis as a selection criterion

The rotation of the flagellar motor in *E. coli* is another important cellular process powered by pmf [28], which drives the movement of the cell towards or away from a chemical source. In the absence of a chemical gradient, *E. coli* exhibits random swimming behavior consisting of alternate "runs" and "tumbles". Upon applying a chemical gradient, the cells modulate their tumbling frequency to swim towards a chemoattractant or away from a chemorepellant [29], termed as chemotaxis. A recent study showed that the rotation of the *E. coli* flagellar motor could be inhibited by treatment with azide, but could be rescued by expression and activation of PR [7]. Based on these findings, we conceived the idea of using bacterial chemotaxis towards a chemoattractant in energy-depleted cells as a potential selection criterion. We were inspired by the pioneering work of Julius Adler to measure and quantify bacterial chemotaxis using capillary tubes [30, 31], showing that bacteria brought into contact with a capillary filled with a chemoattractant will readily migrate into the tube. We adapted this concept using U-shaped glass capillary tubes and converted a conventional 96 well microplate into a chemotaxis screening set-up. Serine was selected as a chemoattractant in our assay, since it is very potent and has been commonly employed to measure and quantify chemotaxis in *E. coli*. [8, 9]. A pre-determined step-gradient of serine was filled in the capillaries and wells, which would produce a more or less continuous gradient by diffusion. The migratory rate of healthy *E. coli* cells towards serine is reported to be between 15-20 $\mu m.s^{-1}$ [8]. Given the dimensions of

the capillaries used and the starvation of the cells, we estimated that the distance between 5 wells could be covered in 5-6 hours under high-intensity white light illumination, while requiring longer time-spans with low-intensity NIR illumination.

4.4.3.2 Potential of the developed chemotaxis assay

E. coli MG16555 Δ*iscS* transformed with MUT and PR/GR was selectively induced to generate CTRL, WT and MUT cells. All cell populations were energy depleted for a day by starvation and treatment with 30 mM azide. The cells were loaded in the chemotaxis assay and allowed to migrate under illumination through the capillaries following the serine gradient. Plating the contents of the wells at the end of the assay and counting the individual cells allowed us to determine how far and how many cells had migrated in the setup. We observed that under white light illumination, PR_{WT} cells indeed were able to reach well-5 in about 6 hours. Importantly, we found that under white light illumination, PR_{WT} and GR_{WT} migrated substantially further than their corresponding controls assayed without retinal supplementation, consistently across several trials.

The assay showed excellent discriminatory potential. Out of the about 10^9 cells in the starting cells, only several tens of control cells made it into well-3, while for PR_{WT} and GR_{WT} this number varied between 5-10 x 10^3. In fact, up to several tens of the latter cells could reach well-5. Not unexpectedly, both PR_{MUT} and GR_{MUT} showed impaired migration as compared to PR_{WT} and GR_{WT}. Induction of MUT, which suppresses proof-reading and enhances error-prone lesion bypass, would generate a diverse library of non-specific mutations [3]. In this case it is impossible to exclude the possibility of mutations in the bacterial genome, which could impair chemotactic migration, or generate non-functional mutations of the PR/GR gene. This would decrease the viability of a significant part of the cell population and should account for the lower migration seen for the mutant population,

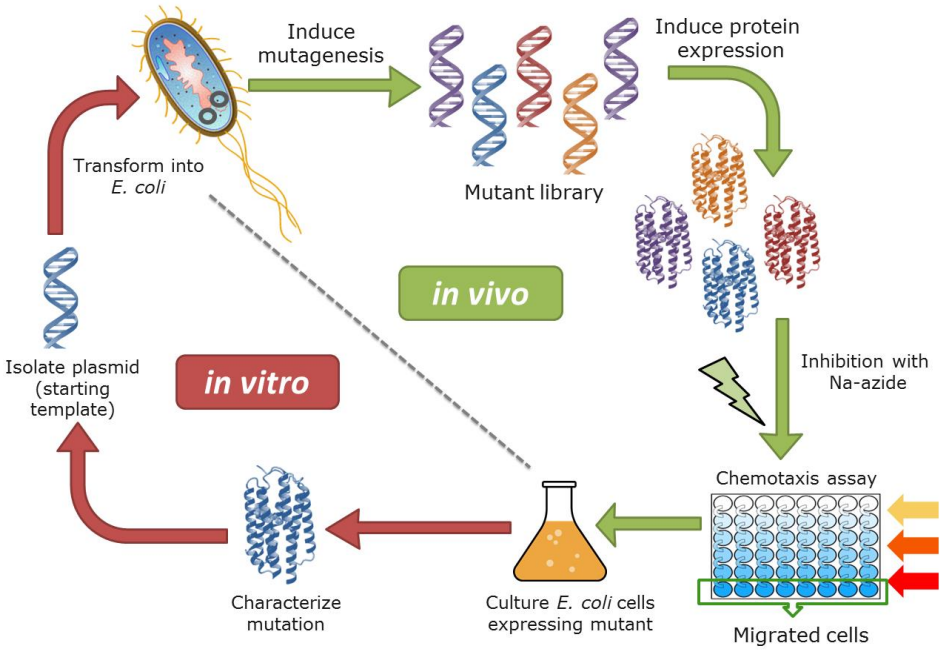

Figure 4.7 A schematic of the developed directed evolution assay using chemotaxis

Nonetheless, we were bolstered by the fact that GR_{MUT} and PR_{MUT} in particular showed better migration as compared to the corresponding controls. Hence, we proceeded to the planned assay conditions, starting with red-light illumination (>590 nm). In a first test, we additionally used the red-shifting analog A2 as a chromophore (c.f. chapters 2 and 3). In view of its absorbance spectrum, peaking at 552 nm (c.f. chapter 3), the A2 pigment of PR_{WT} migrated less well than under white light as expected. However, now the A2 pigment of GR_{WT} showed improved migration relative to PR_{WT}, most likely due to its more red-shifted action spectrum, and yielded a distribution pattern over the wells quite similar to that under white-light illumination. Most importantly, a very positive result was that A2 pigments of PR_{MUT} showed a substantial improvement in migration as compared to PR_{WT}. Preliminary characterization of these migrated cells indeed gave evidence for the presence of red-shifted action spectra.

4.4.3.3. Prospects of the chemotaxis assay

The red-light screen described above should be repeated several times to sample as many positive mutants as possible, in view of the random character of the mutagenesis process. Promising mutants will be subjected to additional screens with further red-shifted photons (> 650 nm). If sufficient intensity can be attained in the 650-800 nm range (> 1000 $\mu E.cm^{-2}.s^{-1}$), the assay will also be performed with MMAR as a ligand (c.f. chapter 3), aiming at further enhancing the NIR absorbance band and increasing the proton pumping activity.

4.5 Conclusion

In summary, we designed a novel assay, which uses bacterial chemotaxis as a selection criterion in a directed evolution scheme (Figure 4.7). This assay was aimed towards the evolution of red-shifted rhodopsin proton-pumps, which have much potential as synthetic biology tools and for various nanobiotechnological devices [32]. The developed assay shows strong discriminatory power, and in principle, can be easily modified to evolve other cellular systems dependent on illumination, energy or transport.

References

[1] Cobb, R. E., Sun, N. and Zhao, H. "Directed evolution as a powerful synthetic biology tool ", *Methods*, 2013. **60**(1): p. 81-90.

[2] Packer, M. S. and Liu, D. R. "Methods for the directed evolution of proteins ", *Nat Rev Genet*, 2015. **16**(7): p. 379-394.

[3] Esvelt, K. M., Carlson, J. C. and Liu, D. R. "A system for the continuous directed evolution of biomolecules ", *Nature*, 2011. **472**(7344): p. 499-503.

[4] Ezraty, B., Vergnes, A., Banzhaf, M., Duverger, Y., Huguenot, A., Brochado, A. R., Su, S. Y., Espinosa, L., Loiseau, L., Py, B., Typas, A. and Barras, F. "Fe-S cluster biosynthesis controls uptake of aminoglycosides in a ROS-less death pathway ", *Science*, 2013. **340**(6140): p. 1583-7.

[5] Chen, Q., van der Steen, J. B., Dekker, H. L., Ganapathy, S., de Grip, W. J. and Hellingwerf, K. J. "Expression of holo-proteorhodopsin in Synechocystis sp. PCC 6803 ", *Metab Eng*, 2016. **35**: p. 83-94.

[6] Chen, Q., Arents, J., Ganapathy, S., de Grip, W. J. and Hellingwerf, K. J. "Functional expression of Gloeobacter rhodopsin in *Synechocystis* sp. PCC6803 ", *Photochem Photobiol*, 2017. **93**(3): p. 772-781.

[7] Walter, J. M., Greenfield, D., Bustamante, C. and Liphardt, J. "Light-powering *Escherichia coli* with proteorhodopsin ", *Proc Natl Acad Sci U S A*, 2007. **104**(7): p. 2408-12.

[8] Vuppula, R. R., Tirumkudulu, M. S. and Venkatesh, K. V. "Chemotaxis of *Escherichia coli* to L-serine ", *Phys Biol*, 2010. **7**(2): p. 026007.

[9] Mesibov, R. and Adler, J. "Chemotaxis toward amino acids in *Escherichia coli* ", *J Bacteriol*, 1972. **112**(1): p. 315-26.

[10] Ling, M. M. and Robinson, B. H. "Approaches to DNA mutagenesis: an overview ", *Analytical biochemistry*, 1997. **254**(2): p. 157-78.

[11] Hsu, P. D., Lander, E. S. and Zhang, F. "Development and Applications of CRISPR-Cas9 for Genome Engineering ", *Cell*, 2014. **157**(6): p. 1262-1278.

[12] Reetz, M. T. and Carballeira, J. D. "Iterative saturation mutagenesis (ISM) for rapid directed evolution of functional enzymes ".

[13] Engqvist, M. K., McIsaac, R. S., Dollinger, P., Flytzanis, N. C., Abrams, M., Schor, S. and Arnold, F. H. "Directed evolution of *Gloeobacter violaceus* rhodopsin spectral properties ", *J Mol Biol*, 2015. **427**(1): p. 205-20.

[14] Kim, S. Y., Waschuk, S. A., Brown, L. S. and Jung, K. H. "Screening and characterization of proteorhodopsin color-tuning mutations in *Escherichia coli* with endogenous retinal synthesis ", *Biochim Biophys Acta*, 2008. **1777**(6): p. 504-13.

[15] Maiti, T. K., Yamada, K., Inoue, K. and Kandori, H. "L105K Mutant of Proteorhodopsin ", *Biochemistry*, 2012. **51**(15): p. 3198-3204.

[16] Yamada, K., Kawanabe, A. and Kandori, H. "Importance of alanine at position 178 in proteorhodopsin for absorption of prevalent ambient light in the marine environment ", *Biochemistry*, 2010. **49**(11): p. 2416-23.

[17] Martinez, A., Bradley, A. S., Waldbauer, J. R., Summons, R. E. and DeLong, E. F. "Proteorhodopsin photosystem gene expression enables photophosphorylation in a heterologous host ", *Proc Natl Acad Sci U S A*, 2007. **104**(13): p. 5590-5.

[18] Lee, K. A. and Jung, K.-H. "ATP Regeneration System Using *E. coli* ATP Synthase and *Gloeobacter* Rhodopsin and Its Stability ", *J Nanosci Nanotechnol*, 2011. **11**(5): p. 4261-4264.

[19] Beja, O., Spudich, E. N., Spudich, J. L., Leclerc, M. and DeLong, E. F. "Proteorhodopsin phototrophy in the ocean ", *Nature*, 2001. **411**: p. 786-789.

[20] Gómez-Consarnau, L., González, J. M., Coll-Lladó, M., Gourdon, P., Pascher, T., Neutze, R., Pedrós-Alió, C. and Pinhassi, J. "Light stimulates growth of proteorhodopsin-containing marine Flavobacteria ", *Nature*, 2007. **445**(7124): p. 210-213.

[21] Wang, Y., Li, Y., Xu, T., Shi, Z. and Wu, Q. "Experimental evidence for growth advantage and metabolic shift stimulated by photophosphorylation of proteorhodopsin expressed in *Escherichia coli* at anaerobic condition ", *Biotechnol Bioeng*, 2015. **112**(5): p. 947-56.

[22] Walter, J. M., Greenfield, D. and Liphardt, J. "Potential of light-harvesting proton pumps for bioenergy applications ", *Curr Opin Biotechnol*, 2010. **21**(3): p. 265-70.

[23] Gómez-Consarnau, L., Akram, N., Lindell, K., Pedersen, A., Neutze, R., Milton, D. L., González, J. M. and Pinhassi, J. "Proteorhodopsin phototrophy promotes survival of marine bacteria during starvation *", PLoS Biol*, 2010. **8**(4): p. e1000358.

[24] Schwartz, C. J., Djaman, O., Imlay, J. A. and Kiley, P. J. "The cysteine desulfurase, IscS, has a major role in in vivo Fe-S cluster formation in *Escherichia coli", Proc Natl Acad Sci U S A*, 2000. **97**(16): p. 9009-14.

[25] Lauhon, C. T. and Kambampati, R. "The iscS gene in Escherichia coli is required for the biosynthesis of 4-thiouridine, thiamin, and NAD *", J Biol Chem*, 2000. **275**(26): p. 20096-103.

[26] Noumi, T., Maeda, M. and Futai, M. "Mode of inhibition of sodium azide on H+-ATPase of Escherichia coli *", FEBS Letters*, 1987. **213**(2): p. 381-384.

[27] Lichstein, H. C. and Soule, M. H. "Studies of the effect of sodium azide on microbic growth and respiration: II. The action of sodium azide on bacterial catalase *", J Bacteriol*, 1944. **47**(3): p. 231-8.

[28] Gabel, C. V. and Berg, H. C. "The speed of the flagellar rotary motor of Escherichia coli varies linearly with protonmotive force *", Proc Natl Acad Sci U S A*, 2003. **100**(15): p. 8748-51.

[29] Vladimirov, N. and Sourjik, V. "Chemotaxis: how bacteria use memory *", Biological chemistry*, 2009. **390**(11): p. 1097-104.

[30] Adler, J. "Chemoreceptors in Bacteria *", Science*, 1969. **166**: p. 1588-1597.

[31] Adler, J. "Chemotaxis in Bacteria *", Annu. Rev. Biochem.*, 1975. **44**: p. 341-356.

[32] Wagner, N. L., Greco, J. A., Ranaghan, M. J. and Birge, R. R. "Directed evolution of bacteriorhodopsin for applications in bioelectronics *", J R Soc Interface*, 2013. **10**(84).

Chapter 5

The effect of a detergent or lipid microenvironment on the properties of PR and GR

The insoluble nature of membrane proteins presents a major drawback in their structural and functional investigation, since they require excessive solubilization by detergents and subsequent purification steps. The choice of detergent is important, as the surfactant environment often affects the stability, oligomeric assembly, and activity of the resulting protein. We compared the efficacy of several commonly used detergent systems on the solubilization and stabilization of wild type PR and GR. We further investigated the spectral properties, stability and oligomeric distribution of the resulting pigment-detergent complexes. The pressure and membrane potential has an impact both on the structure and dynamics of intrinsic membrane proteins. For this reason, various membrane mimetic systems have been put forward, which allow these pigments to be studied in a near-native-like lipid environment. We investigate the properties of PR and GR in different open and closed bilayer systems, namely nanodiscs and liposomes. Finally, we present examples of the structural and functional studies made possible by using such native-like membrane systems.

5.1 Introduction

Membrane proteins account for roughly 30% of all gene transcripts, yet they make up less than 0.5% of the solved protein structures in the protein data bank. This presents a serious bottleneck, given that these proteins are integral to cellular life and are responsible for a wide range of functions ranging from cell to cell communication to signal transduction and ionic transport. The scientific community has invested much effort to overcome the difficulties inherent in the isolation and characterization of these insoluble proteins. Due to multiple membrane spanning domains, these proteins usually require amphipathic molecules for their extraction from the membrane. Solubilization by detergent micelles is the most popular method of choice, and is particularly useful for their initial biophysical characterization (Figure 5.1). The detergent DDM is among the most widely used detergent for the solubilization of membrane proteins, since it has relatively minor deleterious effects on structure and stability of most membrane proteins, thereby behaving as a very mild detergent. In the previous chapters, we have primarily used DDM micelles to solubilize and purify the pigment complexes that were generated. However, some novel variants like GR-FS:MMAR have low thermal stability even in DDM, confirming that protein and ligand engineering affect the structure and stability of the pigment-micelle complex. Hence, it is usually preferable to transfer purified membrane proteins in detergent solution back into a native-like membrane mimicking environment. Towards this end, various phospholipid bilayer systems such as proteoliposomes and nanodiscs (Figure 5.1) have been developed to stabilize these pigments, allowing their properties to be studied in a native-like membrane environment.

Proteoliposomes are commonly used for vectorial studies, and in the solid-state NMR investigation of protein structure [1, 2]. However, due to the light scattering induced by their large size (200 nm-10 um diameter), they are less suitable for optical studies.

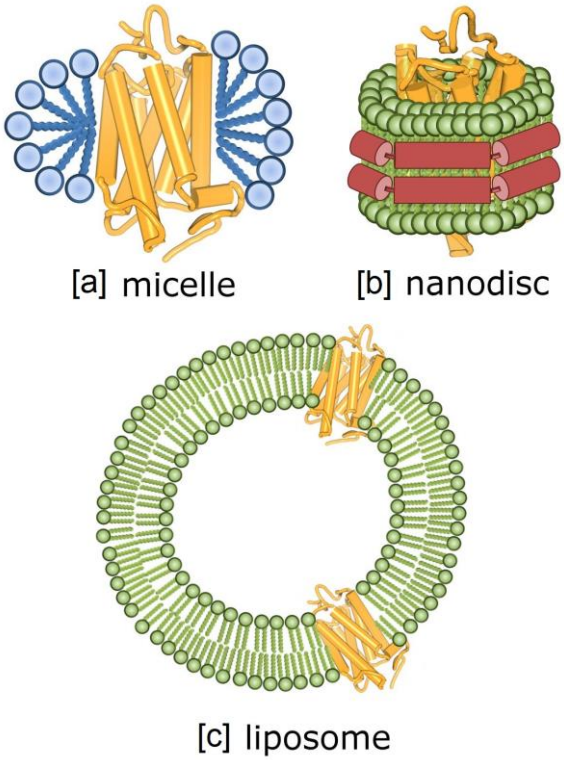

Figure 5.1. Schematic representation of the microenvironments for membrane proteins, which have been investigated in this chapter, after their extraction from their biological membranes [3]. Detergent molecules are represented in blue, lipids in green and membrane scaffold components in red. See the text for the difference in size range between the systems.

The much smaller discoid open nanodisc systems (10-30 nm diameter) are a suitable alternative. Nanodiscs consist of the protein of interest embedded in a phospholipid bilayer contained by a scaffolding amphipathic agent. Traditionally, nanodiscs are made using two molecules of the amphipathic membrane scaffold protein (MSP) [4]. However, these MSP-nanodiscs require prior detergent solubilization of the pigment, which then allows subsequent insertion into a non-native membrane environment. SMA-nanodiscs using styrene maleic acid copolymer as a scaffolding component, are an alternative emerging option which can allow detergent free insertion of membrane proteins into nanodisc structures [5].

SMA self-inserts into the cell membrane extracting native-nanodisc patches, which can be further purified to isolate the nanodiscs embedded with the protein of interest.

In this chapter, the effect of the local microenvironment on properties of wild type PR and GR was investigated. We compare a number of detergent and phospholipid bilayer systems, and study their influence on the spectral properties, stability, size and oligomeric state of the resulting pigment-complexes, in preparation for further extensive biophysical characterization.

5.2 Experimental section

Besides the methods described in Chapters 2 and 4, additional methods used for this chapter are described below. The source of special chemicals is given in the Appendix (A1.).

5.2.1 Cell lines, plasmids, and cell culturing

E. coli BL21 transformed with either plasmid pJBS1255 or pJBS1257, constructed as described elsewhere [6], was used to express 6x-His tagged PR or GR, driven by the inducible P_{trc} promoter. A main culture was grown from a 1:50 dilution of an overnight culture in LB at 37°C. Expression of the opsin was induced with 0.5 mM IPTG at an OD_{600} of 0.5-0.6. The cells were grown for an additional 14-16 h, and harvested by centrifugation at 3200xg for 20 minutes at RT. *E. coli* BL21 was also used to express the plasmid pET-28a containing the insert for the 6x-His tagged membrane scaffold protein MSP1E3D1 [4]. A main culture was grown from a 1:50 dilution of an overnight culture in Terrific broth at 37°C. Expression of MSPDE31 was induced using 0.5 mM IPTG at an OD_{600} of 0.6-0.7. The cells were grown for 2-4 h and harvested by centrifugation at 3200xg for 20 min at RT.

5.2.2 Hydrolysis of SMA

10 g of styrene maleic acid copolymer SMA2000 was refluxed in 100 mL 1M KOH for 3 h at 100°C. The solution was cooled to RT and kept at 4 °C overnight. The hydrolyzed SMA was precipitated with 1 M HCl, by lowering the pH to 7. SMA was spun down in a tabletop centrifuge at 6000xg for 20 min, and the pellet was further washed 4-5 times with 100 mM HCl. The supernatant was drained and the powder was lyophilized overnight. From the refluxed solution, 98 % of SMA was recovered. A stock solution of 10 % SMA (w/v) was made in 50 mM Tris, pH 8.

5.3.3 Extraction of PR and GR into SMA-nanodiscs

E. coli UT5600 cell pellets expressing PR or GR (c.f. chapter 2) were resuspended in 50 mM Tris, 0.6 M NaCl, pH 8 (3 mL per 100 mL culture), and were sonicated to generate membrane vesicles (4s on, 5s off, 30 % amplitude, 10 min, 4°C). 3 ml of 10 % SMA was added and the solution was sonicated again and left on the roller at RT for 2-3 days. The insoluble fraction was spun down at 147,000xg for 45 min at 4 °C. From the coloured supernatant, PR or GR containing SMA-nanodiscs were purified using nickel affinity chromatography (see below).

5.2.4 Purification of MSPDE31

The *E. coli* BL21 cell pellet was resuspended in 40 mM Tris, 0.3 M NaCl, 5 mM β-mercaptoethanol, pH 8 (10 mL per L culture) supplemented with one protease inhibitor tablet, 10 mg lysozyme and 6 µL benzonase nuclease solution. After 30 min incubation on ice, 250 µL of 10% Tergitol NP-40 was added and the pellet was sonicated 5 times, 45s, 30 % amplitude, 4°C. The cell debris was spun down at 16,000xg for 30 min at 4°C). The lysate was subjected to batch purification using 6 mL Ni^{2+} NTA resin, as described previously [7]. The fractions of pure MSPDE31 were combined and

concentrated using a 10 kDa centrifugal filter (Amicon). The purity was assessed using SDS-PAGE.

5.2.5 Formation of MSP-nanodiscs

PR and GR solubilized and purified in DDM, DPC or TritonX-100 were used to generate MSP-nanodiscs. A solution of 2 mg/mL asolectin or *E. coli* polar lipid was made in 40 mM nonylglucose, 50 mM HEPES, 100 mM NaCl, pH 7.8. The entire protocol was carried out at 4°C with continuous mixing during the incubation steps. Purified PR/GR was combined with the lipid solution using a molar ratio of 2:240 for PR/GR : asolectin/*E. coli* lipid. This mixture was incubated for 30 min. Then MSP1E3D1 was added in a molar ratio of 1:2; PR/GR : MSP. The solution was vortexed and incubated for 30 min. Subsequently, the detergent was complexed by the addition of β-cyclodextrin, which induces the formation of the MSP-nanodiscs [8]. β-cyclodextrin was added in three equal parts, with 15 min incubation steps for each addition, to achieve a final molar ratio of 1:1.5 for detergent:β-cyclodextrin. The insoluble material was then spun down at 14,000xg for 30 min at 4°C.

5.2.6 Purification of SMA- and MSP-nanodiscs

The SMA- and MSP-nanodiscs containing PR or GR were purified by nickel-affinity chromatography. 0.3 or 1 mL Ni^{2+} NTA-resin in 0.6 or 5 mL columns was spun down in a table top centrifuge at 2700xg for 1 min and washed once with Buffer A (20 mM bis-tris propane, 20 mM imidazole, 0.5 M NaCl, pH 8). The crude nanodisc solution was added to the column, incubated at RT for 20 min, and the unbound lysate was spun down. The columns were washed ten times with 0.6 mL of Buffer A. The bound nanodiscs were eluted using 600 µL of 500 mM imidazole, 20 mM bis-tris propane, 0.5 M NaCl, pH 8. The absorbance spectra of the purified nanodiscs were recorded, and their purity was assessed by SDS-PAGE.

5.2.7 Insertion of purified PR/GR into liposomes

A 15 mg/mL *E. coli* lipid solution was made in 40 mM nonylglucoside, 50 mM HEPES, 100 mM NaCl, pH 7.8. Purified PR/GR was added to the lipid solution using a ratio of 1 protein monomer : 25 *E. coli* lipid molecules and left mixing continuously for 1 h, RT. β-cyclodextrin was then added in three equal parts as described above using a molar ratio for β-cyclodextrin : detergent of 1.5:1. The resulting liposomes were pelleted in a table top ultracentrifuge (21191xg, 30 min, 4˚C). The resulting pellet was washed twice with 50 mM phosphate buffer, 150 mM NaCl, pH 8.

5.2.8 Size exclusion chromatography:

Size exclusion chromatography (SEC) of purified PR/GR in DDM or OGNG was done using a mobile phase containing 50 mM phosphate buffer, 150 mM NaCl, 0.2 % OGNG, pH 8 or 20 mM bis-tris propane, 150 Mm NaCl, 0.1% DDM, pH 8 with a Amersham Pharmacia biotech äkta column at standard pressure and flow rate. The absorbance was measured at 215, 280 nm, 500 nm, 520 nm and 540 nm. Blue Dextran (Sigma-Aldrich) was used for molecular weight calibration.

5.2.9 Circular dichroism spectroscopy

Circular dichroism spectra were recorded using 2 mm quartz cuvettes on a J-815 spectrometer (Jasco, Gross-Umstadt, Germany) equipped with temperature control. The following parameters were used: wavelength range, 400-700/900 nm; data pitch, 1 nm; response time, 2 s; band width, 4 nm; scanning speed, 50 nm/min; temperature, 20°C. A sample absorbance of 0.5-1 OD units at the λ_{max} was used throughout.

5.2.10 Dynamic light scattering (DLS)

The size distribution of the purified nanodisc samples was analyzed using the Zetasizer Nano-S (Malvern Instruments Ltd, Malvern UK), equipped

with a 633 nm laser. The samples were spun down in a table-top centrifuge at 13,000xg for 10 min prior to the measurement. The signals were analyzed using the internal software of the equipment and converted into a size distribution with scatter intensity.

5.2.11 Kinetic spectroscopy

Transient absorption measurements were performed at the LaserLaB of the Vrije Universiteit Amsterdam, using a femtosecond to sub-millisecond pump-probe setup as described previously [9]. A 2-mm sapphire plate was used for supercontinuum white light generation, and a selected wavelength region was detected by the photodiode array. The data was acquired within a time window of -50 ps to 300 μs, relative to time zero of the pump, with a minimum temporal step of 50 fs. The diameters of the pump and the probe beams at the sample position were ~200 μm and ~70 μm, respectively. The wavelength of the pump beam was centered at 520 or 620 nm. Global analysis was performed using Glotaran as described previously [9, 10].

5.2.12 Solid-state NMR measurements

ssNMR measurements were recorded using an Avance-I spectrometer operating at a field strength of 17.6 T, equipped with a 4 mm triple resonance MAS probe (Bruker, Karlsruhe, Germany). At this field, the ^{1}H resonates at 750 MHz while the ^{13}C resonates at 187.5 MHz. The optimum length of 90° proton and carbon pulse was determined on uniformly labelled ^{13}C tyrosine. For ^{13}C CP-MAS, a mixing time of 2ms with a recycle delay of 1s and total a number of 2048 scans were collected. 2D ^{13}C-^{13}C correlation PARIS experiments were performed using a mixing time of 20 ms, 30 ms and 50 ms with a recycle delay of 1s, at a total number of 192 scans with indirect dimensions of 128 scans. ^{13}C CP-MAS experiments were measured at 10, 13 and 14 kHz spinning frequencies, to identify the

spinning side bands. All solid-state NMR measurements were performed at 236 K. The NMR data were processed in Topspin 3.2 and MestReNova.

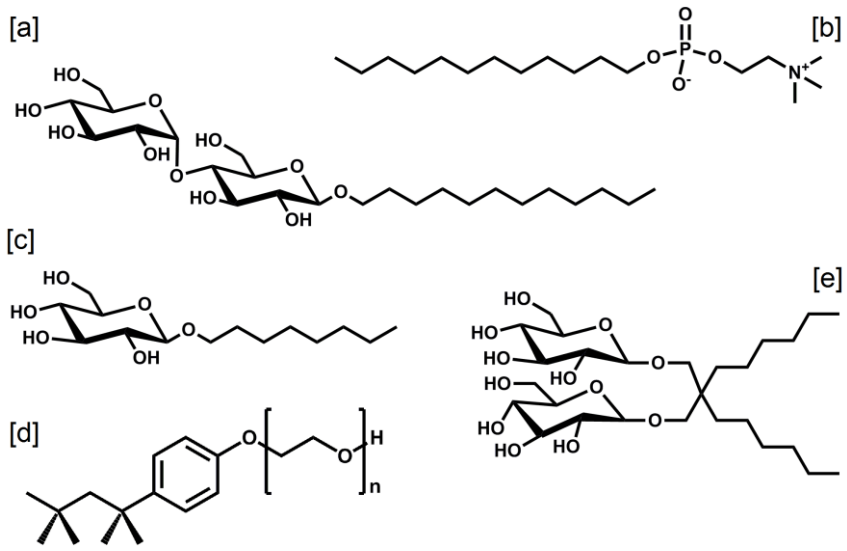

Figure 5.2 Chemical structures of detergents used in this study to solubilize and/or purify the pigments. DDM [a], DPC [b], OG [c], TritonX-100, n=9-10 [d] and OGNG [e].

5.3 Results

5.3.1 Effect of the detergent environment on properties of PR and GR

In the previous chapters, we used the mild nonionic detergent DDM for the solubilization and subsequent purification of all pigments generated. In this chapter, we compare the effect of several different detergent environments on the spectral properties and stability of wild type PR and GR (Figure 5.2). We included the popular nonionic detergents TritonX-100 and n-octyl-β-D-glucopyranoside (OG), and the recently synthesized glucose neopentyl glycol derivative OGNG, which produces smaller micelles, but has similar

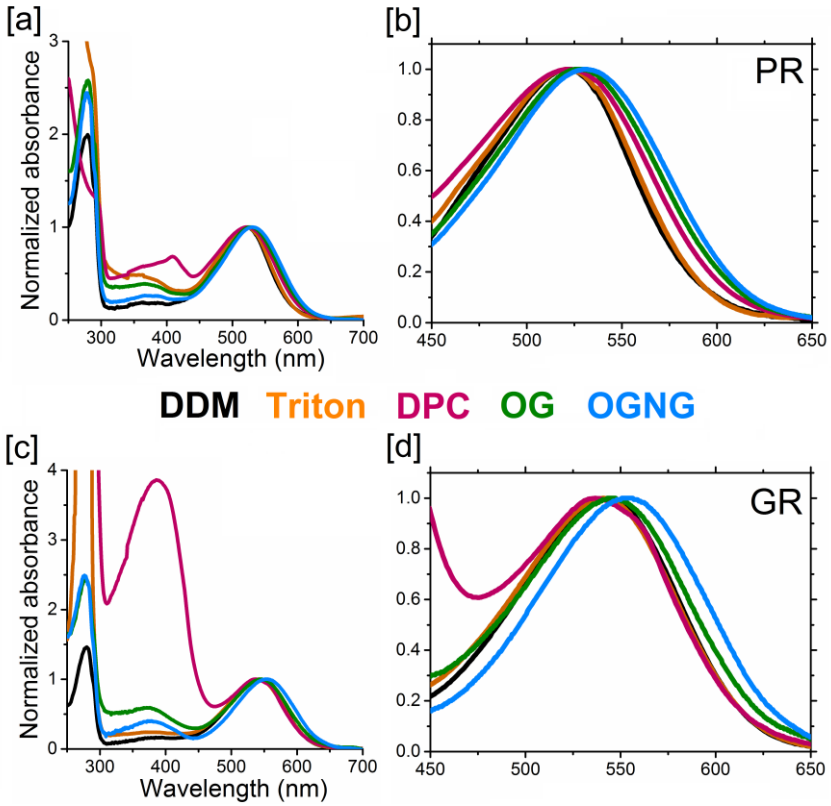

Figure 5.3 Absorbance spectra of purified PR [a,b] and GR [c,d] in various detergent environments, normalized at the main absorbance band. Color codes are as shown by the detergent abbreviations in the figure.

stabilization potential as DDM [11]. We further included the zwitterionic detergent dodecyl phosphocholine (DPC), which is commonly used to investigate membrane proteins with liquid-state NMR, since it generates relatively small mixed micelles [12].

The membrane vesicles containing PR or GR, isolated from the *E. coli* host cells, were solubilized using 2.5-5% of the detergent of choice and were subsequently purified and concentrated to a final detergent concentration of 2%. The exception to this was OGNG, which required solubilization of the pigments in 4% DDM, followed by several on-column washes and subsequent elution of purified pigment in 0.5% OGNG. The thermal

stability of the purified pigments was assessed by following the decay of the main absorbance band.

DPC was found to be the most destabilizing detergent. Even upon short solubilization for 1 h at 4°C followed by rapid purification, a strong peak was observed around 390 nm in the absorbance band of the purified protein (Figure 5.3). This band represents retinal released from denatured pigment. The destabilization was more pronounced for GR. The highest solubilization efficiency was obtained with TritonX-100 which required 1 hour solubilization at RT (or overnight at 4°C). The purified PR samples were stable at 4°C for several days (data not shown). However, GR purified in Triton did not survive RT incubation, long-term storage at 4°C, or repeated freeze-thaw cycles. OG required overnight solubilization at RT, but showed similar results to Triton in terms of stability of the pigments. Complete solubilization with DDM required 2-3 days at RT. The resulting pigments showed the highest stability and could be stored in DDM at RT for up to a week. The poorest solubilization efficiency was seen for OGNG, which achieved less than 10% solubilization of the pigments after a week of extraction at RT.

Detergent	[a]cmc (mM)	[b]conc (mM)	[c]diameter (nm)	[d]λ_{max} PR (nm)	[d]λ_{max} GR (nm)
DDM	0.2	40	5.4	520	540
DPC	1.1	57	3.6	522	537
TritonX-100	~1	31	6.4	521	541
OG	20	65	4.3	527	545
OGNG	~1	35	nd	531	553

Table 5.1 Absorbance maximum of PR and GR in different detergent environments. [a] critical micelle concentration provided by the manufacturer, [b] detergent concentration used in this experiment, [c] average diameter of detergent micelle determined by DLS, accuracy ±1 nm [d] λ_{max} value of purified pigment at pH 8, accuracy ±2 nm. nd=not determined.

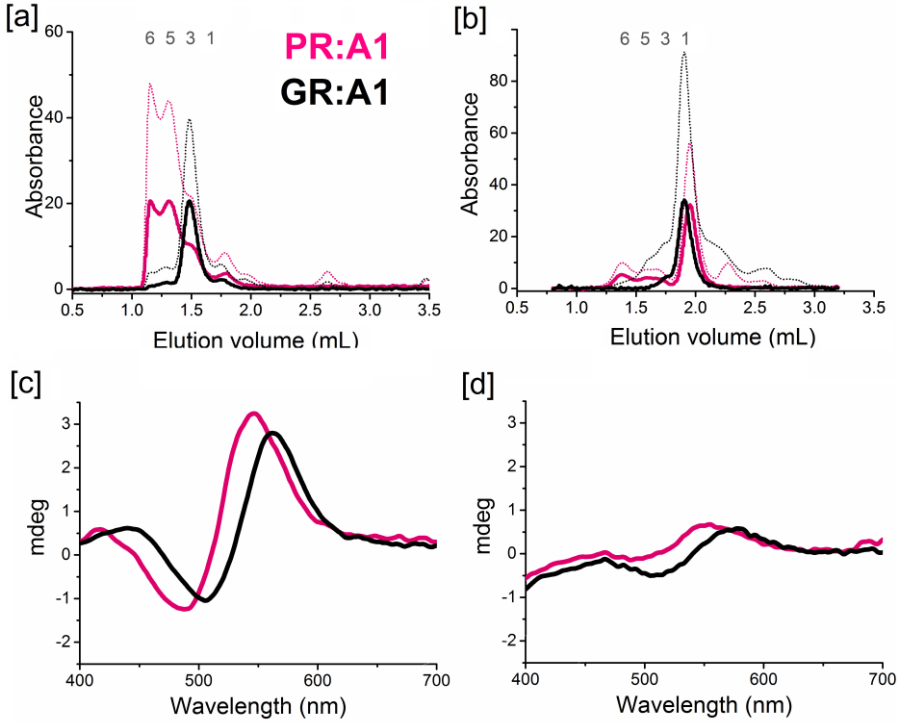

Figure 5.4 Top panel: SEC chromatograms of PR (pink) and GR (black) in 0.2% DDM [a] or 0.2% OGNG [b] dotted line, absorbance at 280 nm; solid line, absorbance ~500 nm. Bottom panel: Circular dichroism spectra in 2% DDM [c] or 2% OGNG [d].

However, the resulting pigments purified in OGNG were stable at RT for several days, similar to DDM. Solubilization with TritonX-100, DPC and DDM yield about the same absorbance maximum for the pigments (Table 5.1). However, both OG and OGNG cause a noticeable red-shift in the λ_{max} of PR as well as GR (5-13 nm). In view of the stability of the pigments in OGNG and their red shifted absorbance, we investigated their oligomeric status using SEC and CD. From the size exclusion pattern (Figure 5.4, top panels), we conclude that both DDM and OGNG micelles contain a relatively uniform population of PR and GR. However, while DDM maintains mainly a higher oligomeric state (hexamers and pentamers for PR, trimers for GR), OGNG micelles appear to predominantly contain smaller units, most likely dimers or monomers. The bilobal CD spectrum for PR and GR in DDM (Figure 5.4,

panel c) is in agreement with an ordered oligomeric state, since it implies close-range communication between the retinylidene ligands of the subunits. The CD spectrum of PR and GR in OGNG shows low intensity and has lost most of this bilobal character. (Figure 5.4, panel d).

5.3.2 Formation and characterization of nanodiscs

PR and GR purified in DPC, TritonX-100 and DDM were used to generate MSP-nanodiscs. The phospholipid mixture from soybean (asolectin), and *E. coli* (polar extract) were both tested as suitable lipid environments and yielded similar results. The purified pigment was mixed with lipid and MSPDE31 in a defined ratio, and the detergent was extracted with β-cyclodextrin [8]. This extraction step concomitantly cajoles the assembly of the MSP-nanodisc. The MSP-nanodisc was purified from the cyclodextrin mixture by nickel affinity chromatography exploiting the 6x-His tag on the opsin and MSP. The purified MSP-nanodiscs were characterized using absorbance spectroscopy, SDS-PAGE and DLS.

The yield of pigment MSP-nanodiscs generated with purified PR (~10% insertion of pigment) was consistently substantially lower than that obtained with GR (~95% insertion). Furthermore, the absorbance band of PR:MSP-nanodiscs at pH 8 was red-shifted by about 10 nm, relative to PR:DDM (Figure 5.5, Table 5.2). SDS-PAGE analysis of the purified PR MSP-nanodisc complexes suggests an assembly ratio of 2 MSPDE31 molecules per incorporated protein monomer (Figure 5.5). DLS measurements indicate a hydrodynamic diameter of 14-15 nm for both the PR- and GR-MSP-nanodiscs (Table 5.2). The pigments were extremely stable in the MSP-nanodisc environment and could be stored at 4°C for several months.

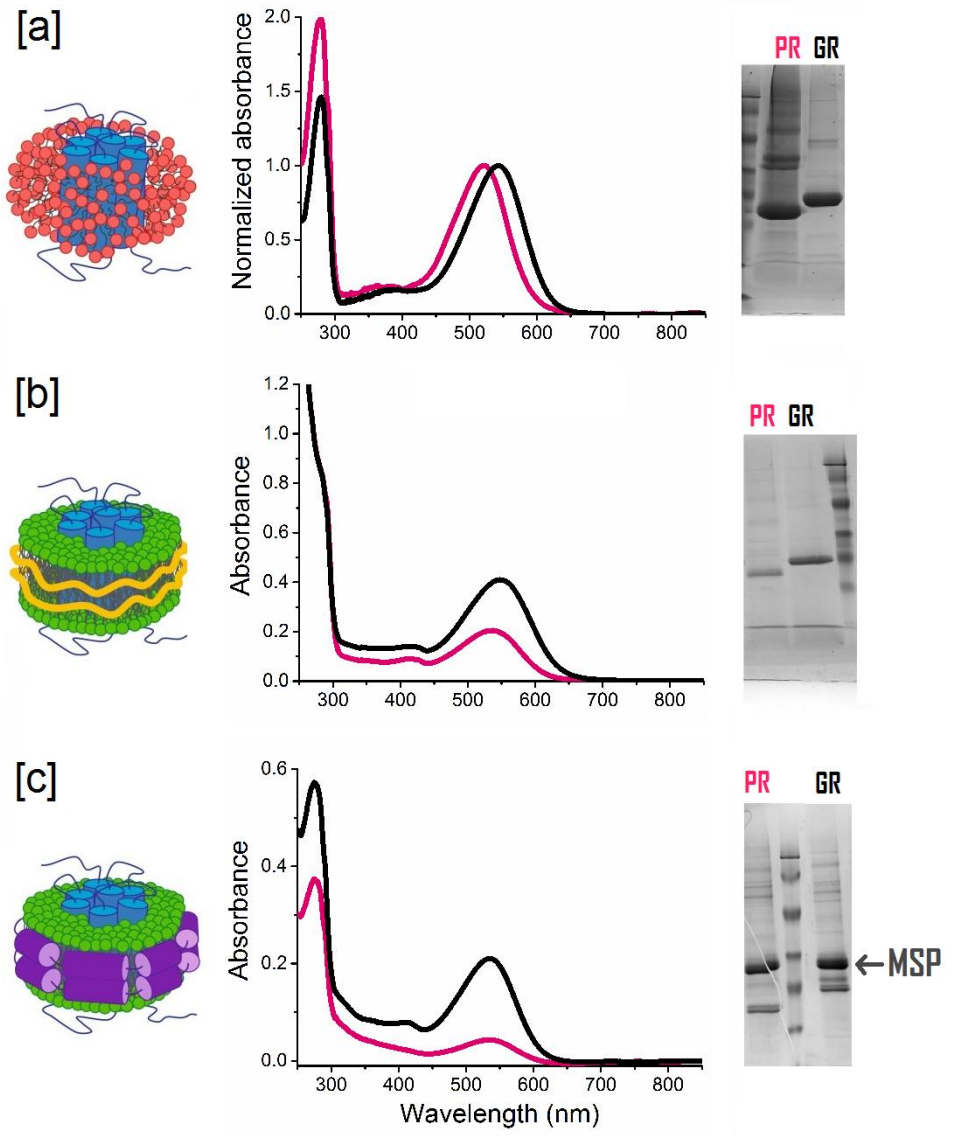

Figure 5.5 Comparison between the different soluble membrane-mimetic environments for PR (pink curves) and GR (black curves)in [a] DDM micelles, [b] SMA nanodiscs, or [c] MSP nanodiscs. Left panel: a schematic illustration of the environment with detergent molecules in red, lipids in green, SMA in yellow and MSP in purple, adapted from [13]. The middle panel shows absorbance spectra of the purified pigment-detergent/nanodisc complexes of PR (pink) and GR (black). Right panel: SDS-PAGE images of the purified fractions, lanes 1 and 2 representing PR and GR, respectively.

Environment	pigment	λ_{max} (nm) [a]	d (nm) [b]	yield (%)[c]
DDM	PR	520	nd	>90
	GR	540	nd	>95
SMA-nanodisc	PR	537	28	20
	GR	548	21	40
MSP-nanodisc	PR	531	15	10
	GR	538	14	95

Table 5.2 Comparison of purified pigment-detergent and nanodisc complexes. [a] λ_{max} determined from the absorbance bands of the pigments at pH 8, accuracy ±2 nm. [b] average diameter of the nanodiscs determined by DLS, accuracy ±1 nm. [c] % yield or insertion of purified pigment in-nanodisc complexes, accuracy ±10% , nd=not determined.

To generate the SMA-nanodiscs, the cell pellets expressing the holo-protein were directly extracted with hydrolyzed SMA under high salt conditions at pH 8. The extraction required multiple rounds of sonication and incubation at RT for 5-7 days. About 60% of GR present in the *E.coli* membrane was extracted, in comparison to 30% extraction of PR. However, significant losses were incurred upon the subsequent purification steps, due to irreversible binding of these SMA-nanodisc complexes to the Ni^{2+} column. Nonetheless, the nanodiscs could be isolated with a high degree of purity, as determined from the absorbance bands of the pure fractions, and SDS-PAGE analysis (Figure 5.5). The absorbance bands of both PR and GR:SMA-nanodiscs are significantly red shifted, as compared to the absorbance of the pigments in DDM (Table 5.2). However, in contrast to the MSP-nanodiscs, the SMA-nanodiscs were not stable and did not survive long-term storage at -80 °C.

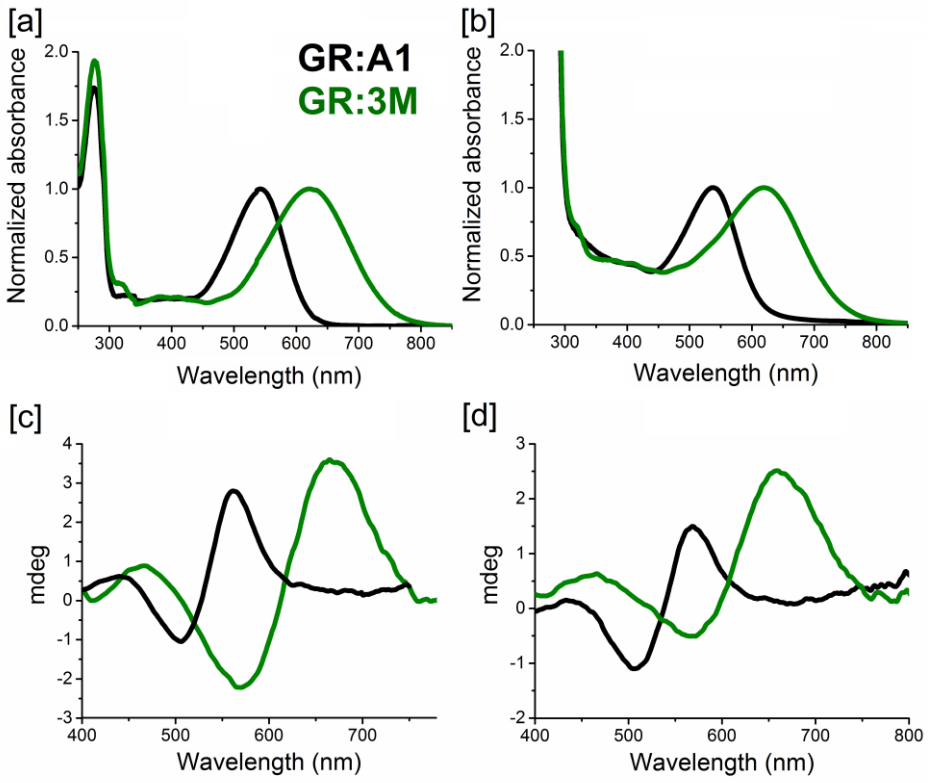

Figure 5.6 Top panel: Absorbance spectra of GR:A1 (black curve) and GR:3M (green curve) purified in 2% DDM [a] or in MSP-nanodisc complexes [b] at pH 8. Bottom panel: circular dichroism spectra of the above in 2% DDM [c] or MSP-nanodiscs [d].

5.3.3 Photocycle dynamics of GR in a nanodisc environment

The feasibility of generating and using MSP-nanodiscs to study the photocycle dynamics of the rhodopsin pigments was assessed using optical spectroscopy (Figure 5.7). GR:A1 and GR:MOA2 were taken as a first test, since the photocycle of GR:A1 has been investigated before [14] and GR:MOA2 is quite red-shifted with poor proton pumping (c.f. chapter 3). About 2-3 mg of each pigment was solubilized and purified in DDM, and subsequently inserted into MSP-nanodiscs as described above.

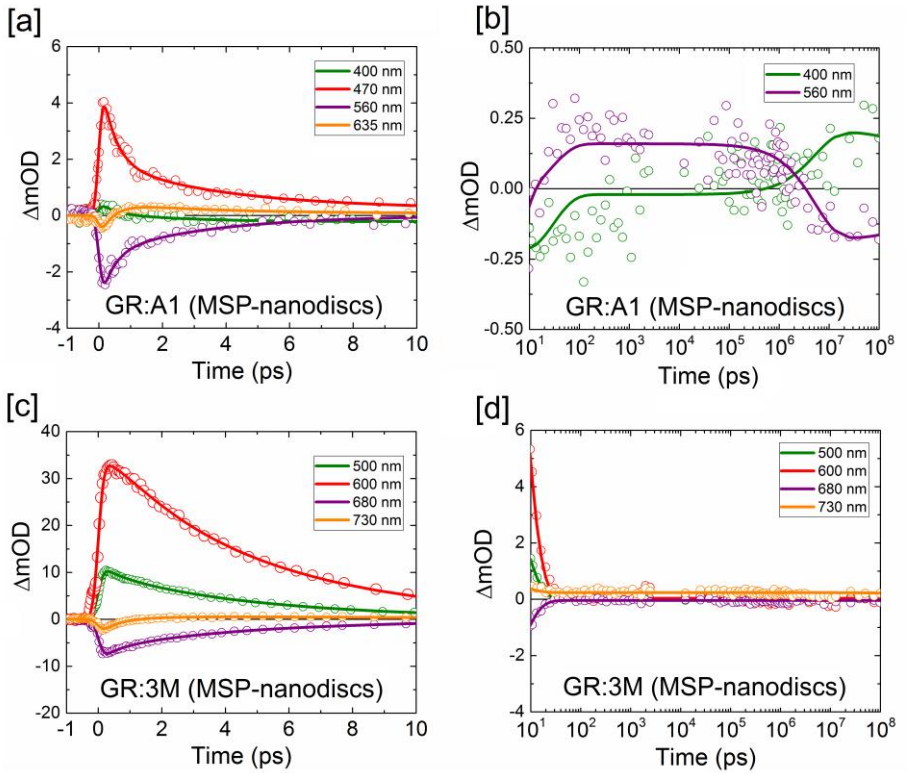

Figure 5.7 Time traces of different spectral intermediates extracted from a pump-probe transient absorption measurement of GR:A1 (top) and GR:MOA2 (bottom) in a MSP-nanodisc environment. The spectral intermediates evolve in the ps [a, c] and μs [b, d] range. 3M stands for MOA2.

The MSP-nanodiscs were concentrated and their steady state absorbance and circular dichroism spectra were measured, which showed good agreement with results obtained with DDM (Figure 5.6). The nanodiscs were further used for pump-probe transient absorption spectroscopy, to identify early photocycle intermediates, upon excitation with 520 nm (GR:A1) or 620 nm (GR:MOA2). Figure 5.7 shows the spectral evolution of different photointermediates in the picosecond and microsecond range. For GR:A1, the characteristic photocycle intermediates of a rhodopsin proton-pump were observed. The excited state absorption was observed at 470 nm, and persisted for several picoseconds. An early 635 nm absorbance

was attributed to the vibrationally hot J intermediate, which blue shifts to 560 nm indicating the rise of a K-L equilibrium. The decay of this signal with a concomitant rise in absorbance at 400 nm (Figure 5.7, panel b) implies the deprotonation of the Schiff base and the rise of an M-state. Surprisingly, in the case of GR:MOA2, only an initial excited state absorption was observed at 730 nm, following which all the signals decayed homokinetically to the ground state.

5.3.4 Proteoliposomes as a membrane model for a solid-state NMR study of the retinal binding pocket

E. coli BL21 was used for large scale cultivation and expression of PR and GR. The cell pellets were lysed to generate the membrane vesicles containing the opsin. The opsin was regenerated using a retinal A1 labeled with 13C at 10 carbons (8-15, 19 and 20; Figure 5.7), and subsequently solubilized and purified in DDM according to the protocols described in chapter 2. Proteoliposomes were generated using this purified PR and GR as a starting material. The pure protein was mixed with the E. coli lipid solution, following which the detergent was extracted using β-cyclodextrin as described in section 5.2.7. The resulting pink coloured proteoliposomes were pelleted and tightly packed into 4 mm NMR rotors.

1D CP-MAS and 2D ^{13}C-^{13}C dipolar correlation spectroscopy using the RFDR and PARIS pulse programs were used to identify the chromophore resonances. The analysis of the resulting spectra (Figure 5.7) will not be explained further. They showed good resolution and relatively narrow resonances for the labelled carbons, which allowed the assignment of the chemical shifts of all ^{13}C carbons of the retinylidene chromophore in PR and GR (Table 5.3).

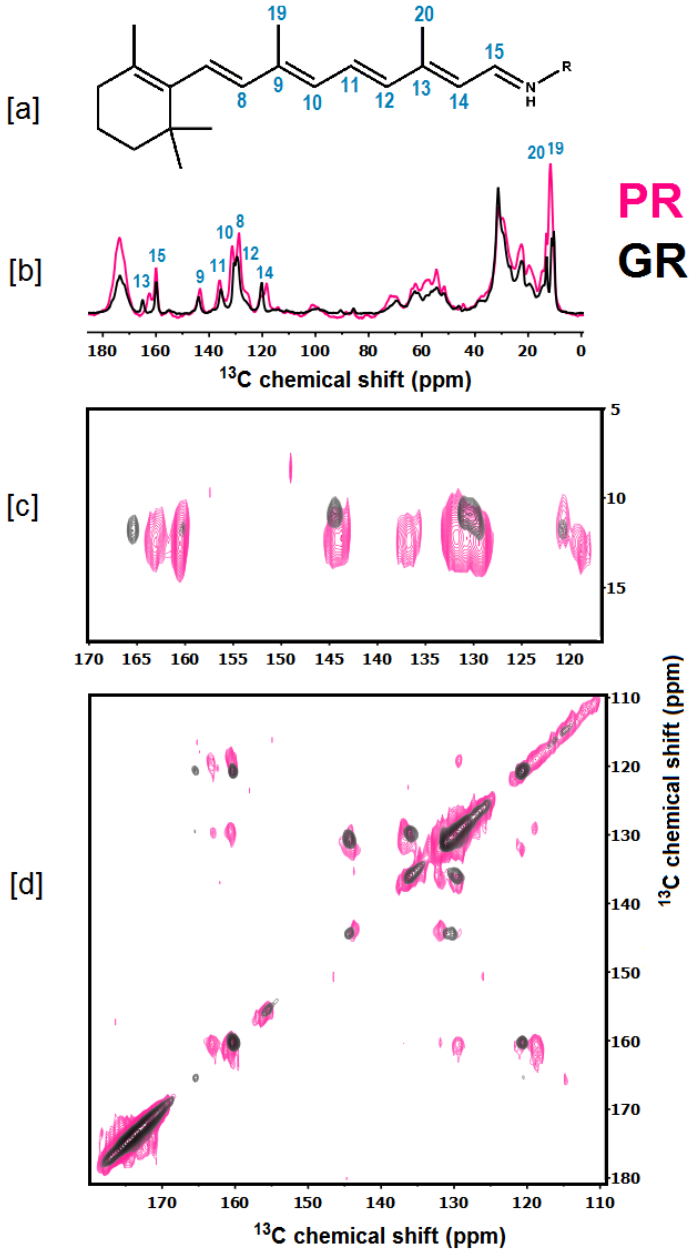

Figure 5.7 ssNMR spectroscopy of PR (pink) and GR (black) regenerated with a $^{13}C_{10}$ retinal. Chemical structure of the retinylidene group showing the positions of the ^{13}C atoms [a] 1D CP-MAS spectra [b] and 2D ^{13}C-^{13}C RFDR [c, d] and PARIS (not shown) spectra were used to assign the chemical shifts of all the ten ^{13}C atoms of the retinylidene chromophore.

^{13}C	8	9	10	11	12	13	14	15	19	20
PR	131.7	143.9	131	136.5	129.2	162.8	118.3	160.4	12.0	12.0
GR	131.0	144.4	130	136.0	129.9	165.4	120.7	160.3	10.7	11.5

Table 5.3 Chemical shifts (ppm) of the ^{13}C resonances of the retinylidene chromophore in PR and GR

5.4 Discussion

5.4.1 General properties of the studied microenvironments

Here we briefly describe the most relevant properties of the various systems used in this chapter to extract, purify and characterize PR and GR.

Detergents are amphipathic molecules, containing hydrophilic and hydrophobic segments, similar to lipids. When their concentration exceeds their individual single molecule solubility, they self-assemble in an aqueous medium by extruding water to form micelles. Detergent micelles contain a hydrophobic interior and hydrophilic exterior and associate with membrane proteins, which share this amphipathic nature, yielding soluble protein-detergent complexes (Figures 5.1, 5.5). The size of these complexes usually depends on the polar tails of the detergent. A wide variety of detergents exist with different combinations of head and tail groups [15]. Choosing a suitable detergent to solubilize and stabilize a particular membrane protein is a challenge, both because of difficulty of choice and ill-defined properties of pigment-detergent complexes.

Micellar systems are suitable for studying the photophysical properties of colored membrane proteins. However, proteins are dynamic structures, and usually undergo functional conformational changes like the opening and closing of channels. The loss of protein-lipid and lipid-lipid interactions makes these pigments vulnerable to destabilization in the micellar

environment. The lateral pressure induced by the membrane has a stabilizing influence on membrane proteins. Therefore a number of systems have been devised which simulate the membrane environment of these proteins.

MSP-nanodiscs are discoid monodisperse open complexes, which consist of the protein of interest embedded in a phospholipid bilayer, enclosed by two amphipathic MSP molecules (Figures 5.1, 5.5). These nanodiscs are usually 9-20 nm wide, with the diameter of the nanodisc controlled by the length of the MSP used [16]. SMA-nanodiscs should be an attractive alternative to MSP-nanodiscs, since they do not require prior solubilization of the protein by detergents. The small size of these nanodisc systems leads to optical near-transparency of the sample, due to which nanodiscs have been widely used in a variety of spectroscopic techniques.

While nanodiscs work well to simulate the fluidity and lateral pressure of a membrane, the impact of membrane curvature and protein (hetero)-oligomerization on structural and functional properties can become lost in this environment. Furthermore, vectorial properties of the proteins, such as proton transport, are not easily studied in these open systems [17]. For such studies, the closed proteoliposome system is much more suitable. Proteoliposomes are 10-100 times larger than nanodiscs and their light-scattering properties render them less suitable for optical studies. However, they are widely used for the structural determination of membrane proteins by ssNMR, in functional assays and in a variety of biotechnological applications.

5.4.2 Differences between the detergent systems investigated

The choice of surfactant has an important effect on the oligomeric distribution and stability of membrane proteins. The nonionic sugar based detergent DDM [18] has been extensively used in membrane protein

studies. DDM forms large well-structured micelles (56-71 kDa) thereby stabilizing protein dynamics and protein-protein contacts and minimizing denaturation [15]. Previous studies have shown that the native oligomeric assembly of PR is preserved in DDM micelles, which contain a predominant fraction of hexamers and a minor monomeric population [19]. This agrees with our analyses (Figure 5.4). However, the large protein-detergent complexes formed by DDM make it less suitable as a detergent of choice for crystallization trials, and for structural studies using solution-state NMR. Smaller protein-detergent complexes, which would stabilize a solubilized monomer of these proteins are highly desirable. Here, we compare a number of commonly used detergent environments, and their influence on the thermal stability, oligomeric structure and spectral properties of PR and GR.

A variant of the zwitterionic detergent DPC was recently used to solve the solution NMR structure of PR [20]. DPC forms much smaller micelles (18-21 kDa) and is hence more useful to isolate the monomeric form of these proteins. However, in our study, DPC was found to be the most destabilizing of all detergents tested. Despite rapid solubilization and purification steps in the cold, extensive denaturation of in particular GR was observed accompanied by release of retinal (Figure 5.3). We thereby decided to focus on nonionic detergents such as TritonX-100, OG and OGNG, which also form smaller protein-detergent complexes. Prior studies have shown that solubilization of PR with 13% TritonX-100 stabilizes a monomeric red-shifted fraction of PR [21]. However, we found that though the solubilization efficiency of TritonX-100 was high, at concentrations higher than 10% it did not stabilize the pigments sufficiently for long-term storage or further characterization. Despite its poor solubilization potential, OGNG came out as the most stabilizing detergent of this triad, with no significant loss of intact pigment, even upon incubation at RT for several days. We thereby decided to investigate the oligomeric distribution

of PR and GR in OGNG using SEC and CD, so as to compare it to the well-characterized DDM microenvironment. From the SEC distribution, we conclude that in OGNG micelles, both PR and GR most likely largely exist as a monomeric fraction.

The CD spectra of PR and GR in DDM exhibit a strong bilobal bandshape (Figure 5.4c), centered around the absorption maxima of the pigments. Such a bandshape was also observed in the CD spectrum of bR [22, 23] and XR [24]. It is thought to originate from an oligomeric complex of the pigment due to excitonic interactions between the retinal molecules, and an asymmetric conformation in the protein. Hence, such a strong bilobal bandshape is not expected for monomeric units of these pigments. Indeed, the CD spectra of the pigments purified in OGNG (Figure 5.4d), particularly PR, show a strong reduction in the bilobal structure. Previous CD spectra of the pigments in a high concentration of 15% Triton-X 100 have shown an unordered mono-peak absorbance band, indicating a purely monomeric fraction (data not shown). We interpret this as supporting the spectral and SEC data in that predominantly PR or GR monomers are present in OGNG micelles, which have low CD activity in their main absorbance band.

In OGNG micelles, a significant red-shift in the absorbance bands of both PR and GR was observed relative to DDM micelles (Table 5.1). Saccharide headgroups are likely to have minimal effect on the retinal-protein interaction. Besides, such a red-shift is also observed for PR in SMA- as well as MSP-nanodiscs and for GR in SMA nanodiscs (Table 5.2). Rather, the oligomeric state of PR and GR will have a predominant impact. It was shown that in the hexameric and pentameric complexes of PR, the pKa of D97 (6.5-6.7) is about one unit lower than in monomeric PR (7.4-7.8) [25]. Presumably this originates in the cross-protomer interaction between H75-W34, which reduces the weakening effect of H75 on the acidity of D97 [22]. The absence of this H75-W34 interaction in the monomer thus enhances

protonation of D97 in the pH range 6-9, thereby inducing a red-shift. This is further evidence for a monomeric state of PR in OGNG micelles. The red-shift in the absorbance band of GR however is still unexplained, since the equivalent counterion D121 in GR has a lower pKa (≈ 4.5) and its absorbance band shows little pH dependence in the range 6-9 (Table 2.1).

5.4.3 Differences between bilayer systems

We investigated the potential of different bilayer systems, namely the open soluble nanodiscs and closed insoluble proteoliposomes, and tested their application towards the structural and functional characterization of PR and GR in a membrane environment.

We generated two different types of nanodiscs, namely MSP and SMA-nanodiscs. Generation of SMA-nanodiscs requires longer incubation steps, and we noticed that the SMA-nanodiscs had poor thermal stability, despite the native membrane environment. The multiple sonication steps could have had an impact on the structure of the resulting complexes. We further observed that in general, GR was more readily incorporated into the nanodisc environment than PR. This is attributed to an oligomeric assembly of the pigments in the membrane.

Various studies have shown that PR exists predominantly as hexamers or pentamers in the membrane environment via crystallography of blue absorbing PR [26, 27], pulsed EPR [28], mass spectrometry [29] and atomic force microscopy in lipid bilayers [30]. Crosslinking studies have further shown that hexamers of PR can be found in the native *E. coli* membrane, indicating that this assembly is physiological [25]. A previous study showed that PR was reconstituted into MSP-nanodiscs as photoactive monomers after solubilization with TritonX-100 [21]. Considering the diameter of the MSP-nanodiscs, we generated, (14-15 nm) and that of the oligomeric PR complexes (ca 10 nm; [22, 25]), we conclude that the predominantly hexa-

meric population of PR is too large to be comfortably contained within a MSP-nanodisc. Thus, we primarily isolate nanodiscs containing the smaller monomeric fraction of PR, which explains the much lower yield of PR nanodiscs, as compared to GR nanodiscs. This is further corroborated by the red-shifted absorbance bands of the purified PR-nanodiscs relative to DDM micelles (c.f. previous section), due to the higher pKa of D97 in the monomers. On the other hand, GR is thought to exist as a trimer in DDM [31], which agrees with our data (Figure 5.4) and is likely to represent its physiological form in the membrane. Presumably, trimers of GR would easily incorporate within MSP-nanodiscs, since trimeric bR and LHCII, proteins of similar size, are well contained in these nanodiscs [7, 32].

The puzzling observation of the significant red-shift of PR (17 nm) and GR (8 nm) after incorporation into SMA-nanodiscs (Table 5.2) is still unexplained. The measured size of these nanodiscs (diameter of 28 and 21 nm, for PR and GR respectively), suggests that they could easily contain PR and GR in their oligomeric state. With better yields, analysis by CD spectroscopy would probably have brought more insight. Currently, we cannot exclude that the harsh conditions required to generate the SMA-nanodiscs has led to conformational deformation, affecting protein structure as well as protein-ligand and protomer-protomer interaction. Possibly, supplementing with extra lipid during protein extraction would alleviate these conditions, as recently reported for some G protein-coupled receptors [33].

5.4.4 Potential applications of bilayer systems

Due to the high thermal stability of MSP-nanodiscs, and the ease of incorporation of a physiologically relevant assembly of GR, we decided to test GR:MSP-nanodiscs as a biomimetic system for kinetic spectroscopy. Using pump-probe spectroscopy, we could observe the early photointermediates in the photocycle of GR:A1 up until the formation of

the M-intermediate that corresponds to the deprotonation of the Schiff-base. However, we observed little evidence of a photocycle for the red-shifted GR:MOA2, as the photointermediates could not be resolved (Figure 5.7c and d). This is in line with previous measurements in DDM (data not shown) which suggests that GR:MOA2 does not have an active photocycle under these experimental conditions, which in part could account for its low proton pumping activity reported in chapter 3. MSP-nanodiscs thus have potential in characterizing the photocycle dynamics of these proteins in a natural membrane environment.

Proteoliposomes are less suited for kinetic spectroscopy due to the light scattering induced by their large size. However, they are much more suited for structural studies using ssNMR. Here we employed proteoliposomes embossed with PR and GR containing a $^{13}C_{10}$ labeled retinal chromophore. Using high-resolution 1D CP-MAS and 2D correlational spectroscopy, we could assign the chemical shift values of all ^{13}C atoms of the retinylidene chromophore in the binding pocket of PR and GR. Further discussion of these data is outside the scope of this thesis. This first-stage effort will pave the way towards a full structural assignment of PR and GR in a natural lipid micro-environment.

5.5 Conclusion

We tested various detergent and membrane based biomimetic systems to assess their effect on the spectral properties, thermal stability and structural state of PR and GR. While there are advantages and drawbacks inherent in each biomimetic system, the ultimate decision of which system to use depends on the research question and technique of choice. While a micellar environment is usually preferred for crystallographic studies, selection of a proper detergent is critical. From our analysis, OGNG appears to be a suitable candidate for small protein complexes, however it is less suited for multimeric protein assemblies. As an emerging alternative, SMA-

and MSP-embedded membrane proteins may have strong potential in lipid-based crystallization screens utilizing cubic and sponge-phase systems. We further recommend the MSP-nanodisc system for more demanding spectroscopic studies of smaller protein complexes. These nanodiscs can also be primed for transport studies. For non-crystallographic structural studies proteoliposomes are the system of choice in combination with solid-state NMR.

References

[1] Opella, S. J. "Solid-state NMR and membrane proteins ", *J Magn Reson*, 2015. **253**: p. 129-37.

[2] Friedrich, T., Geibel, S., Kalmbach, R., Chizhov, I., Ataka, K., Heberle, J., Engelhard, M. and Bamberg, E. "Proteorhodopsin is a light-driven proton pump with variable vectoriality ", *J Mol Biol*, 2002. **321**(5): p. 821-38.

[3] Milic, D. and Veprintsev, D. B. "Large-scale production and protein engineering of G protein-coupled receptors for structural studies ", *Front Pharmacol*, 2015. **6**(66): p. 66.

[4] Bayburt, T. H. and Sligar, S. G. "Membrane protein assembly into Nanodiscs ", *FEBS Lett*, 2010. **584**(9): p. 1721-7.

[5] Dorr, J. M., Koorengevel, M. C., Schafer, M., Prokofyev, A. V., Scheidelaar, S., van der Cruijsen, E. A., Dafforn, T. R., Baldus, M. and Killian, J. A. "Detergent-free isolation, characterization, and functional reconstitution of a tetrameric K+ channel: the power of native nanodiscs ", *Proc Natl Acad Sci U S A*, 2014. **111**(52): p. 18607-12.

[6] Chen, Q., van der Steen, J. B., Dekker, H. L., Ganapathy, S., de Grip, W. J. and Hellingwerf, K. J. "Expression of holo-proteorhodopsin in Synechocystis sp. PCC 6803 ", *Metab Eng*, 2016. **35**: p. 83-94.

[7] Pandit, A., Shirzad-Wasei, N., Wlodarczyk, L. M., van Roon, H., Boekema, E. J., Dekker, J. P. and de Grip, W. J. "Assembly of the major light-harvesting complex II in lipid nanodiscs ", *Biophys J*, 2011. **101**(10): p. 2507-15.

[8] Degrip, W. J., Vanoostrum, J. and Bovee-Geurts, P. H. "Selective detergent-extraction from mixed detergent/lipid/protein micelles, using cyclodextrin inclusion compounds: a novel generic approach for the preparation of proteoliposomes ", *Biochem J*, 1998. **330 (Pt 2)**: p. 667-74.

[9] Hontani, Y., Inoue, K., Kloz, M., Kato, Y., Kandori, H. and Kennis, J. T. "The photochemistry of sodium ion pump rhodopsin observed by watermarked femto- to submillisecond stimulated Raman spectroscopy ", *Phys Chem Chem Phys*, 2016. **18**(35): p. 24729-36.

[10] Snellenburg, J. J., Laptenok, S., Seger, R., Mullen, K. M. and van Stokkum, I. H. M. "Glotaran: A Java-based graphical user interface for the R package TIMP ", *J Stat Softw*, 2012. **1**(3).

[11] Cho, K. H., Bae, H. E., Das, M., Gellman, S. H. and Chae, P. S. "Improved glucose-neopentyl glycol (GNG) amphiphiles for membrane protein solubilization and stabilization ", *Chem Asian J*, 2014. **9**(2): p. 632-8.

[12] Warschawski, D. E., Arnold, A. A., Beaugrand, M., Gravel, A., Chartrand, É. and Marcotte, I. "Choosing membrane mimetics for NMR structural studies of transmembrane proteins", *Biochim Biophys Acta Biomembr*, 2011. **1808**(8): p. 1957-1974.

[13] Dorr, J. M., Scheidelaar, S., Koorengevel, M. C., Dominguez, J. J., Schafer, M., van Walree, C. A. and Killian, J. A. "The styrene-maleic acid copolymer: a versatile tool in membrane research", *Eur Biophys J*, 2016. **45**(1): p. 3-21.

[14] Miranda, M. R., Choi, A. R., Shi, L., Bezerra, A. G., Jr., Jung, K. H. and Brown, L. S. "The photocycle and proton translocation pathway in a cyanobacterial ion-pumping rhodopsin", *Biophys J*, 2009. **96**(4): p. 1471-81.

[15] Sadaf, A., Cho, K. H., Byrne, B. and Chae, P. S. "Amphipathic agents for membrane protein study", *Methods Enzymol*, 2015. **557**: p. 57-94.

[16] Denisov, I. G. and Sligar, S. G. "Nanodiscs in membrane biochemistry and biophysics", *Chem Rev*, 2017. **117**(6): p. 4669-4713.

[17] Henrich, E., Sörmann, J., Eberhardt, P., Peetz, O., Mezhyrova, J., Morgner, N., Fendler, K., Dötsch, V., Wachtveitl, J., Bernhard, F. and Bamann, C. "From gene to function: cell-free electrophysiological and optical analysis of ion Pumps in nanodiscs", *Biophys J*. **in press**: p. DOI: 10.1016/j.bpj.2017.03.026.

[18] De Grip, W. J. and Bovee-Geurts, P. H. M. "Synthesis and properties of alkylglucosides with mild detergent action: improved synthesis and purification of β-1-octyl-, -nonyl-, and -decyl-glucose. Synthesis of β-1-undecylglucose and β-1-dodecylmaltose", *Chem Phys Lipids*, 1979. **23**(4): p. 321-335.

[19] Stone, K. M., Voska, J., Kinnebrew, M., Pavlova, A., Junk, M. J. and Han, S. "Structural insight into proteorhodopsin oligomers", *Biophys J*, 2013. **104**(2): p. 472-81.

[20] Reckel, S., Gottstein, D., Stehle, J., Lohr, F., Verhoefen, M. K., Takeda, M., Silvers, R., Kainosho, M., Glaubitz, C., Wachtveitl, J., Bernhard, F., Schwalbe, H., Guntert, P. and Dotsch, V. "Solution NMR structure of proteorhodopsin", *Angew Chem Int Ed Engl*, 2011. **50**(50): p. 11942-6.

[21] Ranaghan, M. J., Schwall, C. T., Alder, N. N. and Birge, R. R. "Green proteorhodopsin reconstituted into nanoscale phospholipid bilayers (nanodiscs) as photoactive monomers", *J Am Chem Soc*, 2011. **133**(45): p. 18318-27.

[22] Vogel, H. and Gartner, W. "The secondary structure of bacteriorhodopsin determined by Raman and circular dichroism spectroscopy", *J Biol Chem*, 1987. **262**(24): p. 11464-9.

[23] Cassim, J. Y. "Unique biphasic band shape of the visible circular dichroism of bacteriorhodopsin in purple membrane: Excitons, multiple transitions or protein heterogeneity?", *Biophys J*, 1992. **63**(5): p. 1432-42.

[24] Smolensky, E. and Sheves, M. "Retinal-salinixanthin interactions in xanthorhodopsin: a circular dichroism (CD) spectroscopy study with artificial pigments", *Biochemistry*, 2009. **48**(34): p. 8179-88.

[25] Hussain, S., Kinnebrew, M., Schonenbach, N. S., Aye, E. and Han, S. "Functional consequences of the oligomeric assembly of proteorhodopsin", *J Mol Biol*, 2015. **427**(6 Pt B): p. 1278-90.

[26] Shastri, S., Vonck, J., Pfleger, N., Haase, W., Kuehlbrandt, W. and Glaubitz, C. "Proteorhodopsin: characterisation of 2D crystals by electron microscopy and solid state NMR", *Biochim Biophys Acta*, 2007. **1768**(12): p. 3012-9.

[27] Ran, T., Ozorowski, G., Gao, Y., Sineshchekov, O. A., Wang, W., Spudich, J. L. and Luecke, H. "Cross-protomer interaction with the photoactive site in oligomeric

proteorhodopsin complexes", *Acta Crystallogr D Biol Crystallogr*, 2013. **69**(10): p. 1965-80.

[28] Edwards, D. T., Huber, T., Hussain, S., Stone, K. M., Kinnebrew, M., Kaminker, I., Matalon, E., Sherwin, M. S., Goldfarb, D. and Han, S. "Determining the oligomeric structure of proteorhodopsin by Gd3+ -based pulsed dipolar spectroscopy of multiple distances", *Structure*, 2014. **22**(11): p. 1677-86.

[29] Hoffmann, J., Aslimovska, L., Bamann, C., Glaubitz, C., Bamberg, E. and Brutschy, B. "Studying the stoichiometries of membrane proteins by mass spectrometry: microbial rhodopsins and a potassium ion channel", *Phys Chem Chem Phys*, 2010. **12**(14): p. 3480-5.

[30] Klyszejko, A. L., Shastri, S., Mari, S. A., Grubmuller, H., Muller, D. J. and Glaubitz, C. "Folding and assembly of proteorhodopsin", *J Mol Biol*, 2008. **376**(1): p. 35-41.

[31] Tsukamoto, T., Kikukawa, T., Kurata, T., Jung, K. H., Kamo, N. and Demura, M. "Salt bridge in the conserved His-Asp cluster in Gloeobacter rhodopsin contributes to trimer formation", *FEBS Lett*, 2013. **587**(4): p. 322-7.

[32] Bayburt, T. H., Grinkova, Y. V. and Sligar, S. G. "Assembly of single bacteriorhodopsin trimers in bilayer nanodiscs", *Arch Biochem Biophys*, 2006. **450**(2): p. 215-22.

[33] Broecker, J., Eger, B. T. and Ernst, O. P. "Crystallogenesis of Membrane Proteins Mediated by Polymer-Bounded Lipid Nanodiscs", *Structure*, 2017. **25**(2): p. 384-392.

Chapter 6

General discussion and future outlook

In this project, we have made significant progress towards the spectral engineering and characterization of the proton-pumps proteorhodopsin from a SAR 86 γ-proteobacterium (PR) and *Gloeobacter violaceus* rhodopsin (GR). A combinatory strategy of selected protein mutagenesis with chromophore modification was utilized, which yielded several exciting results. We conceived the novel retinal analog MMAR, which has the remarkable potential, particularly when combined with specific opsin modifications, to generate NIR active proton-pumps. In order to screen for and/or optimize red-shifting protein mutants, we developed a novel chemotaxis-based directed evolution assay. This enables the simultaneous screening for desired spectral properties and pump function in a library of mutants. This assay can additionally be combined with retinal analogs, to enhance the proton-pumping function of the respective pigments. The stability of the various pigments generated in our study was assessed in different membrane-mimicking micro-environments, towards their eventual biophysical characterization. We anticipate that the library of retinal analog and rhodopsin proton-pump variants developed in this research will have broad potential in several biotechnological fields. Shifting the action spectra of microbial rhodopsins beyond 700 nm generates exciting applications in phototrophy, optogenetics, membrane-sensor- and nano-bio technologies.

6.1 Characterization and investigation of MMAR pigments

Alterations in the structure and electronic properties of the retinal chromophore have an impact on both the colour and pump activity of the resulting pigments, as demonstrated in **Chapters 2 and 3** of this thesis. Of the retinal analogs tested in **Chapter 2**, retinal A2 was found to induce a red-shift in the absorbance band of all pigments tested, while retaining significant proton-pump activity. Hence we further adapted A2 and tested various A2 analogs in **Chapter3**, of which MMAR was established as the most lucrative. All MMAR pigments showed red-shifted absorbance bands and could be activated by NIR light, thereby representing the first NIR active proton-pumps reported thus far. The properties of these MMAR pigments, particularly within the context of PR, are fascinating. The combination of PR-DNFS with MMAR results in an unprecedented ~740 nm absorbance band. In fact, this band is already intensified in WT PR upon protonation of the counterion. The unusual pH dependence of both PR:MMAR and PR-DNFS:MMAR illustrates the remarkable sensitivity of this analog towards the electrostatic distribution within the retinal binding pocket. We postulate that in MMAR pigments, the positive charge on the pSB has a tendency to delocalize towards the ring element. The 3-monoamine nitrogen provides a stabilizing influence to this charge leading to the resonance structures displayed in figure 3. 7. These structures probably exist in a relatively slow dynamic equilibrium, giving rise to the complex absorbance profile of the resulting pigments. The features of the electronic transitions involved in shaping this absorbance band, the influence of specific binding pocket environments towards the same, and their combined effects on the proton pump activity, provides inspiration for additional experimental and theoretical investigation.

Computational studies using time-dependent density functional theory (TD-DFT) and *ab initio* molecular dynamics (MD) have previously been very useful to simulate the potential energy surfaces involved in the ground

and excited states of the pSB and its photoisomerization dynamics [1, 2]. Such calculations have the advantage of being able to test the influence of different electrostatic environments in the vicinity of the pSB, such as counterion charges or interaction with water molecules. We have made some progress towards the TD-DFT and *ab initio* MD investigation of a minimal retinal binding pocket model of PR, containing the pSB, the His-Asp cluster, a Y200 mimic and three water molecules [3]. Intriguingly, this minimal model could recapitulate the first excitation energies of all analog pigments of PR tested, including PR:MMAR. However, the origin of the 740 nm absorbance band and its pH dependence is still an open question. We anticipate that refinement of the model by inclusion of other binding pocket residues will yield a more comprehensive analysis. The computational load of quantum mechanical calculations often limits their applicability to systems containing a few hundred atoms. This quantum mechanical description of the pSB and its nearby residues is often combined with a classical mechanical description of the residual protein in a hybrid approach termed as quantum mechanical/molecular mechanics (QM/MM) [4]. QM/MM is rapidly becoming an established technique, and has already been used to investigate bovine rhodopsin [5], bR [6]and SR-II [7]. The expansion of our minimal retinal binding pocket into a full QM/MM description would provide crucial information about the role of the opsin environment in colour tuning. Furthermore, such an analysis would have strong predictive potential to aid further chromophore or protein modification.

The photoisomerization and photocycle dynamics of the novel analog pigments generated in our study are still largely undisclosed. As detailed in **Chapter 5**, we tested various detergent and membrane environments on the WT and analog pigments, towards the goal of further extensive characterization using spectroscopic methods. PR pigments retain their native quaternary structure and have high thermal stability in the

detergent DDM. On the other hand, GR analog pigments can benefit from subsequent incorporation into a membrane environment. We describe the assembly and stabilization of GR in soluble MSP-nanodiscs, which are too small to contain the PR oligomeric assembly. The optical transparency of both the detergent and nanodisc assemblies enables them to be studied using kinetic spectroscopy. The characterization of the early photo-intermediates of various analog pigments generated in our study is currently underway using femtosecond time-resolved spectroscopy in a DDM and nanodisc microenvironment. Liposomes are another suitable membrane mimic, which are widely used in the ssNMR investigation of various microbial rhodopsins. We have made an initial effort towards the incorporation of PR and GR containing a $^{13}C_{10}$ retinal chromophore into liposomes. We hope to extend this investigation with uniform ^{15}N labeling of the opsin and ^{13}C labeled retinal analogs, such as MMAR, to study the impact of perturbations to the pSB or the binding pocket.

6.2 Further protein or chromophore engineering

In this thesis, we describe the construction of some site-directed mutants described in **Chapters 2 and 3**, which were further combined yielding several double and triple mutants listed in the appendix (Figure A.5). However, most mutation combinations impair the proton-pump function of the pigments, which presents a serious drawback. The combination of individual red-shifted mutations seems to have a limited additive effect on spectral properties and is increasingly deleterious on pumping activity. This is characteristic for the low predictive power of this approach. To overcome such limitations, we describe the development of a novel chemo-taxis assay in **Chapter 4**, which enables the laboratory scale evolution of PR and GR. The highlight of this assay is the simultaneous selection of spectrally shifted variants with conserved or even improved proton-pumping function from a library of random mutations. We anticipate that this method will be useful to select for novel red-shifted opsin mutants.

Furthermore, it can be combined with the retinal analog and mutant combinations discussed in this thesis. For instance, GR-FS:MMAR, which has significant pump activity under NIR illumination, can be used to evolve further red-shifted pigments or the pump activity of PR-DNFS:MMAR can be augmented under high light illumination.

In **Chapters 2 and 3**, we report on modifications at the ring end of the retinal chromophore. It was previously shown by various groups that introducing electron-withdrawing substituents near the polar end of retinal, such as fluoride or trifluoromethyl (CF_3), generate red-shifts in the absorbance bands of bR and bovine visual rhodopsin (Rh)[8]. 13-CF_3 retinal was found to form active red-shifted analog pigments with Rh [9] and bR [10]. We tested the combination of modifications near the ring and polar end of the retinal by introducing a 13-CF_3 substituent in the retinals A2 and MOA2 (see Appendix, Figure A.3). To our surprise, neither of these analogs generated stable analog pigments of PR or GR. The lack of a corresponding stable holo-pigment suggests that the 13-CF_3 derivative does not constructively fit within the retinal binding pocket, possibly because of higher thermal stability of the 13-*cis* isomeric state. On the other hand, 14-F substituted retinal A1 yielded 40-60 nm red-shifted active analog pigments with PR and GR (data not shown), which was also previously reported for bR [8, 11] and Rh [9]. Furthermore, introduction of a 14-F substituent in retinal derivatives with ring modifications generated additional large red-shifts. 14-F MOA2 induced a ~130 nm red-shift in the absorbance of Rh and iodopsin [12], while 14-F azulenic derivatives were shown to cause 170-230 nm red-shifts in the absorbance bands of bR [8]. However, the activity of these pigments is severely attenuated. In fact, the non-substituted azulenic pigments already have very low activity [8, 12]. Nonetheless, introduction of a 14-F substituent in MMAR would be a realistic option to further red-shift of or enhance the low-energy bands in the absorbance profile. Since enamine resonance structures probably

contribute to these low-energy bands of the MMAR pigments (c.f. figure 3.7), another option would be to enhance the electrodonating character of substituents at the aromatic ring without compromising the fit in the binding pocket.

Such red-shifting retinal derivatives have broad application, since in principle they will directly incorporate in all opsin classes, or can be made to fit using small modifications or protein mutagenesis. Examples of some applications are discussed in the following sections.

6.3 Complementing photosynthesis

Photosynthetic microorganisms such as cyanobacteria and algae hold great promise as autotrophic cell factories in the sustainable conversion of solar energy into liquid fuels and biomass [13]. Cyanobacteria in particular are attractive systems to engineer towards the production of important biomolecules or biofuels due to their high growth rates, well-characterized genome and the potential for the direct conversion of energy towards a desired product [14-17]. However, a major bottleneck in the industrial scale application of these microorganisms is that their photosynthetic efficiency is quite low, maximally in the order of 12% [18]. There are several structural and thermodynamic constraints responsible for this low efficiency . The organisms generate only enough ATP to fuel their needs for growth and survival. Furthermore, the net amount of photon energy utilized by photosynthesis is limited. At higher light intensity, structural changes are activated which lead to non-photochemical quenching of the light harvesting complexes, as a photoprotective mechanism. Another important limitation is the spectral range usable by oxygenic photo-synthesis, termed the photosynthetically active radiation (PAR; 400-700 nm), which accounts for less than half the number of solar photons that reach the earth's surface. This is dictated by the absorbance bands of the predominantly exploited chlorophylls a and b (Chl *a* and Chl *b*) in the blue

and red region of the PAR. By exception, some cyanobacteria are able to produce Chl *d*, extending their PAR to about 720 nm. It was postulated that a method of increasing oxygenic photosynthetic efficiency could be accomplished by expanding the wavelength sensitivity of the system to utilize photons outside the PAR [19, 20]. In fact, using photons up to 750 nm would already increase the available photon energy by 19% [19]. An option could be to utilize bacteriochlorophylls, such as BChl *a* and BChl *b*, which are utilized by anoxygenic photosynthetic organisms. Their action spectra extend into the NIR as far as about 1100 nm [21, 22]. However these are relatively complicated systems to engineer into cyanobacteria, and would certainly cause membrane-crowding. Retinal-based phototrophy may be another viable approach towards this end [23, 24].

Rhodopsin proton-pumps have good potential to complement oxygenic photosynthesis due to their light driven function, relatively small genome, ease of engineering, and lack of photobleaching at high light intensities. In the complementary part of our BSC project, we set out to express the proton-pumps PR and GR in the cyanobacterium Synechocystis sp. PCC 6803 and explore their potential to complement oxygenic photosynthesis [24]. The core aim was to express these proton pumps with a batho-chromically shifted absorbance band in the thylakoid membrane in order to allow the transformed organism to utilize photons outside the PAR. Using WT PR and GR pigments, suitable plasmid based expression systems were generated and characterized for *Synechocystis*, and the functional impact of PR and GR expression was assessed [25, 26]. WT PR showed good expression levels and could even stimulate growth of the organism upon illumination, as compared to the non-functional PR D97N mutant, albeit to only a small extent [25]. Assuming that PR-driven energy production could not compete with PSI, it was decided to test a PSI deletion strain of Synechocystis (ΔPSI). Indeed, in this case PR expression gave a significant growth advantage (Chen et al., submitted). The logical follow-up step, viz.

the transformation of the ΔPSI strain with the NIR active PR-DNFS:MMAR described in **Chapter 3** is in progress. We anticipate that despite the lower pump capacity of this analog pigment, supplementation of the resulting strain with NIR light will significantly benefit its growth. This would set a ground-breaking landmark, which after further optimization of such "rainbow strains", would eventually allow to exploit outside-PAR energy input for the microbial production of fuels and commodities.

6.4 Optogenetics

Various light gated ion channels and pumps have found an important application in the field of optogenetics. These channels, broadly classified as cation channelrhodopsins (CCRS) and anion channelrhodopsins (ACRs), are expressed in neurons and are used to selectively depolarize or hyperpolarize the cells upon illumination. This enables precise spatio-temporal control of the activity of neuronal populations and can be even used to modulate their firing frequency. As a consequence, optogenetics has emerged as a very powerful tool in neuroscience and is now widely used to study brain circuitry, or for the pharmacological investigation of specific drugs [27]. The birth of optogenetics was initiated by the discovery of the CCRs Channelrhodopsins1 and 2 (ChR1 and ChR2), which function as light-gated cation channels in the algal eye membrane of *Chlymydomonas reinhardtii* [28, 29]. These channels are transgenically expressed in the neurons of diverse organisms ranging from zebrafish to mammals. They cause neuronal excitation upon illumination with green light, due to an influx of nonspecific cations which cause depolarization of the membrane. On the other hand, the chloride channel Halorhodopsin (NpHR), a member of the ACR family, causes inhibition of neurons by hyperpolarizing the cell membrane upon illumination, due to Cl^- influx [30].

The CCRs and ACRs used in optogenetics have an absorbance maximum between 450-550 nm. Since blue-green light is strongly absorbed and

undergoes significant scattering in biological tissue, most optogenetic techniques in mammalian brain require the implantation of fibre optic cables to deliver light to subcortical tissue. However, the subsequent mechanical perturbation of the tissue may have several non-specific effects, which limits its usability to more superficial brain regions. Thanks to the much lower loss due to scattering, light ≥ 700 nm penetrates much further into biological tissue than blue-green light. Hence, deep-red-light active optogenetic tools are highly desired, and though some effort has been made in this direction [31], NIR activation is still largely inaccessible in this technique.

Chromophore substitution using retinal analogs described in **Chapters 2 and 3** of this thesis provides a complementary strategy to improve the flexibility of these optogenetic tools. Supplementation with MMAR, for instance, would allow improved light penetration and the stimulation of deeper brain regions using NIR illumination. As another example, All-E-6-s-*trans*-locked retinal A2 would enable to red-shift channelrhodopsins, without significant interference with the visual system or signalling metabolites of retinal A1. Multi-wavelength excitation, where distinct neuronal populations are activated or inhibited, is a valuable technique in optogenetics [32], which can be accomplished using red or blue shifting retinal analogs. These analogs can be supplied to the region of interest by stereotactic injection in the tissue, or by dietary supplementation to null mutants in retinal synthesis. Insights obtained from red-shifted mutants generated in the directed evolution assay described in **Chapter 4** will also aid the design of further red-shifted CCRs and ACRs in the future.

6.5 Membrane potential sensors

The non-pumping mutant PR-D97N (PROPS) was recently engineered as a sensor of membrane potential in *E. coli* [33]. While this pigment has almost no pumping activity, it exhibits strong fluorescence, which is sensitive to

the membrane voltage. This was truly a remarkable study, since PROPS facilitates the membrane studies of a small system such as *E. coli*, which is inaccessible to traditional electrophysiological methods. In initial experiments, we saw an at least five-fold enhancement of the fluorescence intensity of PROPS with MMAR relative to A1, with a concomitant red-shift of about 200 nm (Appendix, figure A.7). Such MMAR based voltage indicators would be very useful for the NIR fluorescent imaging of systems, which are too small or difficult to study by conventional means, such as bacteria, neuronal compartments, mitochondria or other cellular organelles.

PROPS could not yet be adapted to eukaryotic cells, due to poor targeting and lack of localization to the plasma membrane. The proton pump AR3 on the other hand shows excellent expression in mammalian neurons, where it was shown to function as an optogenetic neural silencer [34]. Importantly, AR3 also shows fluorescence which is dependent upon the membrane voltage, enabling its potential as a fluorescent sensor in the live-cell imaging of neurons [35]. Such rhodopsin based fluorescent imaging has an advantage over traditionally used fluorescence indicators or calcium imaging, due to its fast response time and low phototoxicity. The dim fluorescence of AR3 could be enhanced in intensity using site-saturation mutagenesis [36] or in combination with merocyanine retinal analogs to engineer a 8.5 fold brighter NIR fluorescent sensor [37]. Our preliminary results have shown that MMAR red-shifts and broadens the absorbance band of AR3 (data not shown), but its effect on intensity and position of the emission band has not yet been investigated. Nonetheless, we can conclude that dual chromophore and protein modification holds great potential in optimizing NIR fluorescent sensors.

References

[1] Robb, M. A., Garavelli, M., Olivucci, M. and Bernardi, F., "A computational strategy for organic photochemistry" *Reviews in Computational Chemistry*. 2000, John Wiley & Sons, Inc. p. 87-146.

[2] Valsson, O., Filippi, C. and Casida, M. E. "Regarding the use and misuse of retinal protonated Schiff base photochemistry as a test case for time-dependent density-functional theory ", *J ChemPhys*, 2015. **142**(14): p. 144104.

[3] Buda, F., Keijer, T., Ganapathy, S. and de Grip, W. J. "A quantum-mechanical study of the binding pocket of proteorhodopsin: Absorption and vibrational spectra modulated by analogue chromophores ", *Photochem Photobiol*, 2017. **in press**: DOI: 10.1111/php.12800.

[4] Vreven, T. and Morokuma, K. "Hybrid Methods: ONIOM(QM:MM) and QM/MM ", *Annu Rep Comput Chem*, 2006. **2**: p. 35-51.

[5] Coto, P. B., Strambi, A., Ferré, N. and Olivucci, M. "The color of rhodopsins at the ab initio multiconfigurational perturbation theory resolution ", *Proc Natl Acad Sci U S A*, 2006. **103**(46): p. 17154-17159.

[6] Punwong, C., Martinez, T. J. and Hannongbua, S. "Direct QM/MM simulation of photoexcitation dynamics in bacteriorhodopsin and halorhodopsin ", *Chem Phys Lett*, 2014. **610**: p. 213-218.

[7] Altun, A., Yokoyama, S. and Morokuma, K. "Quantum mechanical/molecular mechanical studies on spectral tuning mechanisms of visual pigments and other photoactive proteins ", *Photochem Photobiol*, 2008. **84**(4): p. 845-854.

[8] Liu, R. S., Krogh, E., Li, X. Y., Mead, D., Colmenares, L. U., Thiel, J. R., Ellis, J., Wong, D. and Asato, A. E. "Analyzing the red-shift characteristics of azulenic, naphthyl, other ring-fused and retinyl pigment analogs of bacteriorhodopsin ", *Photochem Photobiol*, 1993. **58**(5): p. 701-5.

[9] Liu, R. S. H. and Asato, A. E., "The binding site of opsin based on analog studies with isomeric, fluorinated, alkylated, and other modified retinals " *Chemistry and Biology of Synthetic Retinoids* M.I.D.a.W.H. Okamura, Editor. 1990, CRC Press, Inc.: Boca Raton, Fl, U.S.A. p. 52-75.

[10] Gaertner, W., Oesterhelt, D., Towner, P., Hopf, H. and Ernst, L. "13-(Trifluoromethyl)retinal forms an active and far-red-shifted chromophore in bacteriorhodopsin ", *J Am Chem Soc*, 1981. **103**(25): p. 7642-7643.

[11] Tierno, M. E., Mead, D., Asato, A. E., Liu, R. S., Sekiya, N., Yoshihara, K., Chang, C. W., Nakanishi, K., Govindjee, R. and Ebrey, T. G. "14-Fluorobacteriorhodopsin and other fluorinated and 14-substituted analogues. An extra, unusually red-shifted pigment formed during dark adaptation ", *Biochemistry*, 1990. **29**(25): p. 5948-53.

[12] Imai, H., Hirano, T., Terakita, A., Shichida, Y., Muthyala, R. S., Chen, R., Colmenares, L. U. and Liu, R. S. H. "Probing for the threshold energy for visual transducin: red-shifted visual pigment analogs from 3-methoxy-3-dehydroretinal and related compounds ", *Photochem Photobiol*, 1999. **70**(1): p. 111-115.

[13] Wijffels, R. H., Kruse, O. and Hellingwerf, K. J. "Potential of industrial biotechnology with cyanobacteria and eukaryotic microalgae ", *Curr Opin Biotech*, 2013. **24**(3): p. 405-413.

[14] Gao, X., Sun, T., Pei, G., Chen, L. and Zhang, W. "Cyanobacterial chassis engineering for enhancing production of biofuels and chemicals ", *Appl Microbiol Biotechnol*, 2016. **100**(8): p. 3401-3413.

[15] Nozzi, N. E., Oliver, J. W. K. and Atsumi, S. "Cyanobacteria as a Platform for Biofuel Production", *Front Bioeng Biotechnol*, 2013. **1**: p. 7.

[16] Chen, Q., Montesarchio, D. and Hellingwerf, K. J. "'Direct Conversion' ", *Advances in Botanical Research*, 2016. **79**: p. 43-62.

[17] Al-Haj, L., Lui, Y. T., Abed, R. M. M., Gomaa, M. A. and Purton, S. "Cyanobacteria as chassis for industrial biotechnology: Progress and prospects", *Life*, 2016. **6**(4): p. 42.

[18] Touloupakis, E., Cicchi, B. and Torzillo, G. "A bioenergetic assessment of photosynthetic growth of Synechocystis sp. PCC 6803 in continuous cultures", *Biotechnol Biofuels*, 2015. **8**(1): p. 133.

[19] Chen, M. and Blankenship, R. E. "Expanding the solar spectrum used by photosynthesis", *Trends in plant science*, 2011. **16**(8): p. 427-31.

[20] Blankenship, R. E., et al. "Comparing photosynthetic and photovoltaic efficiencies and recognizing the potential for improvement", *Science*, 2011. **332**(6031): p. 805-9.

[21] Chen, M., Schliep, M., Willows, R. D., Cai, Z.-L., Neilan, B. A. and Scheer, H. "A red-shifted chlorophyll", *Science*, 2010. **329**(5997): p. 1318.

[22] Croce, R. and van Amerongen, H. "Natural strategies for photosynthetic light harvesting", *Nat Chem Biol*, 2014. **10**(7): p. 492-501.

[23] Claassens, N. J., Volpers, M., dos Santos, V. A. P. M., van der Oost, J. and de Vos, W. M. "Potential of proton-pumping rhodopsins: engineering photosystems into microorganisms", *Trends Biotechnol*, 2013. **31**(11): p. 633-642.

[24] C2.9, C. p. "A complementary photosystem for proton-pumping in Synechocystis PCC6803", *BioSolar Cell Programme*, 2009. http://www.biosolarcells.nl/onderzoek/algen/

[25] Chen, Q., van der Steen, J. B., Dekker, H. L., Ganapathy, S., de Grip, W. J. and Hellingwerf, K. J. "Expression of holo-proteorhodopsin in *Synechocystis* sp. PCC 6803", *Metab Eng*, 2016. **35**: p. 83-94.

[26] Chen, Q., Arents, J., Ganapathy, S., de Grip, W. J. and Hellingwerf, K. J. "Functional expression of Gloeobacter rhodopsin in *Synechocystis* sp. PCC6803", *Photochem Photobiol*, 2017. **93**(3): p. 772-781.

[27] Kushibiki, T., Okawa, S., Hirasawa, T. and Ishihara, M. "Optogenetics: Novel tools for controlling mammalian cell functions with light", *Int J Photoenergy*, 2014. **2014**: p. 1-10.

[28] Nagel, G., Ollig, D., Fuhrmann, M., Kateriya, S., Musti, A. M., Bamberg, E. and Hegemann, P. "Channelrhodopsin-1: A light-gated proton channel in green algae", *Science*, 2002. **296**(5577): p. 2395.

[29] Nagel, G., Szellas, T., Huhn, W., Kateriya, S., Adeishvili, N., Berthold, P., Ollig, D., Hegemann, P. and Bamberg, E. "Channelrhodopsin-2, a directly light-gated cation-selective membrane channel", *Proc Natl Acad Sci U S A*, 2003. **100**(24): p. 13940-13945.

[30] Zhang, F., Wang, L.-P., Brauner, M., Liewald, J. F., Kay, K., Watzke, N., Wood, P. G., Bamberg, E., Nagel, G., Gottschalk, A. and Deisseroth, K. "Multimodal fast optical interrogation of neural circuitry", *Nature*, 2007. **446**(7136): p. 633-639.

[31] Lin, J. Y., Knutsen, P. M., Muller, A., Kleinfeld, D. and Tsien, R. Y. "ReaChR: a red-shifted variant of channelrhodopsin enables deep transcranial optogenetic excitation", *Nat Neurosci*, 2013. **16**(10): p. 1499-508.

[32] Prigge, M., Schneider, F., Tsunoda, S. P., Shilyansky, C., Wietek, J., Deisseroth, K. and Hegemann, P. "Color-tuned Channelrhodopsins for multiwavelength optogenetics", *J Biol Chem*, 2012. **287**(38): p. 31804-31812.

[33] Kralj, J. M., Hochbaum, D. R., Douglass, A. D. and Cohen, A. E. "Electrical spiking in *Escherichia coli* probed with a fluorescent voltage-indicating protein", *Science*, 2011. **333**(6040): p. 345-8.

[34] Chow, B. Y., Han, X., Dobry, A. S., Qian, X., Chuong, A. S., Li, M., Henninger, M. A., Belfort, G. M., Lin, Y., Monahan, P. E. and Boyden, E. S. "High-performance genetically targetable optical neural silencing by light-driven proton pumps", *Nature*, 2010. **463**(7277): p. 98-102.

[35] Kralj, J. M., Douglass, A. D., Hochbaum, D. R., Maclaurin, D. and Cohen, A. E. "Optical recording of action potentials in mammalian neurons using a microbial rhodopsin", *Nat Methods*, 2012. **9**(1): p. 90-5.

[36] McIsaac, R. S., Engqvist, M. K., Wannier, T., Rosenthal, A. Z., Herwig, L., Flytzanis, N. C., Imasheva, E. S., Lanyi, J. K., Balashov, S. P., Gradinaru, V. and Arnold, F. H. "Directed evolution of a far-red fluorescent rhodopsin", *Proc Natl Acad Sci U S A*, 2014. **111**(36): p. 13034-9.

[37] Herwig, L., Rice, A. J., Bedbrook, C. N., Zhang, R. K., Lignell, A., Cahn, J. K., Renata, H., Dodani, S. C., Cho, I., Cai, L., Gradinaru, V. and Arnold, F. H. "Directed evolution of a bright near-Infrared fluorescent rhodopsin using a synthetic chromophore", *Cell Chem Biol*, 2017. **24**(3): p. 415-425.

Appendix

A.1 Sources of special chemicals

Company	Special chemicals/Materials
Addgene	MSPDE31-plasmid
Anatrace	1-n-dodecyl-β-D maltopyranoside (DDM), octyl-β-D-glucopyranoside neopentyl glycol (OGNG)
Avanti polar lipids	*E. coli* polar lipid extract
Buchem	Retinals MOA2, DMAR, MMAR, [8-15, 19, 20]-$^{13}C_{10}$-labelled A1
Cray valley	SMA2000
Gifts	Retinals A2, ALL-E, PHE, MOA2, nonyl β-D-glucopyranoside, asolectin, dodecyl phosphocholine (DPC)
Novagen	1,4-Dithiothreitol (DTT), benzonase nuclease
Promega	isopropyl β-D-1-thiogalactopyranoside (IPTG)
Roche	EDTA-free protease inhibitor tablets, anti-His_6 mouse monoclonal antibody,
Thermo-Scientific Fischer	Ni^{2+}-NTA resin and columns, Coomassie brilliant blue G-250, restriction enzymes, protein ladder, *Pfu* DNA polymerase
Sigma-Aldrich	Retinal A1, ampicillin, valinomycin, lysozyme, carbonyl cyanide m-chlorophenylhydrazone (CCCP), imidazole, bis-tris propane, hydroxylamine, L-Serine, HEPES, β-cyclodextrin, benzoase nuclease, octyl-β-D-glucopyranoside (OG), TritonX-100, Tergitol NP-40, Blue-dextran

A.2 Absorbance spectra, λ_{max} and ε of free retinals and proteorhodopsins

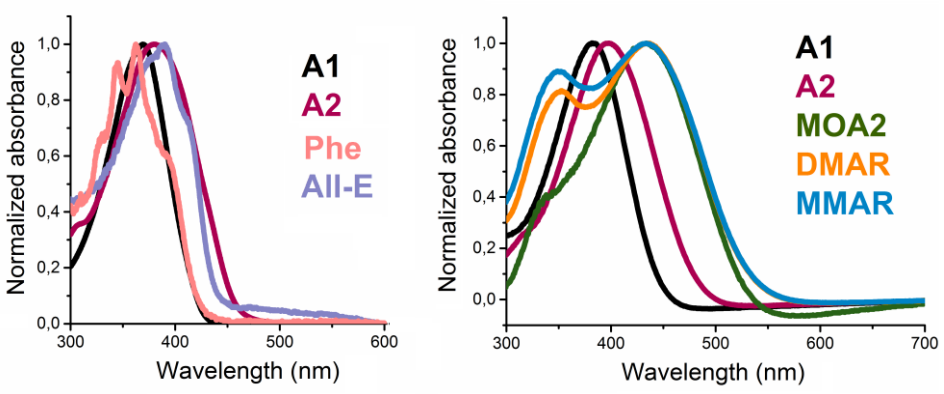

Figure A.2: Absorbance spectra of retinal analogs in organic solvents. [a] A1, A2, ALL-E (hexane); PHE (methanol). [b] A1, A2, MOA2, DMAR, MMAR (DMF).

Retinal	λmax (nm)			
	[a]DMF	[b] 1% DDM	[c] Oxime DMF	[d] Oxime 1% DDM
A1	382	388	365	368
A2	400	404	375	378
PHE	360	nd	nd	nd
ALL-E	395	nd	nd	nd
MOA2	430	441	415	402
DMAR	430	433	358	370
MMAR	423	438	358	350

Table A.2.1: λ_{max} of [a] free retinal in DMF, with the exception of PHE (in methanol) and ALL-E (in hexane). [b] free retinal in 1% DDM solution (pH 7); [c] retinal oxime in DMF solution; [d] retinal oxime in 1% DDM solution (pH 7). Data are the average of at least two measurements, with standard deviation ≤2 nm. nd: not determined.

Retinal	ε ($M^{-1}cm^{-1}$)				
	[a] DMF	[b] 1% DDM	[c] Oxime 1% DDM	[d] PR:retinal 1% DDM	[e] GR:retinal 1% DDM
A1	45600	39500	52500	54200	55500
A2	44500	38000	44000	46800	49200
MOA2	30400	31500	30400	nd	nd
DMAR	31800	29000	42000	40500	nd
MMAR	28000	31000	36000	35200	34200

Table A.2.2: Molar absorbance (ε) of retinals and corresponding proteorhodopsins. [a] free retinal in DMF solution; [b] free retinal in 1% DDM solution; [c] retinal oxime in 1% DDM solution; [d] PR containing the various retinal analogs, after solubilization in 1% DDM solution; [e] GR containing the various retinal analogs, after solubilization in 1% DDM solution. The DDM solution is at pH 7. Data are averages of duplicate assays, with standard deviation ≤ 8%. nd: not determined.

A.3 Fluorinated retinal analogs

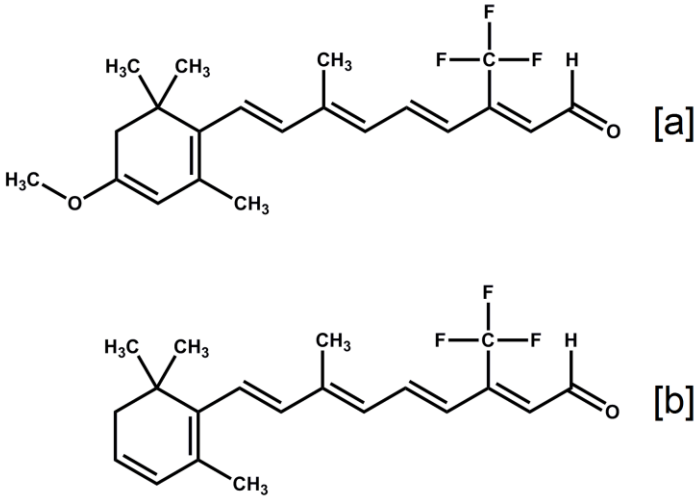

Figure A.3: Chemical structures of retinal analogs that do not yield stable pigments with PR or GR, upon addition to culture or regeneration in membrane vesicles. [a] 3-methoxy-13-trifluoromethyl retinal A2 (λmax = 453 nm in hexane); [b] 13- trifluoromethyl retinal A2 (λmax = 446 nm in hexane). Both are strongly red-shifted relative to retinal A2 (λmax = 381 nm in hexane).

A.4 Primer sequences used in this study for site-directed mutagenesis

Primer name	Sequence
1267_vector_for	GTGAGCGGATAACAATTTCACACAGG
2893_PR_D212N_for	CACAGGTTACCTGATGGGTAACGGTGGATCAGCTCT
2894_PR_D212N_rev	AGAGCTGATCCACCGTTACCCATCAGGTAACCTGTG
2895_PR_F234S_for	GACTTTGTTAACAAGATTCTATCCGGATTAATTATATG
2896_PR_F234S_rev	CATATAATTAATCCGGATAGAATCTTGTTAACAAAGTC
2897_vector_rev	GTATCCGCTCATGAGACAATAACCC
2922_PR_T101A_for	AGATACATTGATTGGTTGCTAGCAGTTCCTCTATTAATATGTG AATTCTAC
2923_PR_T101A_rev	GTAGAATTCACATATTAATAGAGGAACTGCTAGCAACCAATCA ATGTATCT
2924_PR_L105K_for	CATTGATTGGTTACTAACAGTTCCTCTTAAGATATGTGAATTC TACTTAA
2925_PR_L105K_rev	TTAAGTAGAATTCACATATCTTAAGAGGAACTGTTAGTAACCA ATCAATG
2926_PR_A178R_for	CTGCATGCAATACTCGAAGTCCTGCTGTGCAATCAGCT
2927_PR_A178R_rev	AGCTGATTGCACAGCAGGACTTCGAGTATTGCATGCAG
2970_GR_F260S_for	GCCTGTATCAGGTCTACTAGTCTTCGCGA
2971_GR_F260S_rev	GAAGACTAGTAGACCTGATACAGGCTTCGC

for = forward primer

rev = reverse primer

A.5 Site-directed mutants, their λ_{max} and relative proton-pump activity

Site-directed mutants generated in this study	[a]λmax (nm)	[b]H+
GR WT	540	+++
GR F260S	549	+++
PR WT	520	+++
PR D212N	521	+++
PR F234S	540	+
PR L105K	538	+
PR T101A	539	++
PR A178R	540	-
PR D212N, F234S	540	++
PR D212N, F234S, L105K	545	+
PR D212N, F234S, T101A	555	+
PR D212N, F234S, A178R	548	-

Table A.5: WT pigments and their corresponding single, double and triple mutants generated in this study. [a] λ_{max} of the purified pigments in 0.1% DDM solution, pH 8. [b] proton pumping scores relative to the corresponding WT pigment. +++ 70-100% WT, ++ 50-70% WT, + 30-50% WT, - 0-30% WT.

A.6 pH effect with PR-DNFS:MMAR

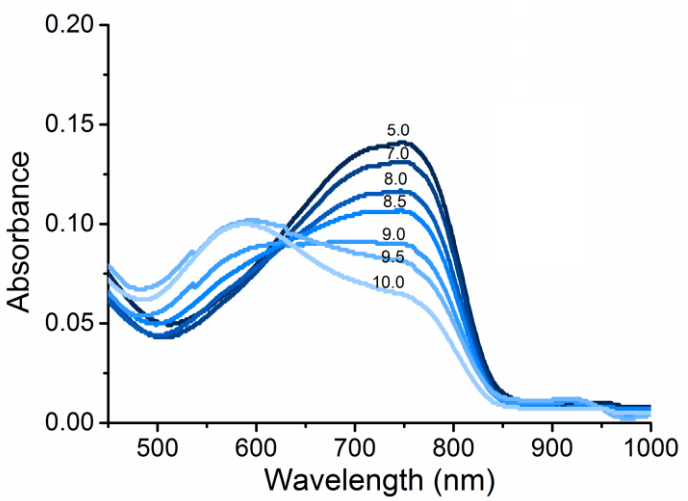

Figure A.6: Absorbance spectra of His-tag purified PR-DNFS:MMAR in DDM solution at pH 5, 7, 8, 8.5, 9, 9.5, 10. pH values are indicated next to the corresponding spectrum in the graph. Spectra represent separate samples, not a titration of a single sample.

A.7 Fluorescence of PROPS with MMAR

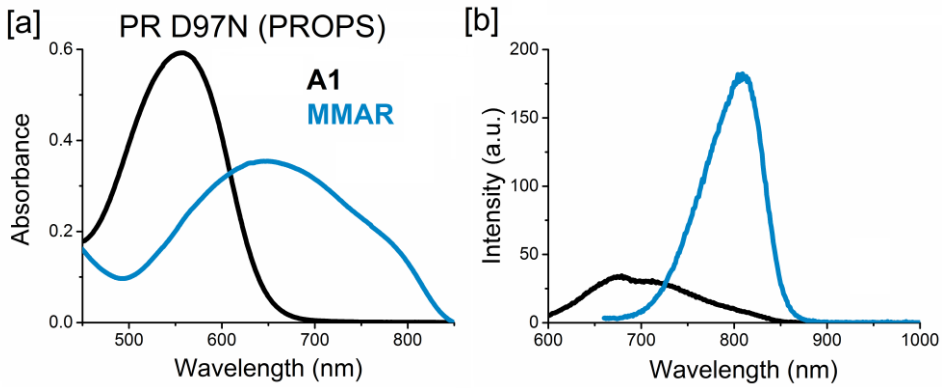

Figure A.7: Absorbance spectra of His-tag purified PROPS: A1 and PROPS:MMAR in DDM solution, pH 8 [a] and their corresponding emission spectra upon excitation at 540 nm for PROPS:A1 and 650 nm for PROPS:MMAR[b].

Summary

Solar energy is the most abundant source of renewable energy available on our planet, which is utilized by plants and certain microorganisms to fuel their growth and survival. Photosynthetic organisms use sunlight to fix atmospheric carbon dioxide and generate chemical energy, which can potentially be channeled towards the sustainable production of biofuels, platform chemicals, secondary metabolites and biomass in bioeconomy applications. However, the industrial applicability of photosynthesis is limited by the yield of the reaction. A significant part of the photon energy utilized by photosynthetic organisms to sustain their growth and maintenance is required to drive the photosynthetic reaction itself. Furthermore, the near-infrared region of the solar spectrum, which accounts for around half of the available photons at the earth surface, is essentially unexploited by photosynthesis.

In this thesis, we propose the use of microbial rhodopsins as an alternative photosystem in a complementary approach towards more efficient use of the photons in the solar spectrum. Microbial rhodopsins are photosensitive pigments implemented in the growth and adaptation of a large population of microorganisms. These relatively simple, tunable photosystems use a molecule of retinal as a chromophore to facilitate the conversion of sunlight to chemical energy. Retinal-based phototrophy is believed to sustain the phototrophic balance of various biospheres and has several important biotechnological applications. In this thesis, we describe the adaptation of two rhodopsin proton-pumps, namely proteorhodopsin (PR) and *Gloeobacter* rhodopsin (GR), to shift their action spectrum into the near-infrared region. In **Chapter 1**, we present a brief introduction to these proton-pumps and their underlying mechanism. We further describe our core research goal, namely, to generate and use near-infrared active proton-pumps as a complement to natural photosynthesis.

In **Chapter 2**, we discuss the first steps towards the spectral modulation of PR and GR using a combination of protein and chromophore engineering. We

describe the use of retinal analogs with different structural and electronic properties. These analogs are further combined with specific protein mutations, which were shown to have a complementary effect on the spectral properties of the analog pigments. Thus, we were able to generate both red and blue shifts in the spectral bands of PR and GR, with a minimal effect on the proton pumping function. From this chapter, we delineate the red-shifting analog retinal A2, which contains an extended conjugation in its ring element, as a template for further chromophore modification.

We focused on increasing the red-shifting potential of retinal A2 in **Chapter 3** with further modifications. The ring conjugation of A2 was extended by introducing electron withdrawing groups at the C3 position on the retinal. Of all analogs tested, one particular analog containing a 3-monomethylamino substituent, namely MMAR, was shown to induce the largest red-shift. MMAR pigments obtained with PR and GR were shown to be active upon illumination with 730 nm light, thereby representing the first near-infrared active proton pumps generated thus far. Quite remarkably, MMAR is very sensitive to the electrostatic environment of the retinal binding pocket, as demonstrated by a ~220 nm red-shift in the absorbance band upon acidification. A similar shift is also effectuated by a specific binding pocket mutation. The corresponding PR-D212N,F234S:MMAR pigment has an absorbance band peaking around 750 nm and thereby is the most red-shifted active microbial rhodopsin reported thus far.

The influence of a variety of site-specific mutations on the absorbance profile and activity of PR and GR were tested over the course of this research. However, a disadvantage inherent in this approach is that it is almost impossible to predict *de novo* whether and how a particular mutation will affect the spectral properties and/or the function of these proteins. To overcome this drawback, we designed a directed evolution based approach to evolve spectral variants of PR and GR, as detailed in **Chapter 4.** We tested various selection criteria, of which bacterial chemotaxis came out as the most efficient. We describe the construction of a novel chemotaxis-based directed

evolution assay, and the initial results obtained are very promising. This assay thus has the potential to evolve rhodopsin proton-pumps with spectral variations and/or augmented function.

The various mutant and analog pigments described in this thesis are ideal templates for further detailed biophysical characterization. Due to the insoluble nature of these membrane proteins, their detergent or lipid microenvironment often has an impact on their structure and dynamics. We assessed the influence of several detergent and lipid complexes on the stability, spectral properties and oligomeric assembly of PR and GR, as described in Chapter 5. We conclude that, ultimately, the choice of a suitable microenvironment depends upon the research question and corresponding methodology. We further provide examples of biophysical characterization of PR and GR made possible using different membrane-mimetic systems.

Chapter 6 presents the future outlook of this thesis. In summary, we have made significant progress towards the generation and characterization of near-infrared active rhodopsin proton-pumps. Follow-up studies involving the theoretical and biophysical characterization of these pigments have already been initiated. The chemotaxis assay described in this thesis has the potential for further evolution of these pigments, and in general, can also be applied towards other energy generating phototrophic systems. In conclusion, the near-infrared active proton-pumps generated in this thesis have important prospects in a number of biotechnological fields such as phototrophy mimetics, optogenetics and membrane sensor technology.

Samenvatting

Zonne-energie is een alom voorkomende en de meest krachtige bron van duurzame energie die beschikbaar is op onze planeet. Zonne-energie wordt benut door de meeste planten en een deel van de micro-organismen voor hun groei en voortbestaan. Fotosynthetische organismen vangen zonlicht in om atmosferische kooldioxide vast te leggen en chemische energie te genereren, die in principe ook bio-economisch toegepast kan worden voor de productie van biodiesel, duurzame chemicaliën, secundaire metabolieten en biomassa. Echter, de industriële toepasbaarheid van fotosynthese wordt beperkt door de opbrengst van de reactie. Een significant deel van de foton-energie wordt gebruikt door het fotosynthetische organisme voor groei en onderhoud en is nodig om het fotosynthetische bedrijf in werking te houden. Daarnaast kan de fotosynthese vrijwel geen gebruik maken van het nabije-infrarood (NIR) deel van het zonnespectrum, dat ongeveer de helft levert van de fotonen-flux op het aardoppervlak.

In dit proefschrift, propageren we het gebruik van microbiële rhodopsines als een alternatief fotosysteem, met tegelijkertijd een complementaire aanpak voor efficiënter gebruik van de fotonen in het zonnespectrum. Microbiële rhodopsines zijn lichtgevoelige pigmenten die een rol spelen bij groei en adaptatie van een grote populatie micro-organismen. Dit relatief simpele, moduleerbare fotosysteem gebruikt een retinal molecuul als chromofoor om de omzetting van zonlicht naar chemische energie te faciliteren. Er zijn duidelijke aanwijzingen, dat fototrofie gebaseerd op rhodopsines van significant belang is voor de balans tussen de verschillende biosferen en bovendien meerdere biotechnologische toepassingen heeft. In dit proefschrift beschrijven we de aanpassing van twee proton-pompende rhodopsines, namelijk proteorhodopsine (PR) en Gloeobacter rhodopsine (GR), met het doel hun actie-spectrum te verschuiven naar het NIR gebied. In hoofdstuk 1, wordt een korte introductie over dit type protonpompen en hun onderliggende mechanisme gegeven. Daarnaast beschrijven we het onderzoeksdoel, namelijk

het genereren en toepassen van NIR-actieve protonpompen als aanvulling op de natuurlijke fotosynthese.

In **hoofdstuk 2**, introduceren we de eerste stap naar spectrale aanpassing van PR en GR door modificatie van zowel het eiwitgedeelte als de chromofoor te combineren. We maken gebruik van retinal analoga, die verschillen qua structurele en elektronische eigenschappen. Combinatie van deze analoga met specifieke eiwitmutanten blijkt een synergistisch effect te geven op de spectrale eigenschappen van de pigment analoga. We zijn daarmee in staat om zowel rood- als blauwverschuivingen in de absorptie-spectra van PR en GR te genereren met slechts een gering effect op de protonpompactiviteit. In dit hoofdstuk beschrijven we onder meer het, dankzij een extra dubbele binding in de koolstofring, bathochrome analogon retinal A2, dat geschikt is als sjabloon voor verdere bathochrome chromofoor aanpassingen.

We concentreren ons in **hoofdstuk 3** op verdere modificatie van retinal A2 met het doel het bathochrome effect te versterken. De conjugatie met de koolstofring in retinal A2 is uitgesmeerd door introductie van elektronenzuigende groepen op de C3 positie. Van alle analoga die zijn getest bleek degene met een 3-monomethylamino subsituent, het MMAR, de grootste roodverschuiving te bewerkstelligen. PR en GR pigment analoga verkregen met MMAR blijken nog actief in NIR licht (730 nm) en zijn daarmee de eerstbekende NIR-actieve protonpompen. Opmerkelijk is dat MMAR zeer gevoelig is voor de elektrostatische omgeving in zijn bindingsplaats. Dit blijkt uit de reusachtige ~220 nm roodverschuiving in de absorptieband bij aanzuren. Een vergelijkbare verschuiving wordt ook bewerkstelligd in combinatie met een specifieke mutatie in het actieve centrum. Het resulterende pigment-analogon PR-D212N,F234S:MMAR vertoont zonder aanzuring al een absorptieband met een piek bij 750 nm en is daarmee het meest rood-verschoven nog actieve microbiële rhodopsine tot nu toe beschreven.

De invloed van een aantal specifieke mutaties op het absorptieprofiel en de activiteit van PR en GR zijn in de loop van dit project getest. Een nadeel inherent aan deze benadering is dat het bijna onmogelijk is om de novo te voorspellen of en hoe een bepaalde mutatie de spectrale eigenschappen en/of functie van deze eiwitten zal beïnvloeden. In een alternatieve aanpak hebben wij een "Directed Evolution" (Gestuurde Evolutie) strategie ontwikkeld om spectrale varianten van PR en GR te genereren, zoals gedetailleerd wordt beschreven in **hoofdstuk 4**. Hiertoe zijn verschillende selectiecriteria getest, waarbij bacteriële chemotaxis het meest effectief blijkt. Dit heeft geresulteerd in een nieuw, op chemotaxis gebaseerd, Gestuurde Evolutie protocol, waarmee de eerste resultaten veelbelovend zijn. Dit protocol biedt de mogelijkheid om spectrale en/of meer actieve varianten van rhodopsine protonpompen te ontwikkelen.

De verschillende mutanten en pigment analoga die beschreven zijn in dit proefschrift vormen een zeer geschikt doelwit voor gedetailleerde biofysische karakterisatie. Door het amfipathische karakter van membraaneiwitten is een vetachtige micro-omgeving vereist, die mede hun structuur en dynamiek bepaalt. In dit verband hebben we de invloed van verschillende op detergentia of lipiden gebaseerde model-systemen getest op stabiliteit, spectrale eigenschappen en oligomerisatie van PR en GR, zoals beschreven in **hoofdstuk 5**. We concluderen dat de keuze van een geschikte micro-omgeving afhangt van de onderzoeksvraag en de bijbehorende methodologie. Daarbij laten we voorbeelden zien van biofysische karakterisatie van PR en GR, waarvoor de verschillende membraan-modelsystemen geschikt zijn.

Hoofdstuk 6 bespreekt de perspectieven van het onderzoek beschreven in dit proefschrift. Samengevat hebben we aanzienlijke vooruitgang geboekt in de ontwikkeling en karakterisatie van NIR-actieve rhodopsine protonpompen. Vervolgstudies gericht op meer theoretische en biofysische karakterisatie van deze pigmenten zijn al in gang gezet. Het op chemotaxis gebaseerde "Gestuurde Evolutie" protocol, beschreven in dit proefschrift, biedt de mogelijkheid tot verdere ontwikkeling van deze pigmenten, en kan in het

algemeen worden toepast op energie-genererende lichtgevoelige systemen. Onze conclusie is, dat de in dit proefschrift beschreven NIR-actieve protonpompen een belangrijk perspectief kunnen bieden bij meerdere biotechnologische toepassingen, zoals in bio-economische en kunstmatige fotosynthese, optogenetica en membraansensor technologie.

Publications

S. Ganapathy, O. Bécheau, H. Venselaar, S. Frölich, J. B. van der Steen, Q. Chen, S. Radwan, J. Lugtenburg, K. J. Hellingwerf, H. J. M. de Groot, W. J. de Grip (2015) "Modulation of spectral properties and pump activity of proteorhodopsins by retinal analogs" *Biochemical Journal* 467: 333-343

Q. Chen, J. B. Van der Steen, H. L. Dekker, **S. Ganapathy**, W. J. De Grip, K. J. Hellingwerf (2016) "Expression of holo-proteorhodopsin in Synechocystis sp. PCC 6803" *Metabolic Engineering* 35:83-94

S. Ganapathy, H. Venselaar, Q. Chen, H. J. M. de Groot, K. J. Hellingwerf, W. J. de Grip (2017) "Retinal-based proton pumping in the near infrared" *Journal of the American Chemical Society* 139 (6): 2338-2344

Q. Chen, J. Arents, **S. Ganapathy**, W. J. de Grip, K. J. Hellingwerf (2017) "Functional expression of Gloeobacter rhodopsin in *Synechocystis* sp. PCC6803" *Photochemistry and Photobiology* 93 (3) :772-781

F. Buda, T. Keijer, **S. Ganapathy**, W.J. de Grip "A quantum-mechanical study of the Binding Pocket of Proteorhodopsin: absorption and vibrational Spectra Modulated by Analogue Chromophores" *Photochemistry and Photobiology* (in press)

Q. Chen, J. Arents, J. M. Schuurmans, **S. Ganapathy**, W. J. de Grip, O. Cheregi, C. Funk, F. B. dos Santos, K. J. Hellingwerf "Proteorhodopsin expression increases growth rate and fitness of a ΔPSI strain of *Synechocystis* sp. PCC6803" (submitted)

Y. Hontani, **S. Ganapathy**, S. Frehan, W. J. de Grip, J. T. M. Kennis "Photoreaction dynamics of near-infrared driven proteorhodopsin with retinal analogues" (submitted)

Q. Chen, J.B. van der Steen, J. Arents, A.F. Hartog, **S. Ganapathy**, W.J. de Grip, and K.J. Hellingwerf "Deletion of *sll1541* in *Synechocystis* sp. PCC6803 allows formation of a far-red shifted *holo*-proteorhodopsin *in vivo*" (submitted)

S. Ganapathy, A. Razumovski, J. B. van der Steen, Q. Chen, H.J.M de Groot, K. J. Hellingwerf and W. J. de Grip "Directed evolution of proteorhodopsin using a novel chemotaxis assay" (manuscript in preparation)

S. Ganapathy, S. Kratz, Q. Chen, K. Rothschild, K. Hellingwerf, H.J.M de Groot, W. J. de Grip "Spectral modulation of Archaearhodopsin-3 using retinal analogs" (manuscript in preparation)

S. Ganapathy, L. Opdam, K. S. Babu, H.J.M de Groot, W.J. de Grip "Solid-state NMR investigation of the retinylidene chromophore in proteorhodopsin and *Gloeobacter* rhodopsin" (manuscript in preparation)

Curriculum vitae

My full name is Srividya Ganapathy, though my friends and colleagues know me simply as Vidya. I was born on the 5th of May 1987 in Rochester, U.S.A and moved to my motherland India when I was barely 5 months old. I grew up in the peaceful and green town of Pune, Maharashtra, where I completed my schooling. I entered the Bachelor of Science Chemistry program in Fergusson College, Pune in 2004 where I graduated with Honors. Having discovered a deep love for all things biochemical, I thereby joined the University of Pune in 2007 to complete a Master's degree in Biochemistry. There I graduated with a first class and won the Prof. Arnikar Lecture competition. For my Master's thesis, I investigated "The antibacterial properties of *Adathoda vasica*, *Holarrhena antidysenterica* and *Cassia fistula*". During my Master's program, I was selected to attend the Making of Mind – a cognitive neuroscience workshop at the National Brain Research Centre, Delhi, India. Following the completion of my Master's degree in 2009, I dabbled for a while in neuroscience and studied "The spatio-temporal features of molecular mechanisms involved in stress induced plasticity" at the National Centre for Biological Sciences in Bangalore, India. After realizing that animal research was not for me, I decided to continue my love affair with the far more docile world of microorganisms. Consequently, in 2012, I started my doctoral studies in Synthetic Biology at Leiden University under the supervision of Prof. dr. Willem J. de Grip and Prof. dr. Huub J. M. de Groot on the project "A Complementary Photosystem", that participated in the large BioSolar Cells programme. During the course of my Ph.D., I had the opportunity to present oral talks about my research at various meetings, such as the BioSolar Cells annual meeting (NL; 2013, 2014), the Gordon Research Seminar in Photosynthesis (Vermont, USA; 2014) and CHAINS (Veldhoven, NL; 2014 and 2016). My research has also been presented in poster form at the BioSolar Cells meeting (2013, 2014, and 2015), the Gordon Research Conference and Seminar in Photosynthesis (2014), CHAINS (2014 and a Poster prize in 2016) and the 17th International Conference on Retinal Proteins (Potsdam, Germany; 2016).